COMPREHENSIVE ANALYSIS OF BOREHOLE STABILITY WITH TEMPERATURE, SWELLING, AND PORE PRESSURE CHANGE FOR LAYERED AND ORTHOTROPIC FORMATIONS

A Thesis

by

FUQIAO BAI

Submitted to the Office of Graduate and Professional Studies of
Texas A&M University
in partial fulfillment of the requirements for the degree of

MASTER OF SCIENCE

Chair of Committee,	Nobuo Morita
Committee Members,	Kan Wu
	Marcelo Sanchez
Head of Department,	Jeff Spath

May 2020

Major Subject: Petroleum Engineering

ABSTRACT

Borehole stability is controlled by various parameters such as rock strength, rock deformation properties, in-situ stress, borehole trajectory, shale swelling, pore pressure change due to osmosis, overbalance mud weight and temperature. The objective of this work is to construct analytical and numerical equations to predict borehole failure including all these parameters and comprehensively evaluate how to improve the borehole instability caused by these parameters.

Analytical solutions are developed for inclined wells including in-situ stress, shale swelling, pore pressure change due to osmosis, overbalance mud weight and temperature. A numerical model is developed for 3D inclined wells with orthotropic formation and layered formation. Using the analytical and numerical models, stress state around inclined wells is evaluated. The breakout angle is predicted using Mohr-Coulomb, Mogi, Lade and Drucker-Prager failure theories. Polar diagrams of mud weights are compared to judge the effect of each parameters and the magnitude predicted by the different failure theories.

Among these parameters, shale swelling, and pore pressure change due to osmosis are the most difficult to estimate. Using with the laboratory measured swelling from cores obtained from various formations, the magnitude to induce breakouts caused by the swelling is the largest comparing with other parameters. Therefore, when shale stability problems occur, we need to estimate the magnitude of shale swelling and osmosis due to water potential difference. Then, to overcome the shale stability problem, we evaluated the sensitivity of human controllable parameters on borehole stability. The

parameters which can be controlled by a drilling engineer are overbalance, type of mud, borehole temperature and borehole trajectory. If the shale swelling is small, the borehole stability is improved by the mud weight. However, from the swelling tests from the cores of Nankai-Trough, we estimated unless we use a swelling inhibitor to reduce the swelling less than 0.1%, the well is not possible to drill through. Actually, the well was abandoned due to instability after trying sidetrack several times.

Unlike previous works, this thesis uses all important parameters (swelling, temperature, pore pressure, orthotropic formation, layered formation) to estimate the stresses around inclined wells. Failure analysis includes Mohr, Mogi, Lade and Drucker-Prager. Finally, the polar diagrams of critical mud weight are used to judge whether we can choose well trajectory, orientation with respect to bedding planes, mud weight, shale inhibitor, and temperature to stabilize the borehole.

DEDICATION

First, I want to dedicate this work to my advisor Dr. Morita. The master life in college station is a tough time to me, which I experienced the medical withdraw and tough research time that I want to give up. However, it is the help and encouragement that Dr. Morita gives to me leading me to this point and compete this work.

Also, I want to dedicate this work to my parents. With my parents' love, I finally complete the research work.

Finally, I want to express my sincere appreciation to my friends for their company. Appreciate all of your encouragement.

ACKNOWLEDGEMENTS

I would like to thank my committee chair, Dr. Morita, and my committee members, Dr. Wu, and Dr. Sanchez for their guidance and support throughout the course of this research.

Thanks also go to my friends and colleagues and the department faculty and staff for making my time at Texas A&M University a great experience.

Finally, thanks to my mother and father for their encouragement

CONTRIBUTORS AND FUNDING SOURCES

Contributors

This work was supervised by a thesis committee consisting of Professor Nobuo Morita [advisor] and Dr. Kan Wu of the Department of Petroleum Engineering and Dr. Marcelo Sanchez of the Department of Civil Engineering.

The analytical and numerical model was continued developed based on the models provided by Professor Nobuo Morita.

All other work conducted for thesis was completed by the student independently.

Funding Sources

Graduate study was supported by a fellowship from Texas A&M University and a dissertation research fellowship from Dr. Nobuo Morita Geomechanics Joint Industry Program.

NOMENCLATURE

σ_{h1}	horizontal stress
σ_{h2}	horizontal stress
σ_v	vertical stress
P_o	pore pressure
σ_{hmax}	maximum horizontal stress
σ_{hmin}	minimum horizontal stress
θ	well azimuth
γ	well inclination
P_w	wellbore pressure
σ_r	radial stress
σ_θ	tangential stress
σ_z	axial stress
σ_r^e	effective radial stress
σ_θ^e	effective tangential stress
σ_z^e	effective axial stress
E	Young's modulus
ν	Poisson's ratio
r_w	wellbore radius
r_d	Normalized wellbore radius
α	Biot constant

η	thermal expansion coefficient
Δp_w	drawdown at the wellbore surface
ΔT_w	temperature change at the wellbore surface
ΔS_w	swelling at the wellbore surface
Δp	pressure drops during drilling
τ_0	cohesion
μ	internal friction coefficient; $\mu = \tan\phi$
ϕ	internal friction angle.
UCS	uniaxial compressive strength
σ_m	mean stress

TABLE OF CONTENTS

Page

LIST OF FIGURES

Page

LIST OF TABLES

Page

CHAPTER I

INTRODUCTION

1.1 Literature Review

Drilling is a significant part of exploration and development cost in petroleum engineering. In most cases, borehole instability related problems may cause seriously high cost for drilling. (Wang, Papamichos and Dusseault 1996). Most oil industries usually make critical mud weight polar charts before drilling wells to select well orientation to minimize downhole borehole instability problems. However, if the reservoir located in the normal faulting regime where the overburden stress is larger than the horizontal stresses, the critical mud weight polar charts will be often ignored during drilling and the well trajectories are selected to maximize oil/gas production. On the other hand, if the maximum horizontal stress exceeds the vertical stress, the critical mud weight polar charts are often honored, and the well trajectory is selected to consider the well stability.

Since other parameters such as well orientation, shale swelling, pore pressure changes due to osmosis, temperature, nonlinearity of stress strain, formation layering and orthotropic elastic modulus can cause borehole instability; effect of these parameters needs to be study to draw accurate critical mud weight polar charts. Stability of horizontal well depends on the well orientation. The well orientation effect is trivial when the maximum stress coincides with overburden pressure and the effect is significant if the maximum stress is in the horizontal direction. (Morita 2004). Shale swelling is caused by the chemical reactions between water-based drilling fluids and

clays present in shale rocks, which, in turn, cause swelling, weakening, and destabilization of the borehole. (Lirkrama and Diaz 2015). It also alters the pore pressure behind cake due to the water potential difference. Temperature changes in a borehole may cause thermal stress that changes in-situ stresses state and therefore leads to borehole failure due to thermal expansion (Wang, Papamichos and Dusseault 1996). Some of these parameters are affecting each other and coupled each other. Although some studies have been done on the effect of each parameter, none of them comprehensively studied the effect of all these parameters on wellbore stability.

1.2 Objective

The objective of this thesis is to use the following procedures to find a proper method to mitigate borehole stability problem caused by shale.

1) Using analytical models, parametric analyses are performed to get stress state for inclined wells with shale swelling, pore pressure change due to osmosis and temperature change due to drilling fluid circulation for typical in-situ stress conditions. The stress state around a borehole is also estimated using a numerical model for layered and orthotropic formations. The author of this dissertation is aware that all of these parameters are coupled each other. For example, if temperature is increased in the borehole, the pore volume behind the mud cake increases resulting in increased pore pressure. If KCL polymer mud is used as a shale inhibitor, the swelling increases and pore pressure increases or decreases depending on the magnitude of dehydration. However, separating the effect of each parameter on borehole stability clarifies its effect

by isolating the effect of other parameters and it can lead a solution to mitigate borehole instability problems.

2) Because the breakout angle depends on the failure criterion of rock, the Mohr, Mogi, Lade and Drucker-Prager failure theories are used to predict the breakout angle round a borehole. Mogi's failure criterion fits well to the failure stresses obtained from the true polyaxial tests for well-consolidated rocks. Lade model is originally proposed for poorly consolidated rock. However, it has been generalized such that it can be used from poorly consolidated rock to consolidated rock by introducing k-value. Mohr Coulomb criterion is often used for fault analysis or weathered rocks with internal cracks or defects or large diameter borehole like a tunnel. Drucker-Prager model is used for predicting a small borehole stability since a small borehole is significantly stronger than a large borehole due to the size effect.

3) Study the effect of controllable parameters on breakout angle around a borehole. Predict critical mud weight to avoid shear collapse under the effect of controllable parameters and plot polar diagrams of safe mud weight for different parameters including swelling, temperature, bedding layers, non-linearity, and anisotropic shales.

4) Compared well orientation effect on the polar diagram of safe mud weight under the normal, the strike-slip and the reverse faulting regimes.

CHAPTER II

EFFECT OF CONTROLLABLE PARAMETERS ON STRESSES AROUND A BOREHOLE

2.1 Analytical Solution to Calculate Stress State around a Borehole

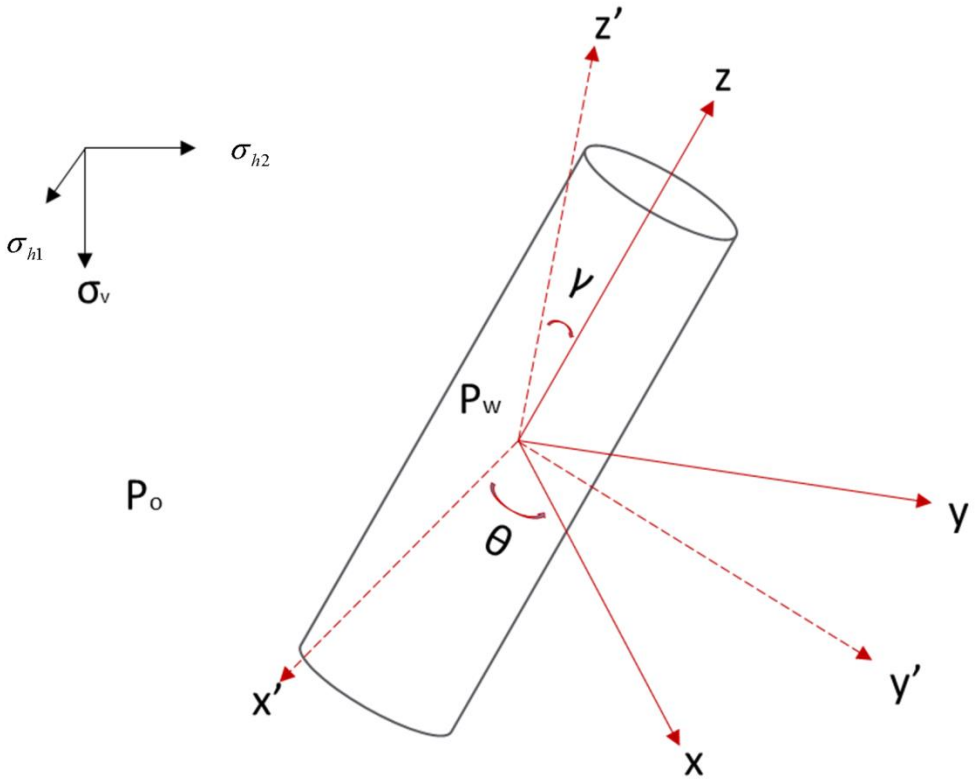

Figure II-1 Coordinate transformation

Suppose the in-situ stresses are given by $(\sigma_{h1}, \sigma_{h2}, \sigma_v)$ in $\left(x', y', z'\right)$ coordinate. The azimuth and inclination of an inclined well is given by (θ, γ) where the coordinate of the inclined well is (x, y, z).

The stress in the well coordinate is given by $\sigma_x, \sigma_y, \sigma_z, \tau_{yz}, \tau_{zx}, \tau_{xy}$, where

$$\sigma_x = \ell_1^2\sigma_{h1} + m_1^2\sigma_{h2} + n_1^2\sigma_v$$

$$\sigma_y = \ell_2^2\sigma_{h1} + m_2^2\sigma_{h2} + n_2^2\sigma_v$$

$$\sigma_z = \ell_3^2\sigma_{h1} + m_3^2\sigma_{h2} + n_3^2\sigma_v$$

$$\tau_{yz} = \ell_2\ell_3\sigma_{h1} + m_2m_3\sigma_{h2} + n_2n_3\sigma_v$$

$$\tau_{zx} = \ell_3\ell_1\sigma_{h1} + m_3m_1\sigma_{h2} + n_3n_1\sigma_v$$

$$\tau_{xy} = \ell_1\ell_2\sigma_{h1} + m_1m_2\sigma_{h2} + n_1n_2\sigma_v$$

Directional cosines are given by:

	x'	y'	z'
x	ℓ_1	m_1	n_1
y	ℓ_2	m_2	n_2
z	ℓ_3	m_3	n_3

$$\ell_1 = \cos\theta\cos\gamma, \ell_2 = -\sin\theta, \ell_3 = \cos\theta\sin\gamma$$

$$m_1 = \sin\theta\cos\gamma, \cdot m_2 = \cos\theta, m_3 = \sin\theta\sin\gamma$$

$$n_1 = -\sin\gamma, n_2 = 0, n_3 = \cos\gamma$$

All the solutions corresponding to the boundary stresses $\sigma_x, \sigma_y, \tau_{xy}, \tau_{yz}, \tau_{xz}$, Pw and Po are added and using the normalized well radius $r_d = r / r_W$, the final solution becomes

$$\sigma_r = 0.5*\left(\sigma_x + \sigma_y\right)\left(1 - rd^{-2}\right) + 0.5*\left(\sigma_x - \sigma_y\right)\left(1 + 3rd^{-4} - 4rd^{-2}\right)\cos(2\theta)$$
$$+ \tau_{xy}\left(1 + 3rd^{-4} - 4r_d^{-2}\right)\sin(2\theta) - P_{WY^{-2}}$$
$$-[E/(1+v)]\beta r^{-2}\int_{r_w}^{r} r\Delta p dr - [E/(1-v)]r^{-2}\int_{r_w}^{r} r(S + \alpha\Delta T)dr$$

$\beta = [(1+v)/(1-v)](1/3B - 1/3Bi)$ for plane strain.

$\beta = (1+v)(1/3B - 1/3Bi)$ for plane stress.

$$\sigma_\theta = 0.5*\left(\sigma_x + \sigma_y\right)\left(1 + r_d - 2\right) - 0.5*\left(\sigma_x - \sigma_y\right)\left(1 + 3r_d^{-4}\right)\cos(2\theta)$$
$$- \tau_{xy}\left(1 + 3rd^{-4}\right)\sin(2\theta) + P_w rd^{-2}$$
$$+[E/(1+v)]\beta r^{-2}\int_{r_w}^{r} r\Delta p dr \cdot [E/(1-v)](1/3B \cdot 1/3B)\Delta p\Big]$$
$$+[E/(1\cdot v)]r^{-2}\int_{r_w}^{r} r(S + \alpha\Delta T)dr$$
$$-[E/(1-v)](S + \alpha\Lambda T)$$

$$\sigma_z = \sigma_{zz} - v\Big\lfloor 2\left(\sigma_x - \sigma_y\right)rd^{-2}\cos 2\theta + 4\tau_{xy}r_d x_d^{-2}\sin 2\theta\Big\rfloor - [E/(1-v)(1/3B - 1/3Bi)\Delta p$$
$$-[E/(1-v)(S + \alpha\Delta T)$$

$$\tau_{r\theta} = 0.5^{*}\left(\sigma_x - \sigma_y\right)\left(-1 + 3rd^{-4} - 2rd^{-2}\right)\sin 2\theta + \tau_{xy}\left(1 - 3rd^{-4} + 2rd^{-2}\right)\cos 2\theta$$

$$\tau_{\theta z} = \left(-\tau_{xz}\sin\theta + \tau_{yz}\cos\theta\right)\left(1 + rd^{-2}\right)$$

$$\tau_{rz} = \left(\tau_{xz}\cos\theta + \tau_{yz}\sin\theta\right)\left(1 - rd^{-2}\right)$$

$$\begin{aligned} u = {} & 0.5\sigma_x r_w[(1+\nu)/(E)]\left\lfloor (1-2\nu)r_d + r_d^{-1}\right\rfloor + \left[r_w P_w(1+\nu)/E\right]rd^{-1} \\ & + \left(\sigma_x - \sigma_y\right)r_w[(1+\nu)/(E\nu)]\left[0.5r_d - 0.5rd^{-3} + 2\nu/(1+\nu)rd^{-1}\right]\cos(2\theta) \\ & + 0.5\sigma_y r_w[(1+\nu)/(E)]\left[(1-2\nu)rd + rd^{-1}\right] \\ & - \tau_{xy} rw[(1+\nu)/(E\nu)]\left[-rd + rd^{-3} - 4\nu/(1+\nu)rd^{-1}\right]\sin(2\theta) \\ & + [(1+\nu)/E]\tau_{xz} z\cos(\theta) + [(1+\nu)/E]\tau_{yz} z\sin(\theta) \\ & + \beta r^{-1}\int_{r_w}^{r} r\Delta p dr + \frac{1+\nu}{1-\nu} r^{-1}\int_{r_w}^{r} r(S + \alpha\Delta T)dr \end{aligned}$$

$$\begin{aligned} v = {} & \left(\sigma_x - \sigma_y\right)_{rw}[(1+\nu)/(E\nu)]\left[-0.25(1+\nu)rd + 0.25(1-3\nu)rd^{-3} - \nu(1-\nu)/(1+\nu)rd^{-1}\right]\cos(2\theta) \\ & + \tau_w r_w[(1+\nu)/(E\nu)]\left[0.5(1+\nu)r_w - 0.5(1-3\nu)rd^{-3} - 2\nu(1-\nu)/(1+\nu)rd^{-1}\right]\cos(2\theta) \\ & - [(1+\nu)/E]\tau_{xz} z\sin(\theta) + [(1+\nu)/E]\tau_{yz} z\cos(\theta) \end{aligned}$$

$$w = [(1+\nu)/E]\tau_{xz} x_w\left(r_d + 2/r_d\right)\cos(\theta) + [(1+\nu)/E]\tau_{yz} r_w\left(r_d + 2/r_d\right)\sin(\theta)$$

The displacement u,v,w include the displacement induced with the in-situ stresses. The displacement induced after drilling the well is given by

$$\begin{aligned} u' = {} & 0.5\sigma_x r_w[(1+\nu)/(E)]r_d - 1 + \left[r_W P_W(1+\nu)/E\right]rd^{-1} \\ & + \left(\sigma_x - \sigma_y\right)_{r_w}[(1+\nu)/(E\nu)]\left[-0.5rd^{-3} + 2\nu/(1+\nu)rd^{-1}\right]\cos(2\theta) \\ & + 0.5\sigma_y r_w[(1+\nu)/(E)]rd^{-1} \\ & - \tau_{xy} r_W[(1+\nu)/(E\nu)]\left[rd^{-3} - 4\nu/(1+\nu)rd^{-1}\right]\sin(2\theta) \\ & + \beta \mathrm{r}^{-1}\int_{r_w}^{r} r\Delta p dr + \frac{1+\nu}{1-\nu}\mathrm{r}^{-1}\int_{r_w}^{r} r(S + \alpha\Delta T)dr \end{aligned}$$

$$v' = \left(\sigma_x - \sigma_y\right) r_w[(1+v)/(Ev)]\left[0.25(1-3v)rd^{-3} - v(1-v)/(1+v)rd^{-1}\right]\cos(2\theta)$$
$$+ \tau_{xy}\, r_w[(1+v)/(Ev)]\left[-0.5(1-3v)rd^{-3} - 2v(1-v)/(1+v)rd^{-1}\right]\cos(2\theta)$$

$$w' = [(1+v)/E]\tau_{xz} r_w\left(2/r_d\right)\cos(\theta) + [(1+v)/E]\tau_{yz} r_w\left(2/r_d\right)\sin(\theta)$$

Stress at the borehole

At the borehole, we have

$r_d = 1$

Hence,

$$\sigma_r = -P_w$$
$$\sigma_\theta = \left(\sigma_x + \sigma_y\right) - 2\left(\sigma_x - \sigma_y\right)\cos(2\theta) - 2\tau_{xy}\sin(2\theta) + P_W - [E/(1-v)](1/3B - 1/3Bi)\Delta p \Big\rfloor$$
$$-[E/(1-v)](S + \alpha\Delta T)$$

$$\sigma_z = \sigma_{zz} - v\Big\lfloor 2\left(\sigma_x - \sigma_y\right) rd^{-2}\cos 2\theta + 4\tau_{xy}\sin 2\theta \Big\rfloor - [E/(1-v)(1/3B - 1/3Bi)\Delta p$$
$$-[E/(1-v)(S + \alpha\Delta T)$$

$$\tau_{r\theta} = 0$$

$$\tau_{\theta z} = 2\left(-\tau_{xz}\sin\theta + \tau_{yz}\cos\theta\right)$$

$$\tau_{rz} = 0$$

Since the net in-situ stresses are used in the above equation, the in situ stresses must be converted from the total in-situ stresses with the following equation.

$$\sigma_{ij}^{net} = \sigma_{ij} + p_o \delta_{ij}$$

Where p_o is the original pore pressure before drilling.

After calculation of the stress around a borehole, the total stresses must be calculated using the following equation.

$$\sigma_{ij} = \sigma_{ij}^{net} - p_o \delta_{ij}$$

Normally, since the effective stresses are needed to calculate the borehole stability, the following equation is used if the pore pressure around the borehole is changed by Δp from the original pore pressre.

$$\sigma_r^e = \sigma_r + \Delta p = -P_w + \Delta p$$

$$\sigma_\theta^e = \sigma_x + \sigma_y - 2(\sigma_x - \sigma_y)\cos(2\theta) - 2\tau_{xy}\sin(2\theta) + \mathrm{P}_w + \Delta p - \frac{E}{1-\nu}\left(\frac{1-2\nu}{E} - \frac{1-2\nu_m}{E_m}\right)\Delta p - \frac{E}{1-\nu}(S + \alpha\Delta T)$$

$$\sigma_z^e = \sigma_{zz} - 2\nu\left[(\sigma_x - \sigma_y)\cos(2\theta) + 2\tau_{xy}\sin(2\theta)\right] + \Delta p - \frac{E}{1-\nu}\left(\frac{1-2\nu}{E} - \frac{1-2\nu_m}{E_m}\right)\Delta p - \frac{E}{1-\nu}(S + \alpha\Delta T)$$

$$\tau_{r\theta} = 0$$

$$\tau_{\theta z} = 2\left(-\tau_{xz}\sin\theta + \tau_{yz}\cos\theta\right.$$

$$\tau_{\mathrm{rz}} = 0$$

We may calculate the effective stresses assuming a simplified pressure, temperature and swelling distributions. The author of this dissertation is aware that all these parameters interact with each other. However, separating each parameter clarifies the contribution of each parameter on wellbore stability. Distributions of temperature, pore pressure and swelling around a borehole are often approximated by logarithmic functions, since they are induced by diffusion process. Therefore, we assume the following equation for pressure, temperature, and swelling distributions within the distance of r_p, r_T, r_s, respectively. Beyond r_p, r_T, and r_s, these parameters are set to be zero.

$$\Delta p = \Delta p_w (1 - \ell n \frac{r}{r_w} / \ell n \frac{r_p}{r_w}) \ \ for \ r_w < r < r_p \ \text{ and } \ \Delta p = 0 \ for \ r_p < r$$

$$\Delta T = \Delta T_w (1 - \ell n \frac{r}{r_w} / \ell n \frac{r_T}{r_w}) \ \ for \ r_w < r < r_T \ \text{ and } \ \Delta T = 0 \ for \ r_T < r$$

$$\Delta S = \Delta S_w (1 - \ell n \frac{r}{r_w} / \ell n \frac{r_S}{r_w}) \ \ for \ r_w < r < r_S \ \text{ and } \ \Delta S = 0 \ for \ r_S < r$$

2.2 Parameter Study with Typical Field Conditions

Borehole stability is controlled by various parameters such as rock strength, rock deformation properties, in-situ stress, borehole trajectory, shale swelling, pore pressure change due to osmosis, overbalance mud weight, temperature, and bedding layers. In this section, effect of these parameters on stresses around a vertical well borehole under the base reservoir conditions shown in Table II-1 is calculated for linear and non-linear elasticity methods, and then effect of these parameters will be analyzed for horizontal well borehole under the depleted reservoir conditions shown in Table II-2. In this thesis, because of using the polar coordinate for critical mud weight, the x-coordinate is selected from South-North and the y-coordinate is selected from East-West. The angle in North is zero and the well azimuth is counted clockwise from North to East.

Table II-1. The base reservoir and stress conditions. Note: the maximum horizontal stress σh2 is oriented in West-East (y-coordinate) and the minimum horizontal stress is oriented in South-North (x-coordinate) in this thesis)

Young's Modulus	**E(psi)**	3.E6
Poison Ratio	**υ**	0.2
Horizontal Stress	**σ_{h1} (psi)**	-8000
Horizontal Stress	**σ_{h2} (psi)**	-8500
Overburden Stress	**σ_{v} (psi)**	-10000
Pore Pressure	**P_o (psi)**	6000
Wellbore Pressure	**P_w(psi)**	6500
Biot 's Constant	**α**	0.8
Wellbore Radius	**r_w (ft)**	0.354

Assume 4000 psi depletion and the change of axial and vertical effective ratio during depletion is assumed to be $\Delta\sigma_h^e / \Delta\sigma_v^e = 0.4$

Then after depletion, the reservoir conditions become

Table II-2 Depleted reservoir and stress conditions (overbalance well pressure is increased to 1000 psi)

Horizontal Stress	**σ_{h1} (psi)**	-5600
Horizontal Stress	**σ_{h2} (psi)**	-6100
Overburden Stress	**σ_v (psi)**	-10000
Pore Pressure	**P_o(psi)**	2000
Wellbore Pressure	**P_w(psi)**	3000

Analytical solutions are developed for inclined wells including in-situ stress, shale swelling, pore pressure change due to osmosis, overbalance mud weight and temperature. A numerical model is developed for 3D inclined wells with orthotropic formation and layered formation. Using the analytical and numerical models, stress state around inclined wells is evaluated.

2.2.1 Stress State around a Borehole for the base Borehole Conditions

1. **Stress state: The base condition shown in Table II-1**

Here, we use the data given in Table II-1 to calculate the stress state around a borehole at the base condition without considering any other controllable parameters. This provides the base stress state without temperature, swelling and pore pressure disturbances.

Orientation: 0°from x axis

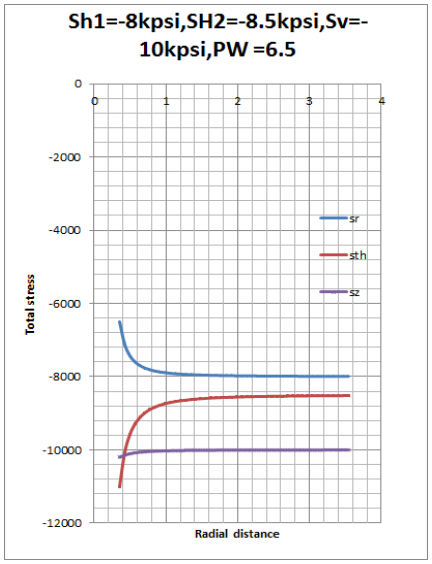

Figure II-2. Total stress state with distance from borehole for base case at 0° from x axis

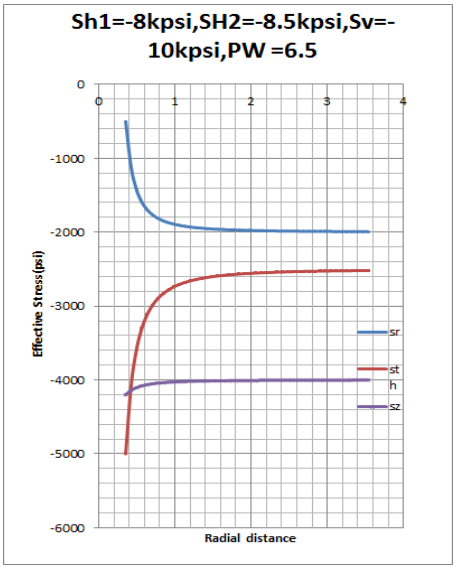

Figure II-3. Effective stress state with distance from borehole for base case at 0° from x axis

Orientation: 90°from x axis

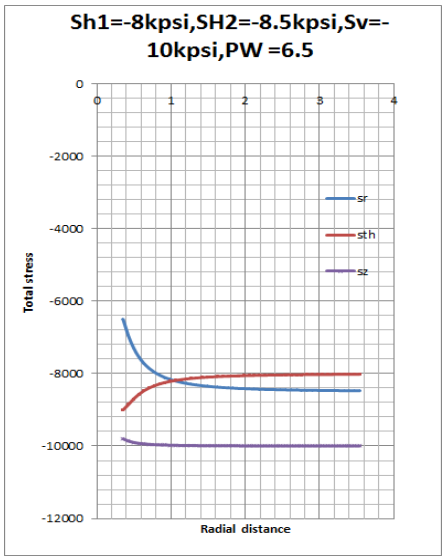

Figure II-4. Total stress state with distance from borehole for base case at 90° from x axis

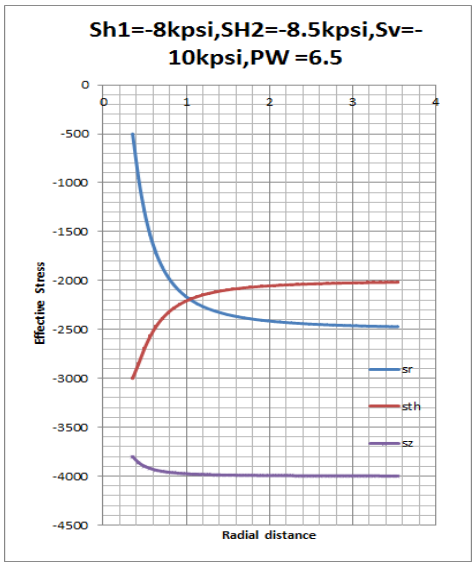

Figure II-5. Effective stress state with distance from borehole for base case at 90° from x axis

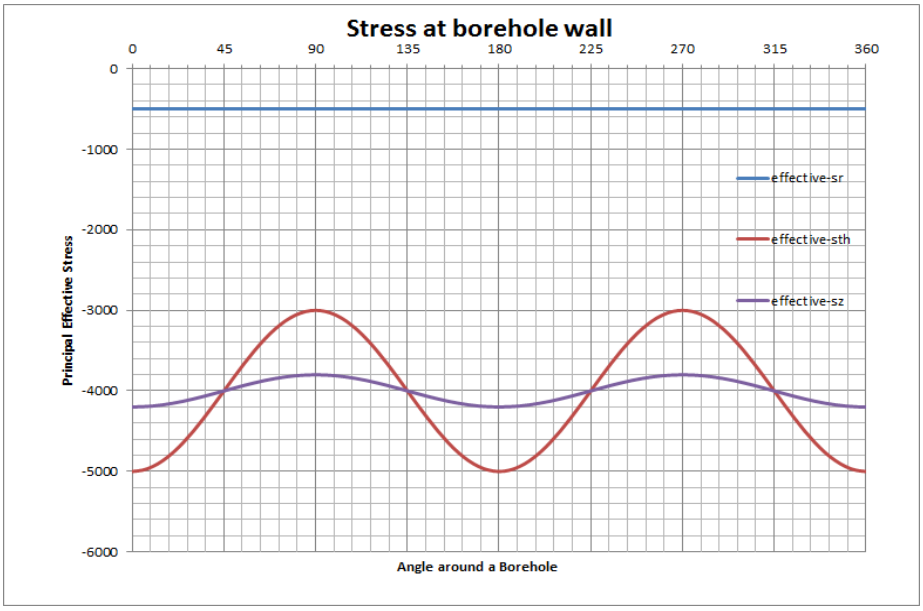

Figure II-6. Effective Stress State at the borehole wall for base case

Figs. II-2 to II-5. illustrate the variation of effective stresses at 0°orientation from x axis (the direction of σ_h) and 90° from x axis (the direction of σ_H) with the radial distance from wellbore. The figures show:

a. The effective stresses only change at and near the borehole, where the magnitude of radial stress increases with distance near the borehole, and the magnitude of tangential stress decreases with distance around borehole. However, all the stresses tend to approach to stable values at far field.
b. Comparing the results of stresses at orientations at 0° and 90° from x axis, we find that the tangential stress, which is in circumferential direction and has most significant effect on the mud weight and borehole stability during drilling, has much larger values at 0° from x axis than the value at 90°. It illustrates that the compressive stress concentration occurs at the borehole in the minimum in-situ stress direction and the extension failure may be induced at the borehole in the maximum in-situ stress direction.

Fig. II-6 shows the effective stresses distribution around borehole. The tangential stress and vertical stress vary like a sine function at the circumferential direction at borehole, while the radial stress remains a constant at borehole wall. And the maximum tangential stress occurs at 90° and 270°. Furthermore, the radial stress is the minimum principal stress. Because the mud overbalance pressure is assumed to be low, a shear failure may be induced.

2. Stress state for well inclination (γ)

The well inclination is set at 0 º, 30º, 60 º, 90 º at the given reservoir conditions.

Well azimuth=0°,well angle=30°

Orientation: 0° from x axis

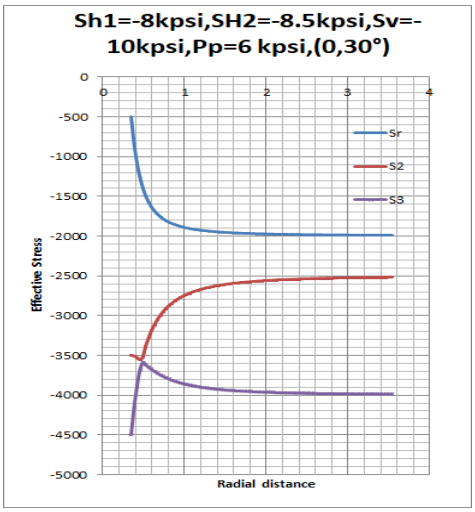

Figure II-7 Effective stress state with distance from borehole for well angle = 30° at 0° from x axis

Orientation: 90° from x axis

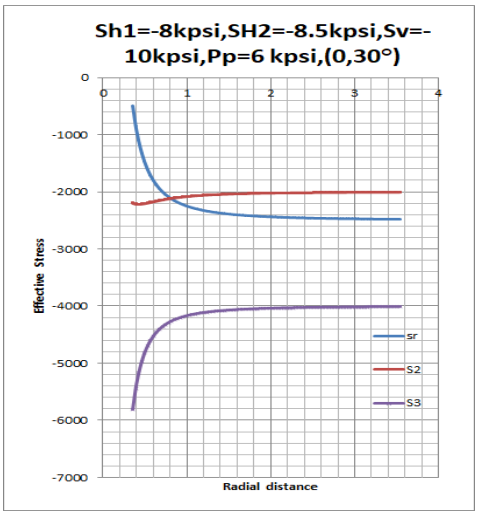

Figure II-8 Effective stress state with distance from borehole for well angle = 30° at 90° from x axis

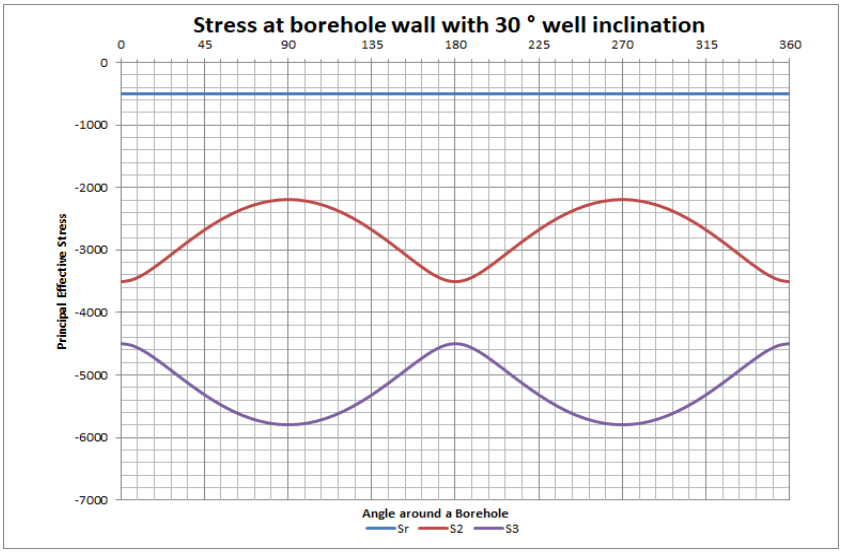

Figure II-9 Effective Stress State at the borehole wall for well angle = 30° at 90° from x axis

As Figs.II-7 and II-8 show, the effective stresses at and near borehole for a 30° inclined well in the orientations at 0° and 90° from x axis also change only at and near the borehole and get closer to stable values at far field (the distance r-∞). The effective stress near borehole is little lower than that that of the base condition. The values of S3 are much smaller at 90° orientation than those at 0°. In addition, the stress state at borehole is $\sigma_r < \sigma_2 < \sigma_3$ and $\sigma_r < \sigma_3 < \sigma_2$ at the far distance from borehole in 0° orientation, while the stress state at borehole is $\sigma_r < \sigma_2 < \sigma_3$ and $\sigma_3 < \sigma_r < \sigma_2$ at the far distance from borehole in 90° from x axis.

Fig.II-9 show effective stress distributions at borehole wall. The orientation of wellbore is ranging from 0° to 360°, and the radial distance is equal to r_w. We can find σ_2 and σ_3 vary like sine and cosine functions, respectively, while the radial stress remains a constant, which is the minimum principal stress. And also, the maximum of σ_2 is at 90° and 270°; the maximum of σ_3 is at 0° and 180°.

Well azimuth=0°,well angle=60°

Orientation: 0° from x axis

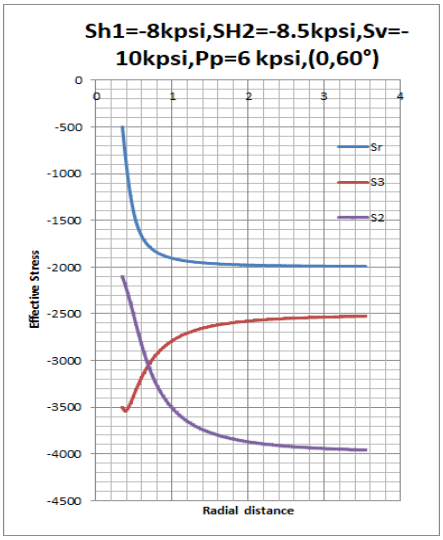

Figure II-10 Effective stress state with distance from borehole for well angle = 60° at 0° from x axis

Orientation: 90° from x axis

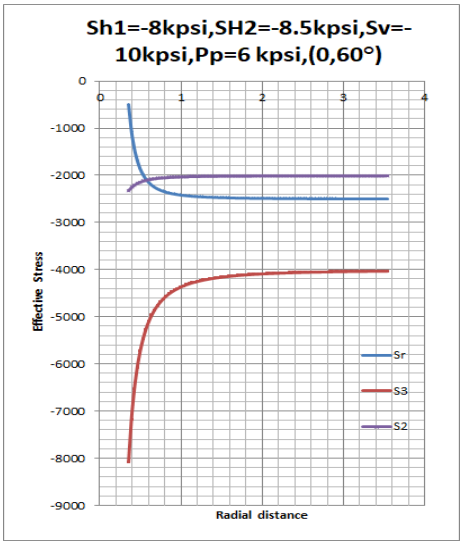

Figure II-11 Effective stress state with distance from borehole for well angle = 60° at 90° from x axis

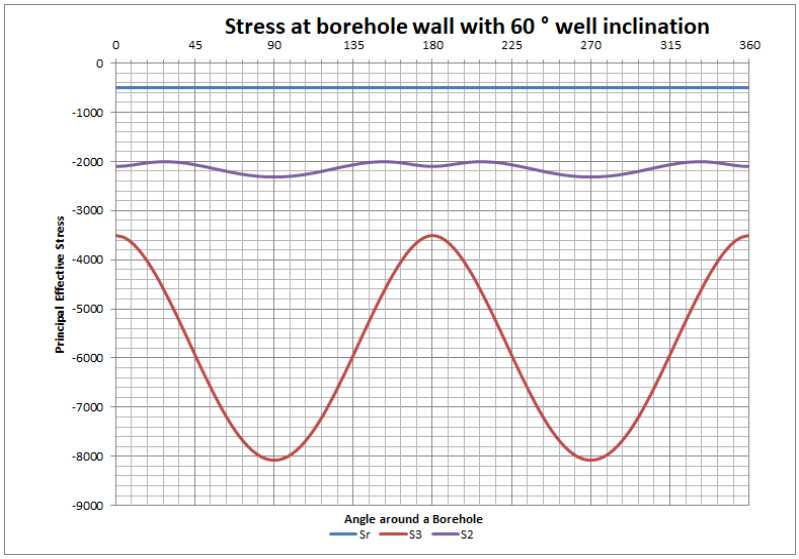

Figure II-12 Effective Stress State at the borehole wall for well angle = 60°

As Figs. II-10 and II-11 show, the effective stress at and near borehole for a 60° inclined well oriented at 0° and 90° azumuth from x aixs also changes only at and near borehole and tends to be stable values at far field (the distance r 1∞). The value of effective stress near borehole is lower than that with the base condition. However, the values of σ_2 and σ_3 are much smaller in orientation at 90° than those at 0° and the values of σ_r are larger in orientation at 90°. In addition, the stress state is $\sigma_r < \sigma_2 < \sigma_3$ at the borehole and $\sigma_r < \sigma_3 < \sigma_2$ at far distance from the borehole in 0° direction, while the stress state is $\sigma_r < \sigma_2 < \sigma_3$ at borehole and $\sigma_3 < \sigma_r < \sigma_2$ at far distance from the borehole at 90° from x axis.

Fig. II-12 shows the effective stress distribution at borehole wall for a 60° inclined well. Under this condition, σ_2 varies around a borehole but it is flatter. σ_3 Varies in larger amplitude like a cosine function, while the radial stress remains a constant, which is the minimum principal stress. The maximum of σ_3 is at 0° and 180°.

Well azimuth=0° ,well angle=90°

Orientation: 0° from x axis

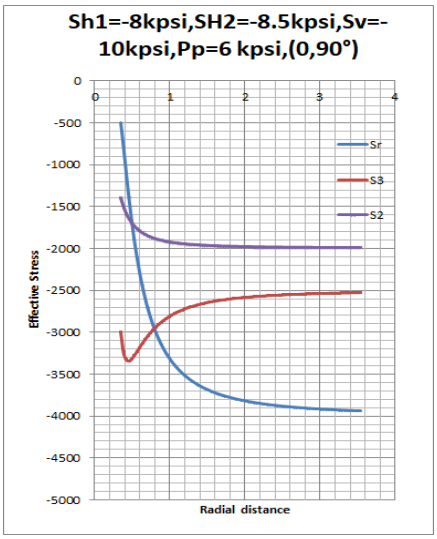

Figure II-13 Effective stress state with distance from borehole for well angle = 90° at 0° from x axis

Orientation: 90° from x axis

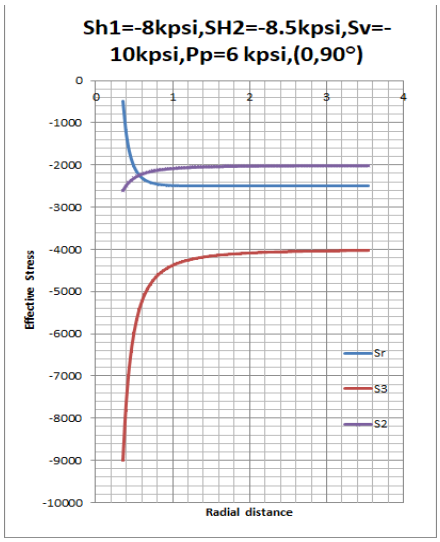

Figure II-14 Effective stress state with distance from borehole for well angle = 90° at 90° from x axis

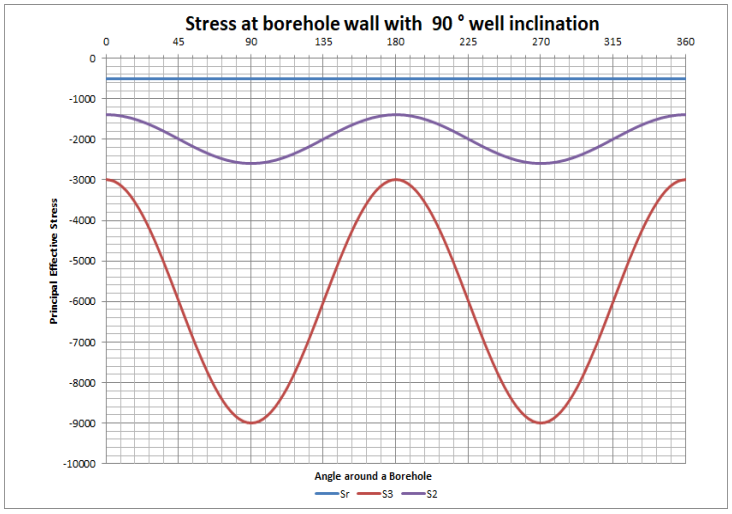

Figure II-15 Effective Stress State at the borehole wall for well angle = 90°

As Fig. II-13 and Fig. II-14 show, the effective stresses at and near borehole for a 90° inclined well with 0° and 90° azimuthes also change only at and near borehole and tend

to be stable values at far field (the distance $r \rightarrow \infty$). The values of effective σ_2 and σ_3 near borehole are lower than those at the base condition, whereas the radial stress is lager with distance away from the borehole than that at the base condition. Furthermore, the values of σ_2 and σ_3 are much smaller at 90°orientation than those at 0° and the values of σ_r is larger at 90°orientation. In addition, the stress state is $\sigma_r < \sigma_2 < \sigma_3$ at borehole and $\sigma_2 < \sigma_3 < \sigma_r$ at far distance from borehole, both at 0° and 90° orientations from x axis.

Figs. II-15 show effective stress distribution at borehole wall for a 90° inclined well . σ_2 and σ_3 vary like sine and cosine functions, respectively, but σ_3 varies in larger amplitude, while the radial stress remains constant, which is the minimum principal stress. And also, the maximum of σ_2 is at 90° and 270°; the maximum of σ_3 is at 0° and 180°.

3. Stress state for pore pressure change due to osmosis effect

Osmosis is caused by water potential difference. Therefore, the osmosis is always considered together with shale swelling. However, recently, polyamine or the same family of shale inhibitors has been used. These inhibitors prevent shale swelling without changing water potential. On the other hand, the conventional shale inhibitors such as KCL polymer or Formate Brine base Mud (KCOOH+NACOOH) rely on the water potential as minimizing the shale swelling and reducing the pore pressure behind the cake. Therefore, in this research, pore pressure change due to osmosis is discussed separately with shale swelling.

In this case, the surface pressure drop of -500 psi is given due to osmosis effect. The radius r_p of the pressure drop is assume to be 2 ft. The wellbore pressure is maitained with 500 psi overbalance.

Orientation: 0°from x axis

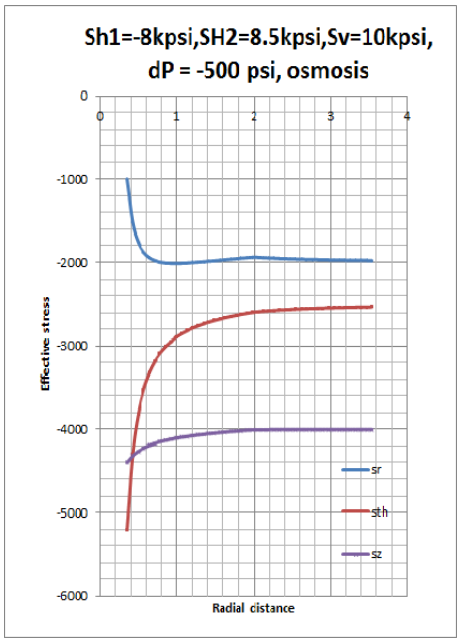

Figure II-16. Effective stress state with distance from borehole due to osmosis at 0° from x axis

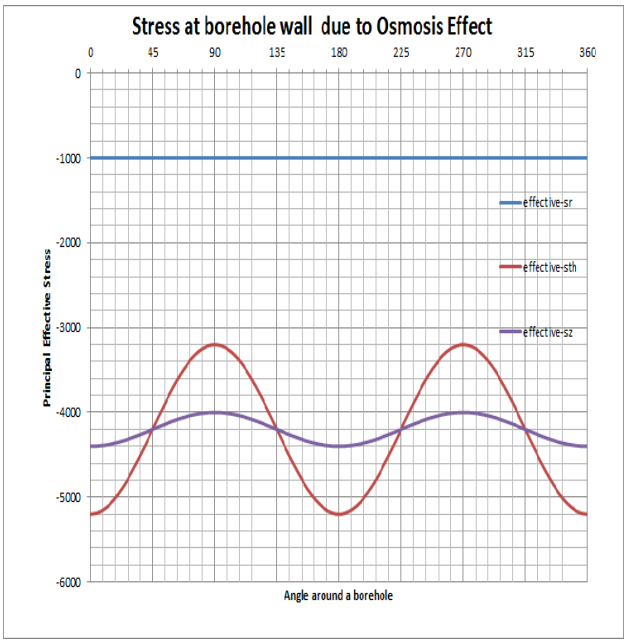

Figure II-17. Effective Stress State at the borehole wall due to osmosis

Orientation: 90° from x axis

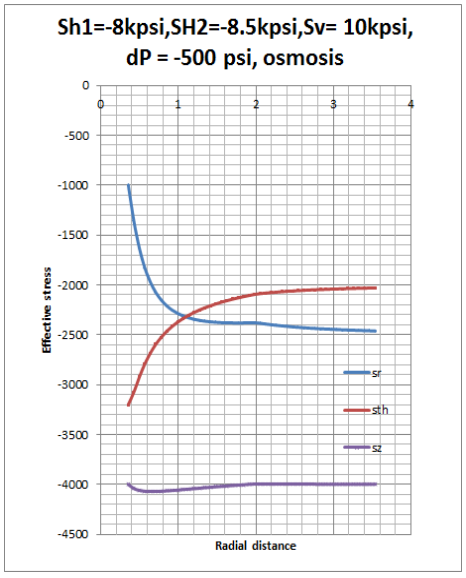

Figure II-18. Effective stress state with distance from borehole due to osmosis at 90° from x axis

As the figures show, when considering the osomosis due to water potential difference, there is almost no change of tangiential and overburden stresses at borehole and at far distance from borehole compared with the base condition where no effect is considered. However, due to the osmosis effect, the radial effective stress increases to -1000 psi from -500 psi at borhole wall, which stabilizes the borehole.

4. Stress state due to swelling effect

75% of drilled formations are consitsed of shale and also shale swelling causes 90% of wellbore instabilities problems. (Tare and Mody 2002). Shale swelling always occurs due to clay (one of the major components of shale) absorbing water, usually from drilling fluid. The proper drilling fluid shale inhibitor can mitigate shale swelling, however, even if the new method and novel drilling fluids additives are used, the shale swelling is still at a high value according to the shale swelling lab test with Nankai trough 319-C0009A 9R-1-WR samples (Takuma 2019).

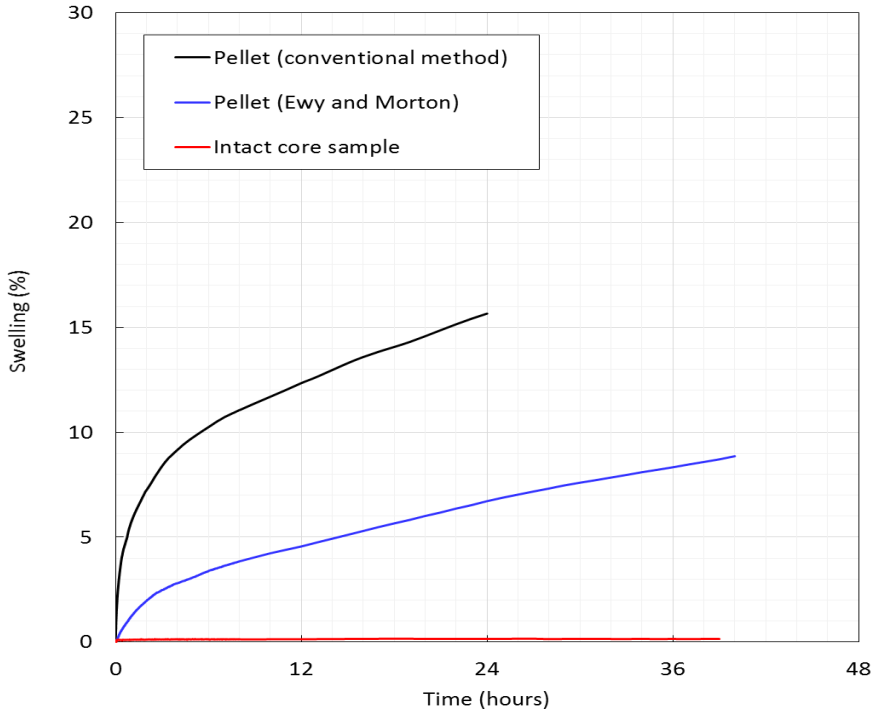

Figure II-19.Linear swelling rate for Nankai trough 319-C0009A 9R-1-WR samples in 3 wt% bentonite mud. Black curve: pellet made by conventional method, Blue curve: pellet made by Ewy and Morton's method, Red curve: intact core sample (Takuma 2019).

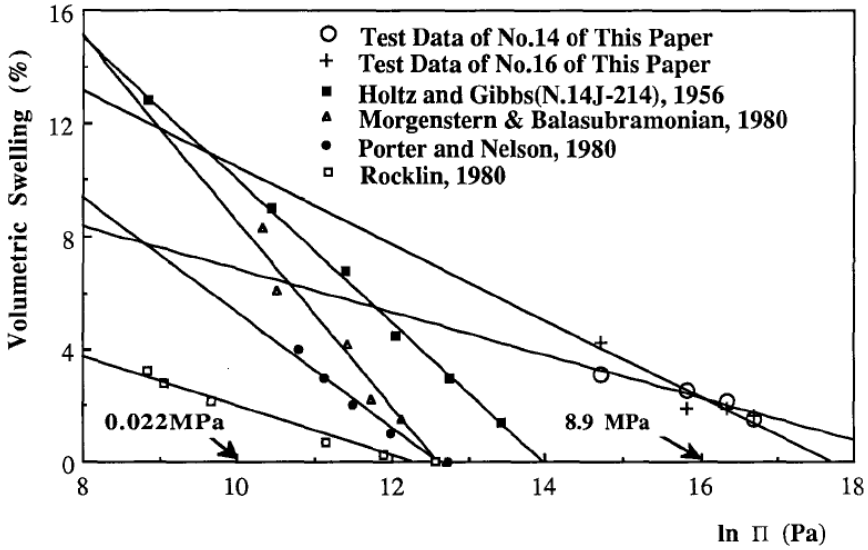

Figure II-20 The relations of confining pressure vs. corresponding volumetric swelling strain (Figure 7 of Zhou et al. 1992)

As shown in Fig.II-19, the magnitude of shale swelling depends on how to measure the swelling. If we use the standard method using pellets, the swelling may be as large as 10-15%. However, if we eliminate the capillary effect using the EWY's method (pore fluid saturation is adjusted to 100%), the measured swelling may be reduced as half as shown in Fig.II-18. In addition, if intact cores are used instead of pellets, the swelling may be reduced below 2% . Table II-3 shows how the swelling changes depending on how to measure. If intact rock is used, the swelling may be reduced less than 2%. Normally, the swelling is measured with small stress (0.4 to 1.7psi axial stress, with a confining steal net). However, the swelling is signifificantly reduced if the effective stress becomes large. Accordidng to the laboratory tests by Zhou (Fig.II-20), the swelling may be reduced to ¼ with in-situ stress comparing with the standard lab test without a confining pressure. Therefore, the magnitude of swelling for hard shale may be as small as 0-0.5%.

Table II-3 Summary of swelling measurement under different stress conditions

	Pellet swelling (%)			Intact swelling (%) *			Intact/Pellet		
Sample	0.4 psi	1.7 psi	3.8 psi	0.4 psi	1.7 psi	3.8 psi	0.4 psi	1.7 psi	3.8 psi
Nankai 319	11.62	5.87	4.25	(2.21)	(2.88)	(1.66)	(0.19)	(0.49)	(0.39)
Nankai 338	6.91	1.23	0.77	3.11	1.39	0.61	0.45	1.14	0.79
Marcellus	4.98	3.23	2.21	0.06	0.14	0.17	0.01	0.04	0.08
Mancos	5.57	2.13	1.86	0.63	0.60	0.56	0.11	0.28	0.30

*Calculated by $1/3 \times$ volumetric swelling

Therefore, in this section, 0.2 % swelling is assumed at the wellbore surface (ΔS) and the swelling radius (rs) is 0.7 ft to evaluate the extent of effect on stresses state around a borehole.

Table II-4 Parameters used for stress calculation around a well for shale swelling

Equation	$\Delta S = \Delta S_w(1-\ell n\frac{r}{r_w}/\ell n\frac{r_S}{r_w})$ *for* $r_w < r < r_S$ and $\Delta S = 0$ *for* $r_S < r$
ΔS_w	0.2%
r_w, r_s	0.354, 0.7ft

According to the analytical solutions, the tangential stress becomes proportionally large as $\{E/(1-\nu)\}$(S+ $\alpha\Delta$T)

As the Fig.II-21-Fig.II-23 show, the stress state is significantly affected by shale swelling. The tangiential and overburden stresses dramatically increase at and near borhole compared with the stress in the base condition, which easily cause borehole instability, but with the distance away from the borehole, the stresses tends to be the same as the state in the base condition, where we assume shale swelling effect is ignored.

Orientation: 0° from x axis

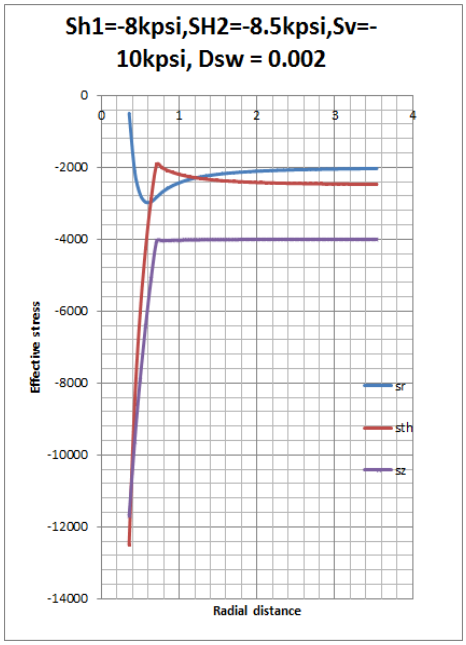

Figure II-21 Effective stress state with distance from borehole due to shale swelling at 0° from x axis

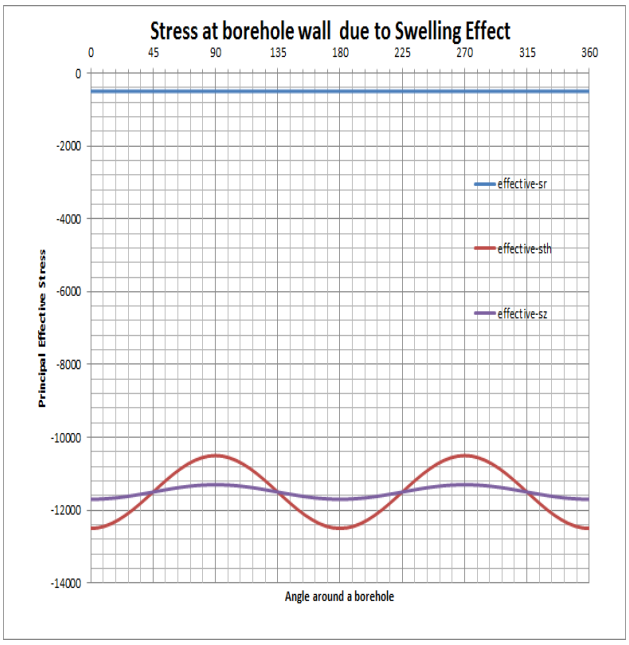

Figure II-22. Effective Stress State at the borehole wall due to shale swelling

Orientation: 90° from x axis

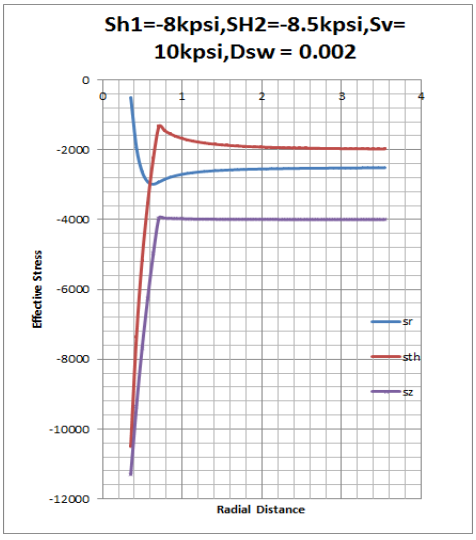

Figure II-23. Effective stress state with distance from borehole due to shale swelling at 90° from x axis

5. Stress state due to temperature effect

During drilling process, one of the key factor that affects borehole stability, is the variation of formation temperature which in turn causes the change in stresses around a borehole. While drilling, the drilling fluid continuously exchanges heat with the formation in the circulation process. The temperature change at borehole anulus below casing shoe can reach to ±50 ° C or even larger which depends on formation temerature gradient and the casing set depth.

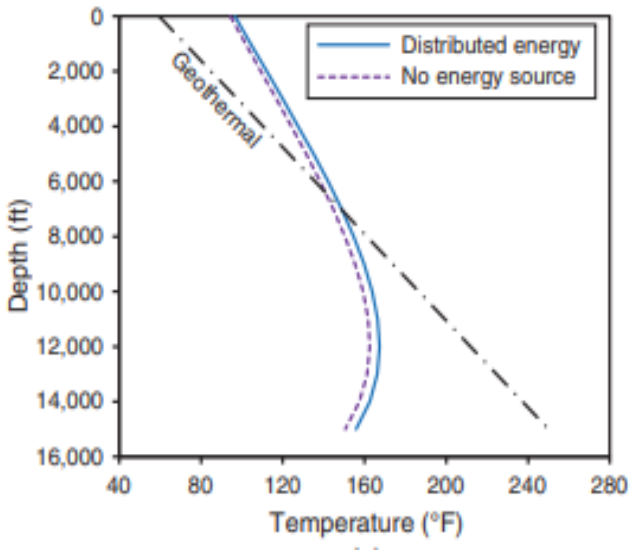

Figure II-24. Annular temperature change during drilling (Al Saedi, Flori et al. 2019)

If there is temperature difference between fluid and formation, the temperature will propagate by diffusion into the formation. And the formations like most other materials expand or shrink when temperature is changing, thus giving rise to thermal contraction or expansion stresses. Thermally induced stress varies by the difference in thermal expansion coefficient of the rock formation. (Prazeres 2015).

Table II-5 Thermal expansion coefficient of different types of rock

Rock Type	α (10^{-6} K^{-1})
Basalt	5.4
Limestone	2.5-20
Granite	7.5-9
Sandstone	10
Marble	5.4-7
Salt	40

Therefore, in this section, a temperature change of -50 °C is assumed at the drill bit and temperature change of 50 °C is assumed at the casing shoe within the radius of 0.7 ft to evaluate the borehole cool down and the borehole warm up effects. The linear expansion coefficient is given as 1.e-5 /ºC.

Table II-6 Parameters used for stress calculation around a well for temperature effect

Equation	$\Delta T = \Delta T_w (1 - \ell n \frac{r}{r_w} / \ell n \frac{r_T}{r_w})$ *for* $r_w < r < r_T$ and $\Delta T = 0$ *for* $r_T < r$
ΔT_w	50ºC
r_w, r_T	0.354, 0.7ft
α (thermal expanion coeeficient)	10^{-5} /ºC

As shown in Fig. II-25-Fig. II-27, a temperature change of 50 °C inside a borehole leads to a significant change of stressses state at and near borehole. The dramatical increase in tangiential and overburden stresses are also observed compared with the base condition. However, Fig. II-28- Fig. II-30 indicate the temperature change of -50 °C reduces the magnetitude of stresses at and near borehole. In contrast with 50 °C increase of tempreature, the temperatrue cooling stabilizes the borehole. The temperature effect on the tangential stress is proportional to $\{E/(1-\nu)\}(\mathrm{S}+\alpha\Delta\mathrm{T})$. Therefore, comparing with the swelling effect, the temperature increase at the casing shoe may be ignored.

Temperature change of 50 °C

Orientation: 0° from x axis

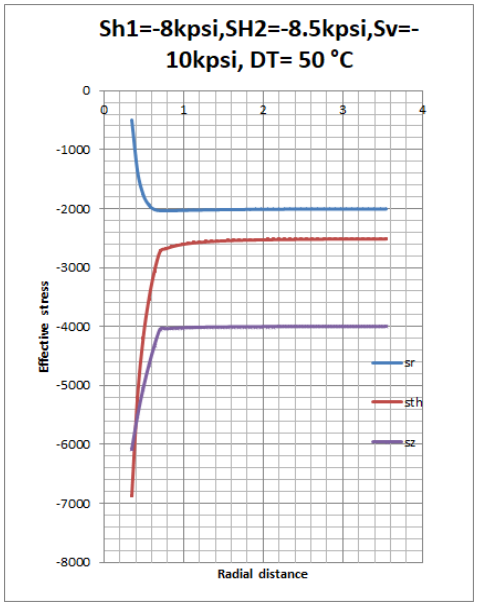

Figure II-25. Effective stress state with distance from borehole due to temperature warm up at 0° from x axis

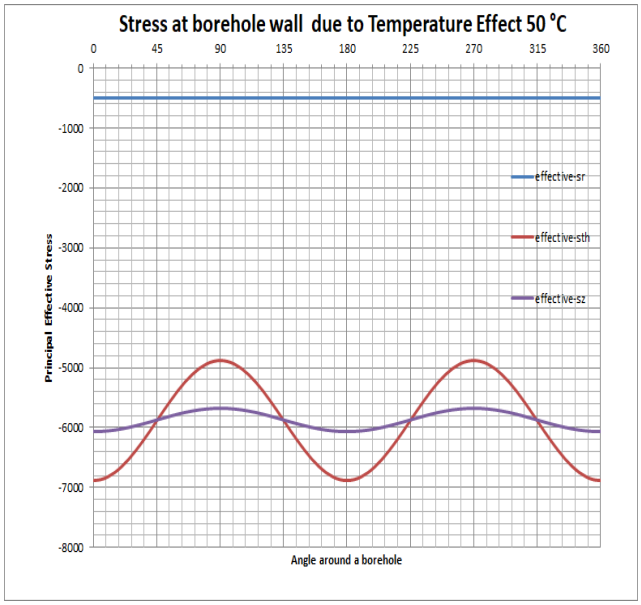

Figure II-26. Effective Stress State at the borehole wall due to temperature warm up

Orientation: 90° from x axis

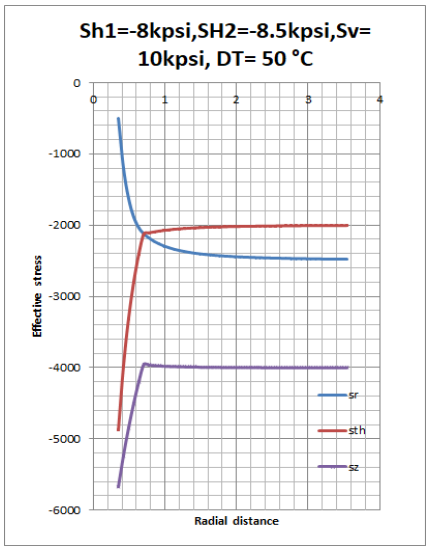

Figure II-27. Effective stress state with distance from borehole due to temperature warm up at 90° from x axis

Temperature change of -50 °C

Orientation: 0° from x axis

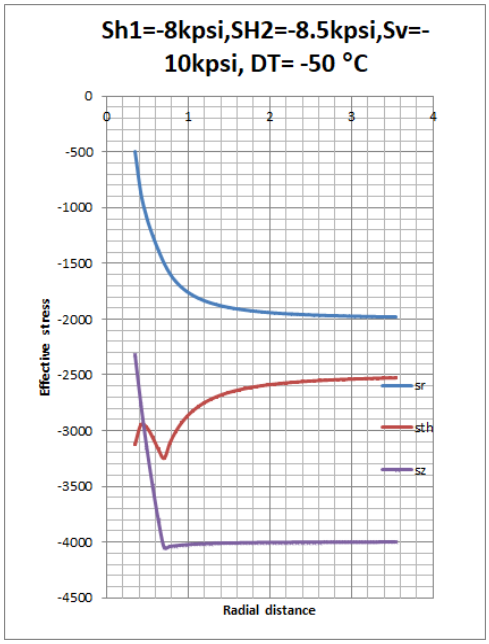

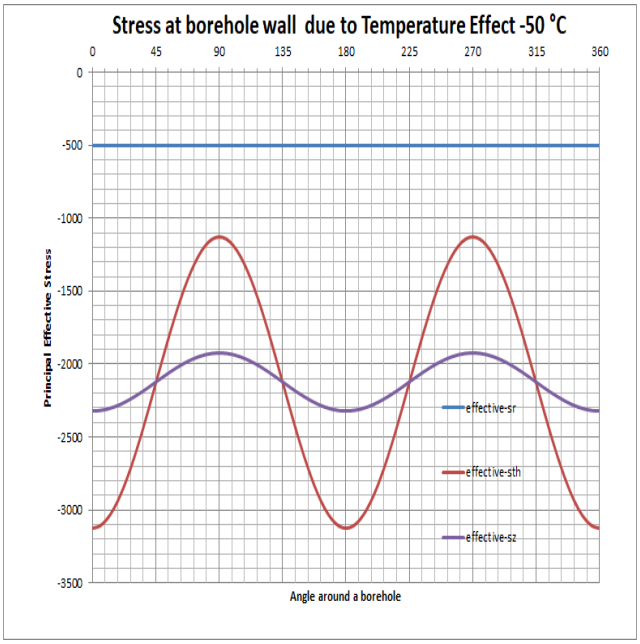

Figure II-28. Effective stress state with distance from borehole due to temperature cool down at 0° from x axis

Figure II-29. Effective Stress State at the borehole wall due to temperature cool down

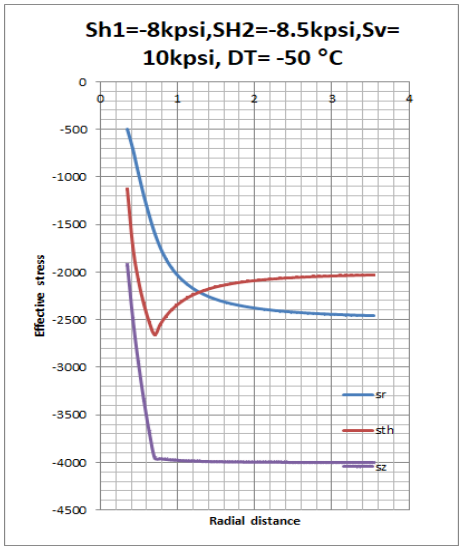

Figure II-30. Effective stress state with distance from borehole due to temperature cool down at 90° from x axis

6. Stress state due to overbalance effect

Normally, overbalance will be increased during the drilling when the breakouts become significant. The wellbore pressure is assumed to increase to 7000 psi from the original formation conditions. As shown in Fig. II-31-Fig. II-33, there is amost no effect on stress state when the overbalance is added. However, the increase of well pressure due to overbalance increases the effective radial stress from 500 psi to 1000 psi and decreases the tangiential stress at borehole wall, resulting in the reduced differenc between the radial and tangiential stresses.

Orientation: 0° from x axis

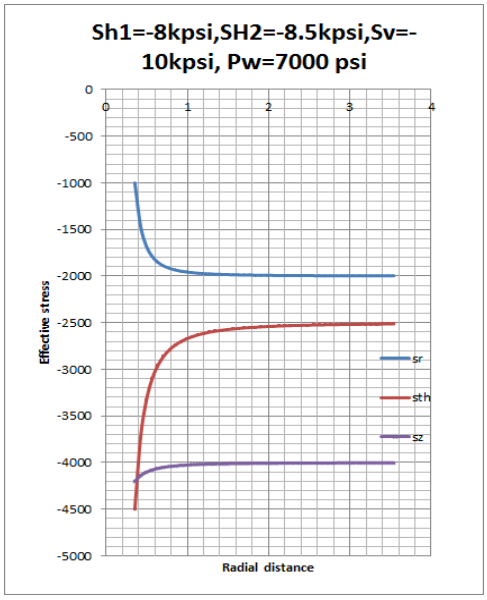

Figure II-31. Effective stress state with distance from borehole due to overbalance at 0° from x axis

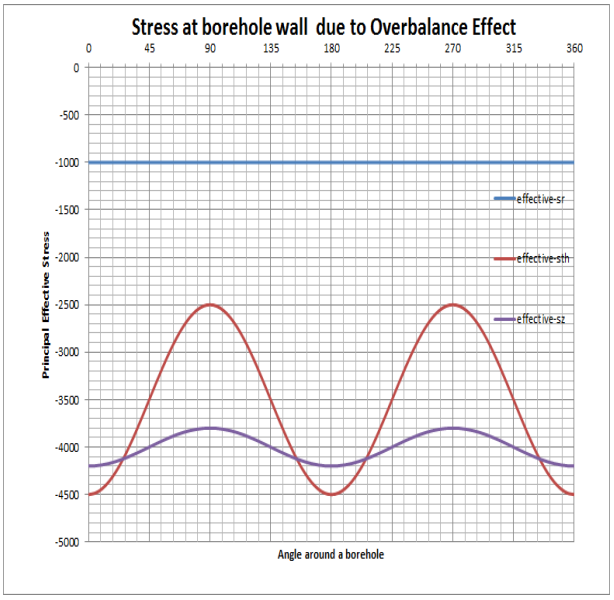

Figure II-32. Effective Stress State at the borehole wall due to overbalance

Orientation: 90° from x axis

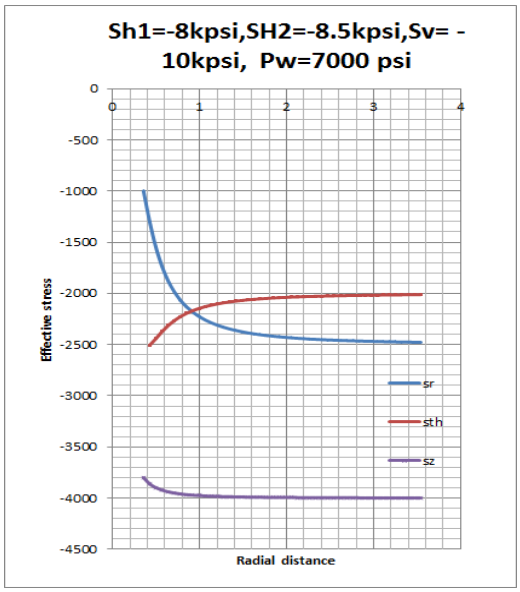

Figure II-33. Effective stress state with distance from borehole due to overbalance at 90° from x axis

7. Stress State due to drawdown effect

In this section, the pore pressure change due to drawdown is – 500 psi and the radius r_p of pressure drop is equal to 2 ft are assumed, considering the underbalance drilling. As shown in Fig. II-34- Fig. II-36, pore presseure change due to drawdown also increases the tangiential stress at and near the borehole wall, which can cause borehole instability. Furethermore, the radial effective stress decreases to 0 due to the pore pressure change, which causes the large difference between radial stress and tangiential stress.

Orientation: 0° from x axis

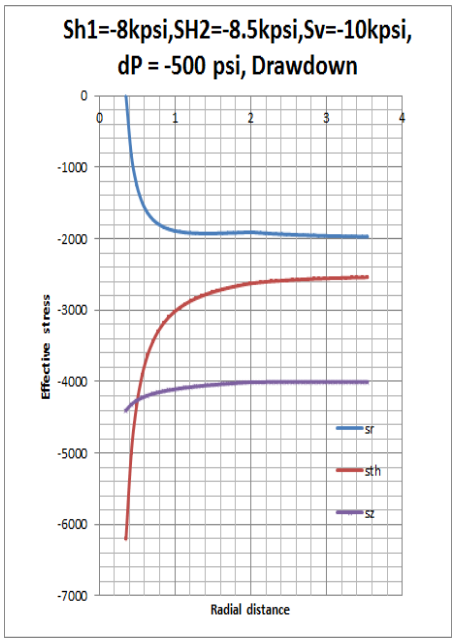

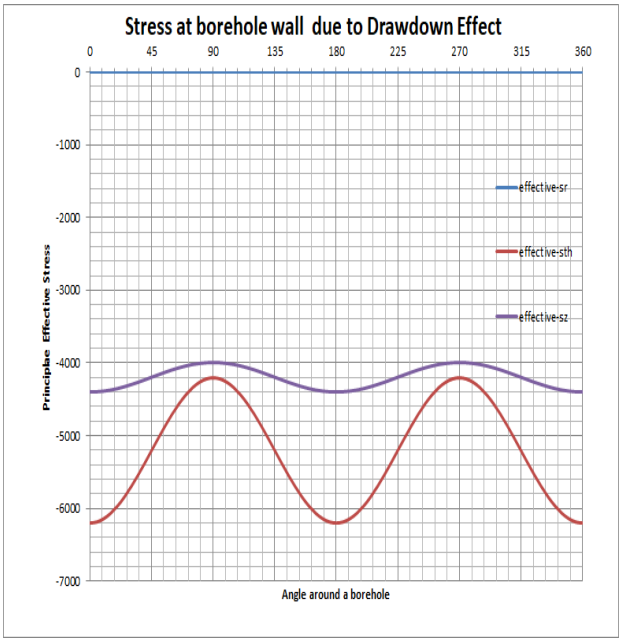

Figure II-34. Effective stress state with distance from borehole due to drawdown at 0° from x axis

Figure II-35. Effective Stress State at the borehole wall due to drawdown

Orientation: 90° from x axis

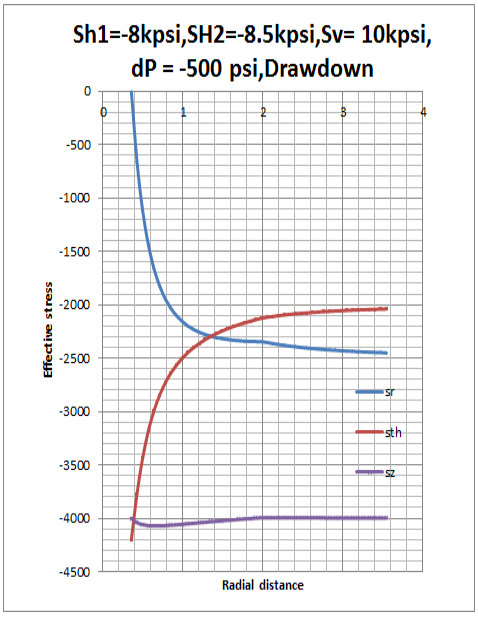

Figure II-36. Effective stress state with distance from borehole due to drawdown at 90° from x axis

8. Stress state due a hard bedding layer ($\gamma = 0°$)

In this case, a hard bedding layer is considered above and below the target layer, which has the young's modulus of 6×10^6 psi, two times as that of the target layer.

Table II-7 Young's modulus of layered formation for hard bedding layer

Young's modulus at the failure analysis	3×10^6 psi
Young's modulus at adjacent layers	6×10^6 psi

Orientation: 0° from x axis

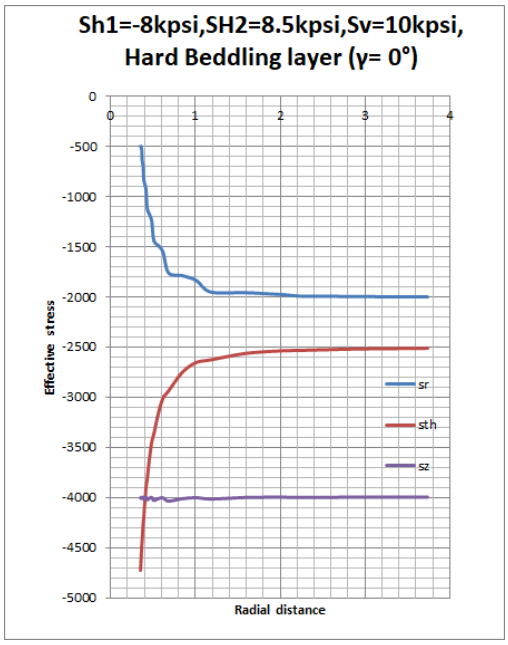

Figure II-37. Effective stress state with distance from borehole with hard bedding layer ($\gamma = 0°$) at 0° from x axis

Orientation: 90° from x axis

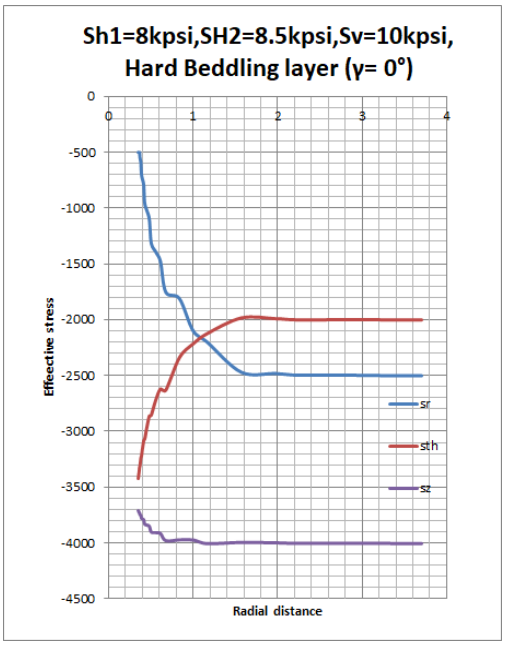

Figure II-38. Effective stress state with distance from borehole with hard bedding layer ($\gamma = 0°$) at 90° from x axis

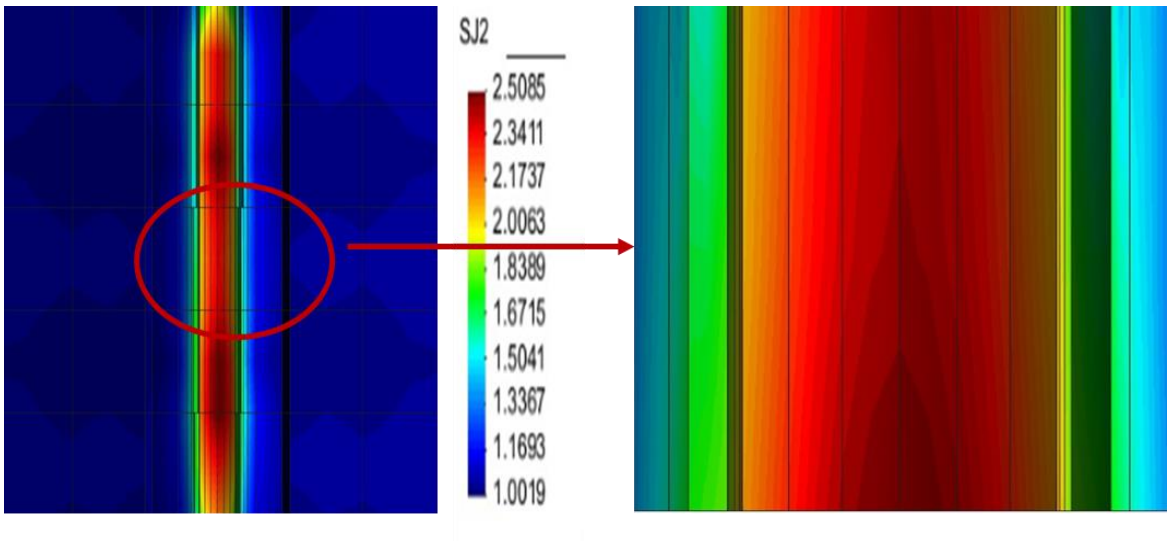

Figure II-39. Stress concentration around borehole with hard bedding layer (γ = 0°)

As shown in Fig. II-37- Fig. II-39, with 0° hard bedding layer, only the tangential stress is reduced a little compared with the base condition and almost no change occurs on radial and overburden stresses.

9. Stress state due to a soft bedding layer existing (γ = 0°)

In this section, a soft bedding layer is considered above the target layer, which has the young's modulus of 1.5×10^6 psi as half as that of the target layer.

Table II-8 Young's modulus of layered formation for soft bedding layer

Young's modulus at the failure analysis	3×10^6 psi
Young's modulus at adjacent layers	1.5×10^6 psi

Orientation: 0° from x axis

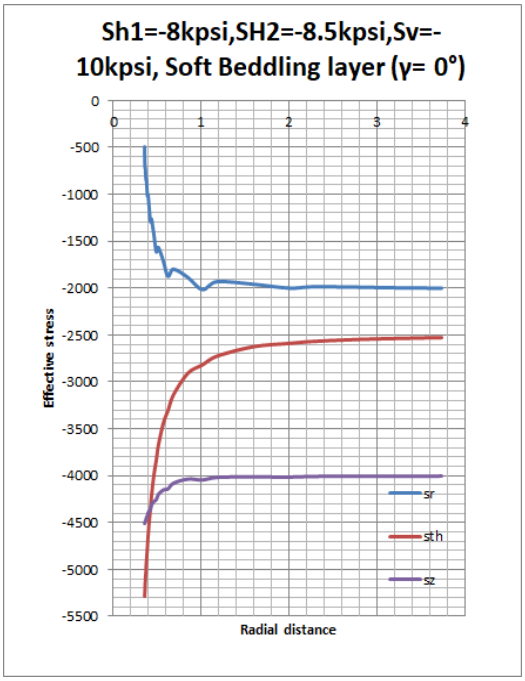

Figure II-40. Effective stress state with distance from borehole with soft bedding layer (γ = 0°) at 0° from x axis

Orientation: 90° from x axis

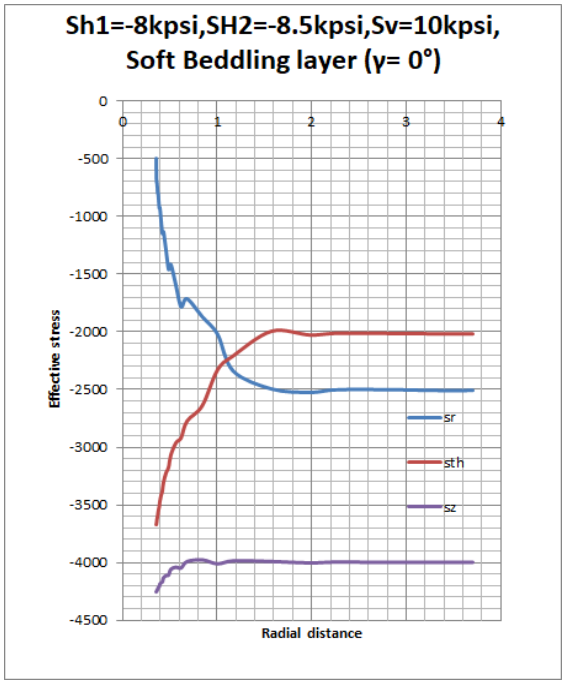

Figure II-41. Effective stress state with distance from borehole with soft bedding layer (γ = 0°) at 0° from x axis

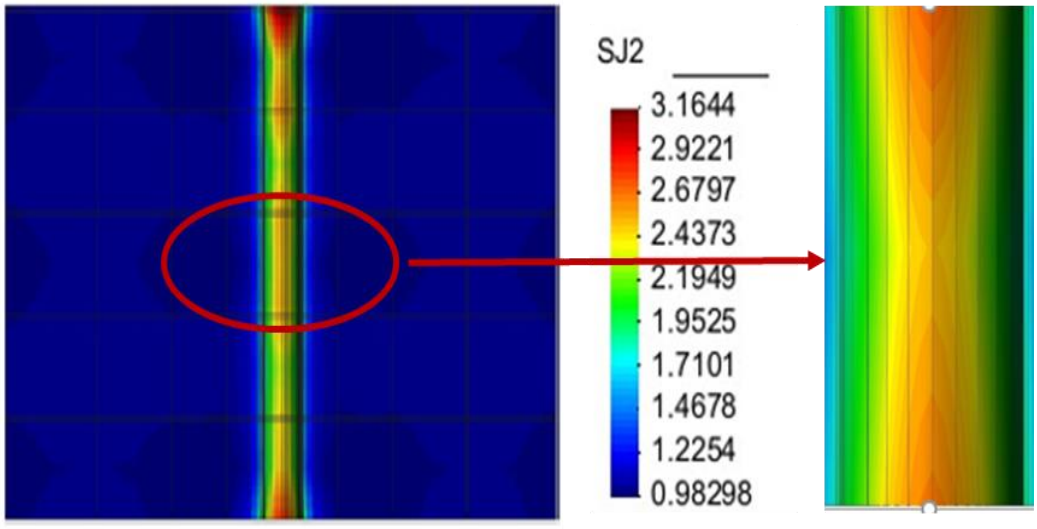

Figure II-42 Stress concentration around borehole with soft bedding layer (γ = 0°)

As shown in Fig. II-40- Fig. II-42, with 0° soft bedding layer, only the tangential stress increases a little compared with the base condition and almost no change occurs on radial and overburden stresses.

10. Stress state with a 60° hard bedding layer (γ = 60°)

In this case, except for the existing hard bedding layer, 60-degree inclination of the bedding layer is considered to analyze the stress state.

Orientation: 0° from x axis

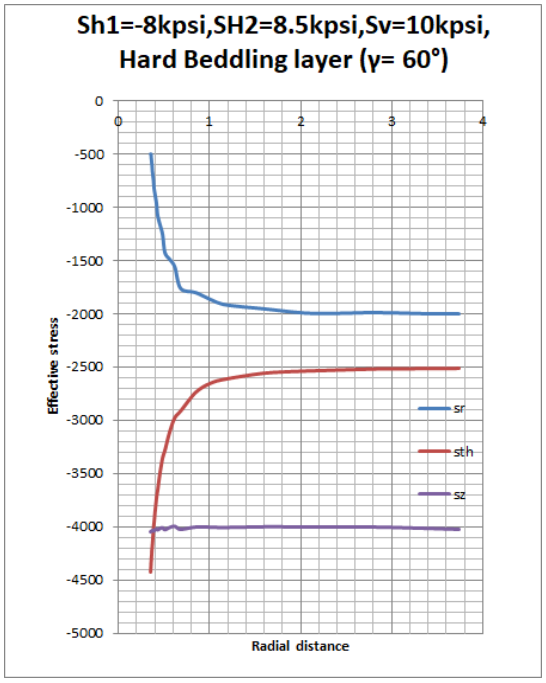

Figure II-43. Effective stress state with distance from borehole with hard bedding layer (γ = 60°) at 0° from x axis

Orientation: 90° from x axis

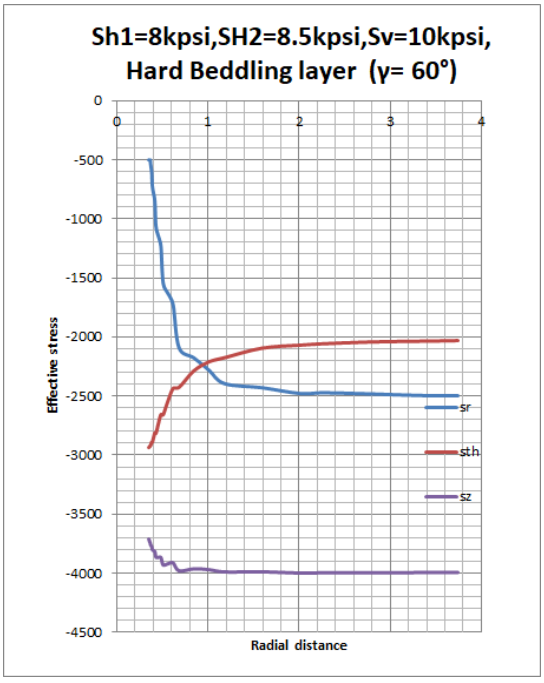

Figure II-44. Effective stress state with distance from borehole with hard bedding layer (γ = 60°) at 90° from x axis

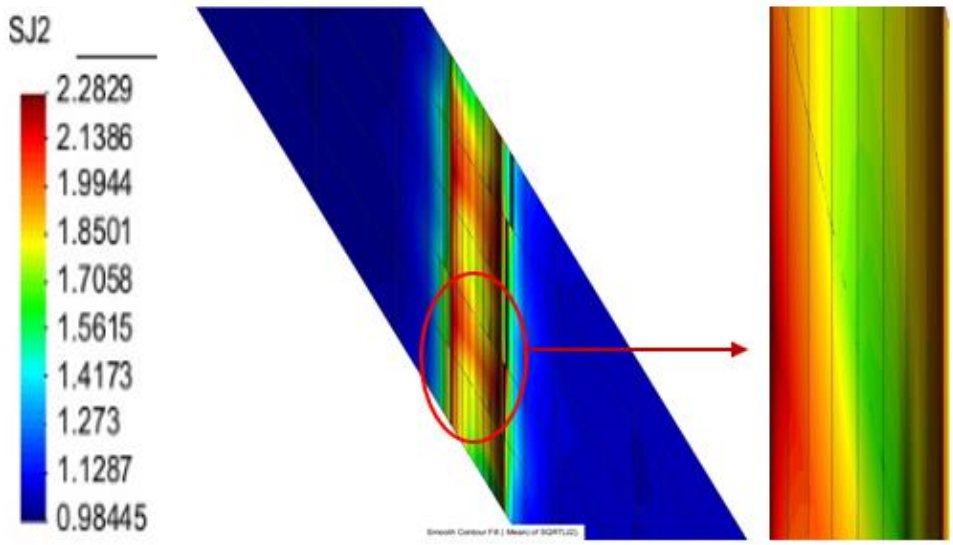

Figure II-45. Stress concentration around borehole with hard bedding layer (γ = 60°)

As shown in Fig. II-43- Fig. II-45, with 60° hard bedding layer, it indicates that the tangential stress continues to decrease a little compared with 0° hard bedding layer and almost no change occurs on radial and overburden stresses.

11. Stress state due to a soft bedding layer with 60 degree inclination (γ = 60°)

In this case, except for the existing soft bedding layer, 60-degree inclination of the bedding layer is considered to analyze the stress state.

Orientation: 0° from x axis

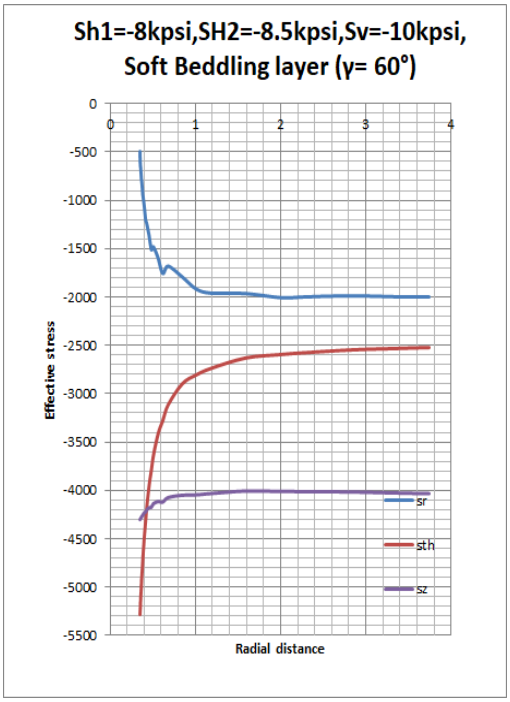

Figure II-46. Effective stress state with distance from borehole with soft bedding layer (γ = 60°) at 0° from x axis

Orientation: 90° from x axis

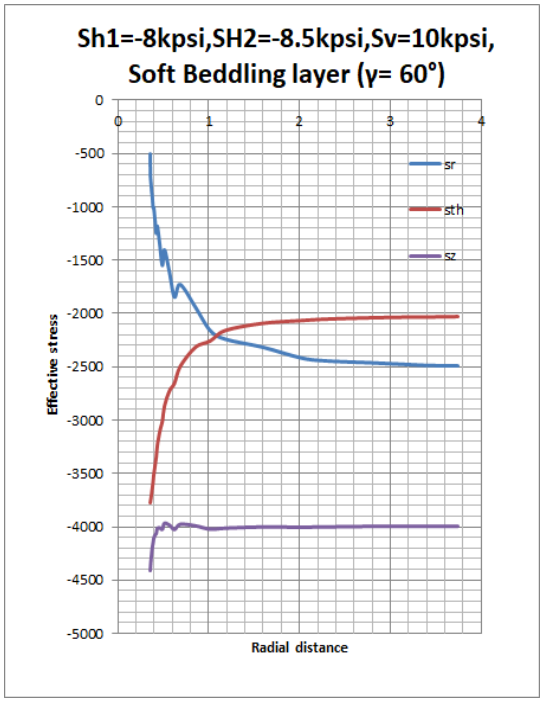

Figure II-47. Effective stress state with distance from borehole with soft bedding layer (γ = 60°) at 90° from x axis

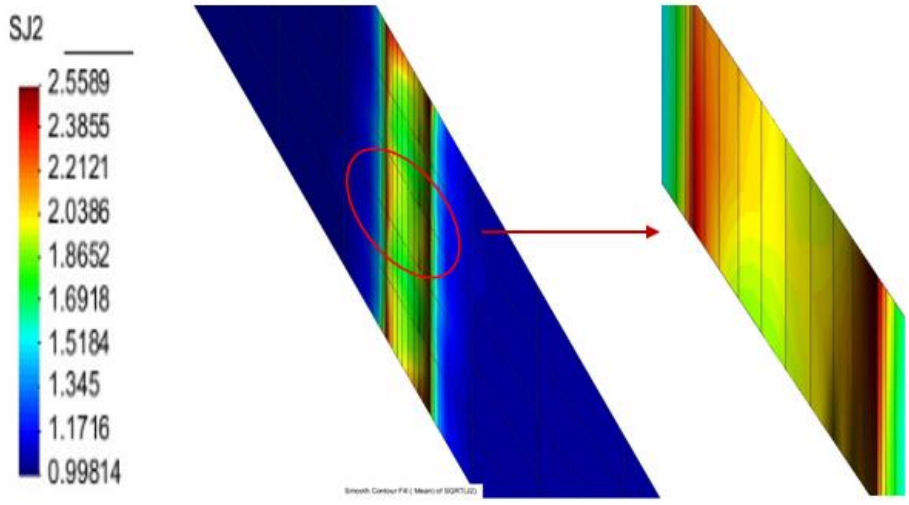

Figure II-48. Stress concentration around borehole with soft bedding layer (γ = 60°)

As shown in Fig.II-46- Fig.II-48, with 60° soft bedding layer, the tangential stress continues to increase a little compared with 0° soft bedding layer and almost no change occurs on radial and overburden stresses.

12. Stress state for formation with transversely isotropic elastic material

Shale formation is laminated with mud and shale layers. The elastic property may be approximated by a transversely isotropic material given by the following five elastic coefficients.

$$D^{-1}=\begin{bmatrix} \frac{1}{E_x} & -\frac{\nu_{xy}}{E_x} & -\frac{\nu_{zx}}{E_z} & & & \\ -\frac{\nu_{xy}}{E_x} & \frac{1}{E_x} & -\frac{\nu_{zx}}{E_z} & & & \\ -\frac{\nu_{zx}}{E_z} & -\frac{\nu_{zx}}{E_z} & \frac{1}{E_z} & & & \\ & & & \frac{1}{G_{zx}} & & \\ & & & & \frac{1}{G_{zx}} & \\ & & & & & 2\left(\frac{1}{E_x}+\frac{\nu_{xy}}{E_x}\right) \end{bmatrix}$$

Then,

$$\sigma^e = D\left(\varepsilon+\frac{1-2\nu_m}{E_m}pI\right)$$

Or

$$\sigma = D\left(\varepsilon+\frac{1-2\nu_m}{E_m}pI\right)-pI = D\varepsilon-(\mathrm{I}-\mathrm{D}\frac{1-2\nu_m}{E_m})pI$$

$$\sigma = D\varepsilon-(\mathrm{I}-\mathrm{D}\frac{1-2\nu_m}{E_m})pI$$

where

$$D=\begin{bmatrix} c_{11} & c_{12} & c_{13} & & & \\ c_{12} & c_{11} & c_{13} & & & \\ c_{13} & c_{13} & c_{33} & & & \\ & & & c_{44} & & \\ & & & & c_{44} & \\ & & & & & \frac{1}{2}(c_{11}-c_{12}) \end{bmatrix}$$

$$c_{11}=\frac{\frac{1}{E_x}-\frac{\nu_{xz}^2}{E_z}}{AE_z},\ c_{12}=\frac{\frac{\nu_{xy}}{E_x}+\frac{\nu_{xz}^2}{E_z}}{AE_z},\ c_{13}=\frac{\nu_{zx}(1+\nu_{xy})}{AE_xE_z},\ c_{33}=\frac{(1-\nu_{xy}^2)}{AE_x^2},\ c_{44}=G_{xz}$$

$$A=\left(1-2\frac{E_x}{E_z}\nu_{xy}\nu_{xz}^2-2\frac{E_x}{E_z}\nu_{xz}^2-\nu_{xy}^2\right)/\left(E_x^2E_z\right)$$

Transformation of elastic coefficient for slanted formation.

The stress and strain is transformed with the transformation matrix T.

$$\varepsilon'=\mathrm{T}\varepsilon,\sigma=D_a\varepsilon$$

Now

$$(\varepsilon')^t\sigma'=(\varepsilon)^t\sigma$$

Hence,

$$(\varepsilon')^tD'\varepsilon'=(\varepsilon)^tD\varepsilon$$

$$(\varepsilon')^tD'\varepsilon'=(\varepsilon)^tD\varepsilon=(\varepsilon')^tT^tD\mathrm{T}\varepsilon'$$

Hence, we have

$$D'=T^tD\mathrm{T}$$

We may also use the following transformation matrix to transform from D to D’

$$\varepsilon'_{ij}=l_{i\alpha}l_{j\beta}\varepsilon_{\alpha\beta}$$

$$T = \begin{pmatrix} l_{11}l_{11} & l_{12}l_{12} & l_{13}l_{13} & l_{i2}l_{j3} + l_{i3}l_{j2} & l_{i3}l_{j1} + l_{i1}l_{j3} & l_{i1}l_{j2} + l_{i2}l_{j1} \\ l_{21}l_{21} & l_{22}l_{22} & l_{23}l_{23} & i, j = 2,2 & & \\ l_{31}l_{31} & l_{32}l_{32} & l_{33}l_{33} & i, j = 3,3 & \text{i, } j = 3,3 & \\ l_{21}l_{31} & l_{22}l_{32} & l_{23}l_{33} & i, j = 2,3 & \text{i, } j = 2,3 & \\ l_{31}l_{11} & l_{32}l_{12} & l_{33}l_{13} & i, j = 3,1 & \text{i, } j = 3,1 & \text{i, } j = 3,1 \\ l_{11}l_{21} & l_{12}l_{22} & l_{13}l_{23} & i, j = 1,2 & \text{i, } j = 1,2 & \text{i, } j = 1,2 \end{pmatrix}$$

Table II-9 Elastic moduli used in this work for the orthotropic rock

E_x	3×10^6 psi
E_y	1.5×10^6 psi
G_{zx}	1.25×10^6 psi
ν_{xy}	0.2
ν_{zx}	0.2

As the shown in figures, formation with transversely isotropic elastic material shows no effect on the stress state at and near the borehole when the well angle is 0 (vertical well). However, as the well inclination increases, both the tangential stress and stress along the well axis significantly change. The magnitudes and changes of stresses at the distance from the borehole are same compared with the stresses state in the base condition and inclined well conditions.

Orthotropic: E2=1.5E6psi, (well angle, well azimuth=0°,0°, θ = 0° and 90°)

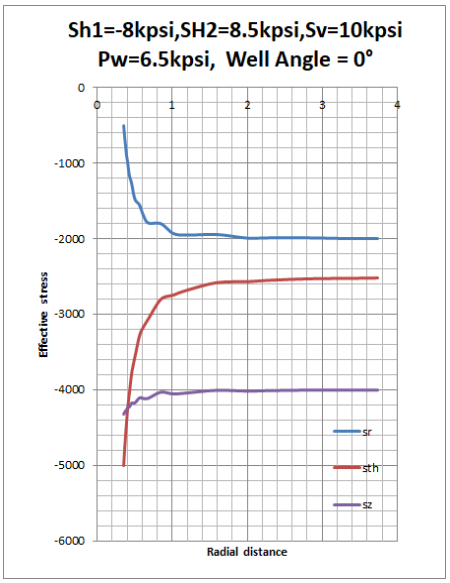

Figure II-49. Effective stress state with distance from borehole for orthotropic formation with well angle = 0° at 0° from x axis

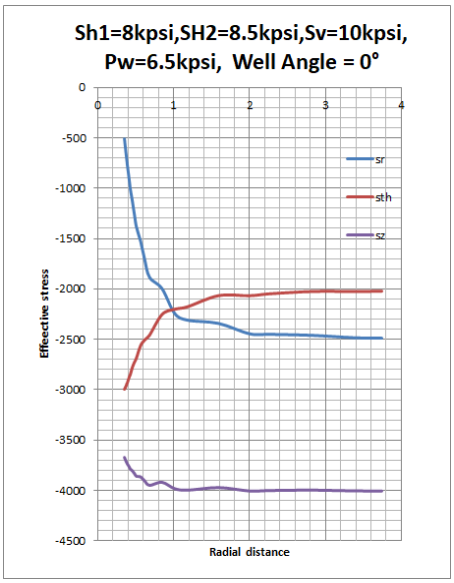

Figure II-50. Effective stress state with distance from borehole orthotropic formation with well angle = 0° at 90° from x axis

Orthotropic: E2=1.5E6psi, (well angle, well azimuth=30°,0°, θ = 0° and 90°)

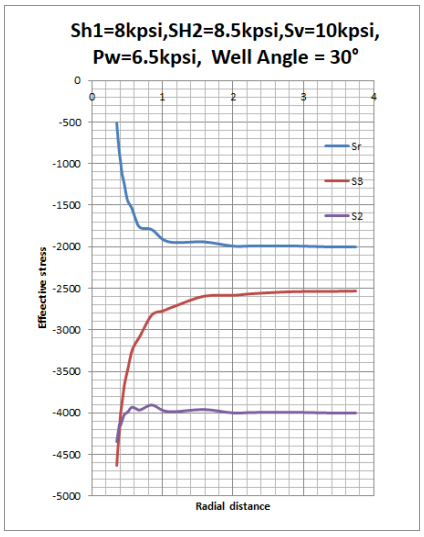

Figure II-51. Effective stress state with distance from borehole orthotropic formation with well angle = 30° at 0° from x axis

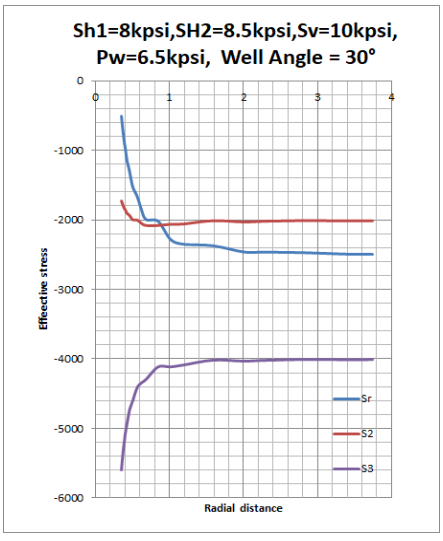

Figure II-52. Effective stress state with distance from borehole orthotropic formation with well angle = 30° at 90° from x axis

Orthotropic: E2=1.5E6psi, (well angle, well azimuth=60°,0°, θ = 0° and 90°)

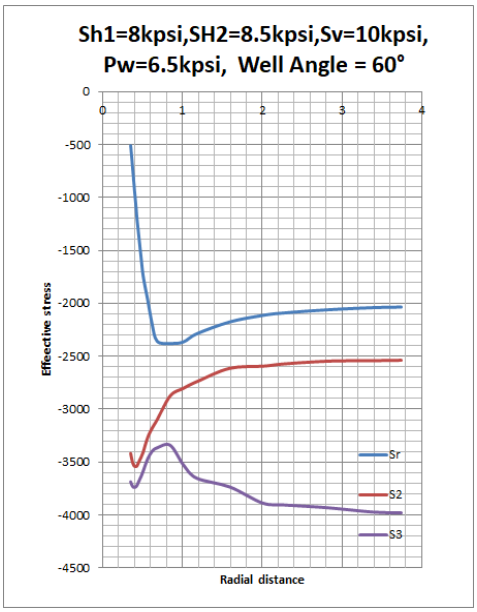

Figure II-53. Effective stress state with distance from borehole orthotropic formation with well angle = 60° at 0° from x axis

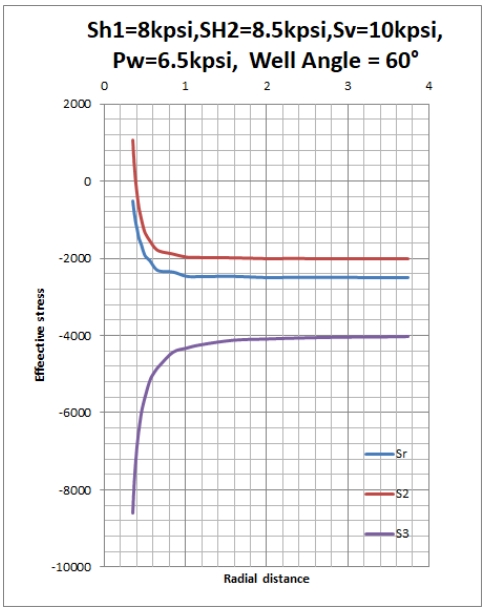

Figure II-54. Effective stress state with distance from borehole orthotropic formation with well angle = 60° at 90° from x axis

Orthotropic: E2=1.5E6psi, (well angle, well azimuth=90°,0°, θ = 0° and 90°)

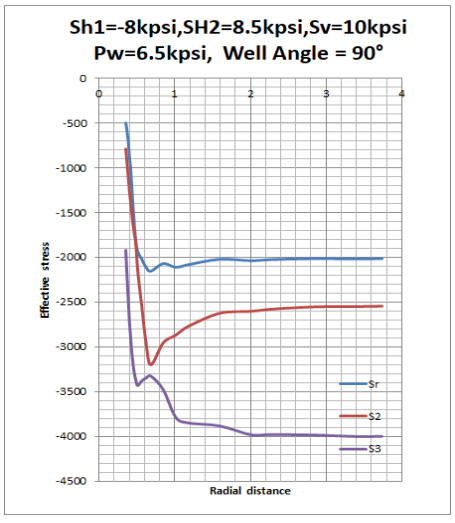

Figure II-55. Effective stress state with distance from borehole orthotropic formation with well angle = 90° at 0° from x axis

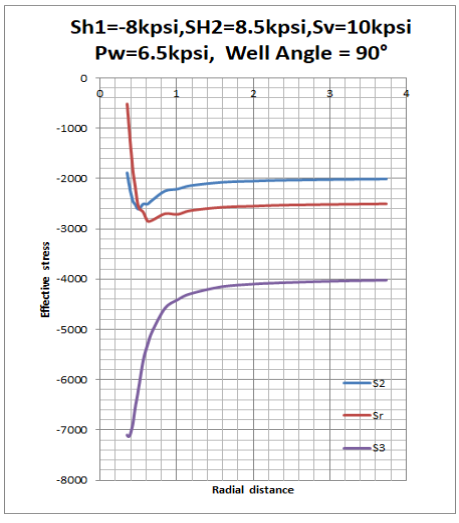

Figure II-56. Effective stress state with distance from borehole orthotropic formation with well angle = 90° at 90° from x axis

2.2.2 Stress State around a borehole in depleted reservoir condition

In this section, parameters effect on the stresses state around a horizontal borehole are studied in depleted reservoir condition which is shown in Table II-2.

1. **Stress state around borehole under the depleted reservoir condition**

Orientation: 0° from x axis

Orientation: 90° from x axis

Total Stress

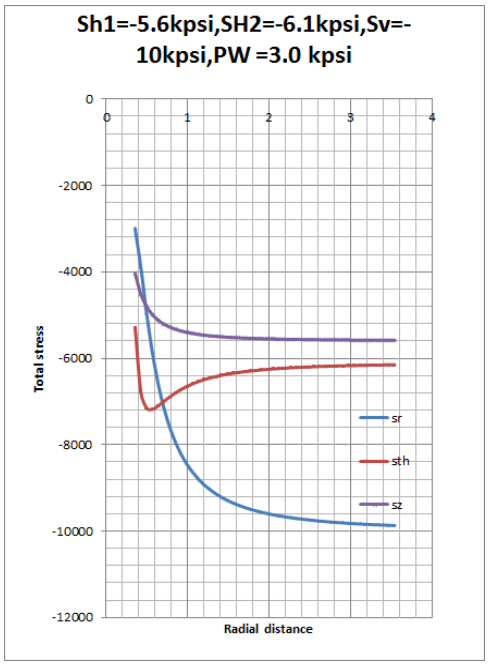

Figure II-57. Total stress state with distance from borehole for depleted reservoir base case at 0° from x axis

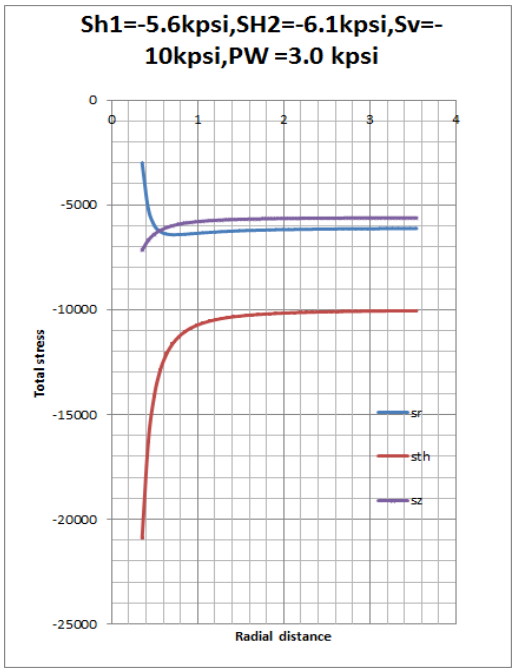

Figure II-58. Total stress state with distance from borehole for depleted reservoir base case at 90° from x axis

Effective Stress

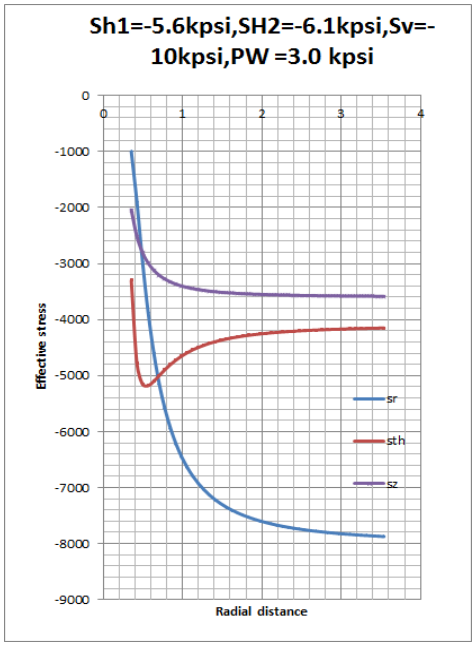

Figure II-59. Effective stress state with distance from borehole for depleted reservoir base case at 0° from x axis

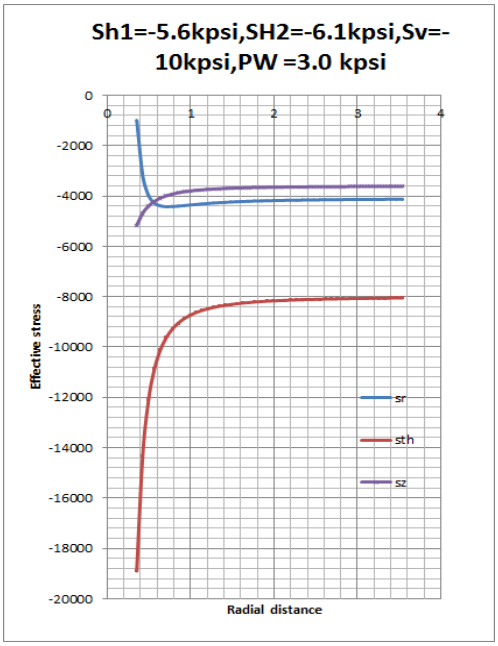

Figure II-60. Effective stress state with distance from borehole for depleted reservoir base case at 90° from x axis

Stress at borehole wall

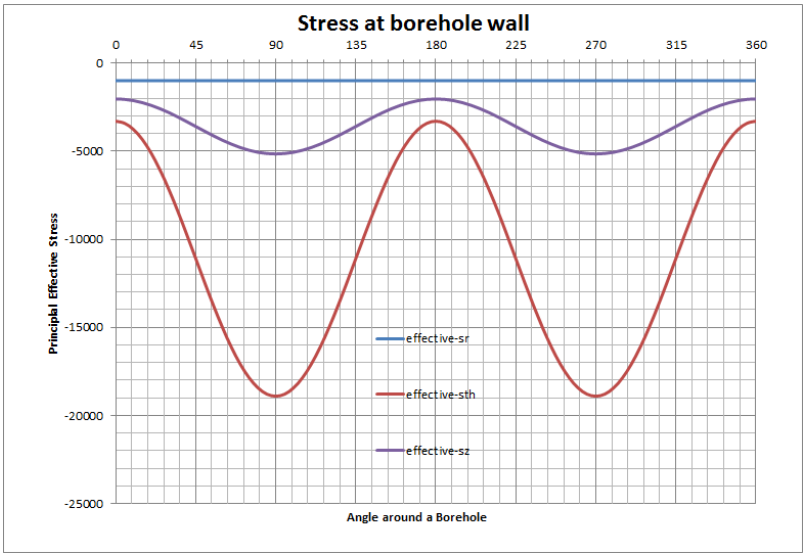

Figure II-61. Effective Stress State at the borehole wall at depleted reservoir condition

Fig. II-59 -Fig. II-60 illustrate the variation of effective stresses at 0° orientation from x axis (the direction of σ_h) and 90° from x axis (the direction of σ_H) with the radial distance from wellbore for a horizontal well at depleted conditions without considering any other effect. As the figures show,

a. The effective stresses only change at and near the borehole, where the magnitude of radial, tangential and vertical stresses increase with distance near the borehole, However, all of the stresses tend to become stable values at far field.
b. Comparing the results of stresses at orientations of 0° and 90° from x axis, it is found that the tangential stress, which is in circumferential direction and has most significant effect on the mud weight and borehole stability during drilling, is extremely larger at 90° from x axis than at 0°. It illustrates that the orientation we choose for drilling also leads to borehole instability.

Fig. II-61 shows the effective stresses distribution around a borehole. The tangential stress and vertical stress vary like a sine function at the circumferential direction at borehole, while the radial stress stays a constant at borehole wall. And the maximum tangential stress occurs at 0° and 90°. Furthermore, the radial stress is the minimum principal stress. Because the mud pressure in this field condition is low, the shear failure may occur.

2. Stress state around borehole under the depleted reservoir condition with swelling effect

Shale swelling is the significant paprameter that need to be estimated in different reservoir conditions. Therefore, for the horizotal well in depleted reservoir condition, 0.2 % swelling is assumed at the wellbore surface (ΔS) and the swelling radius (rs) is 0.7 ft to estimate how the swelling effects the stresses state. As Fig. II-61 to Fig. II-63 show, the stress state is also significantly affected by shale swelling for the horizotal well in a depleted reservoir condition. The tangiential and overburden stresses dramatically increase at and near borehole compared with the stress in the base condition, which cause serious borehole instability, but with the distance away from the borehole, the stresses tends to be constant, that is, the same with the state in the base condition, where we assume shale swelling effect can be ignored.

Orientation: 0° from x axis

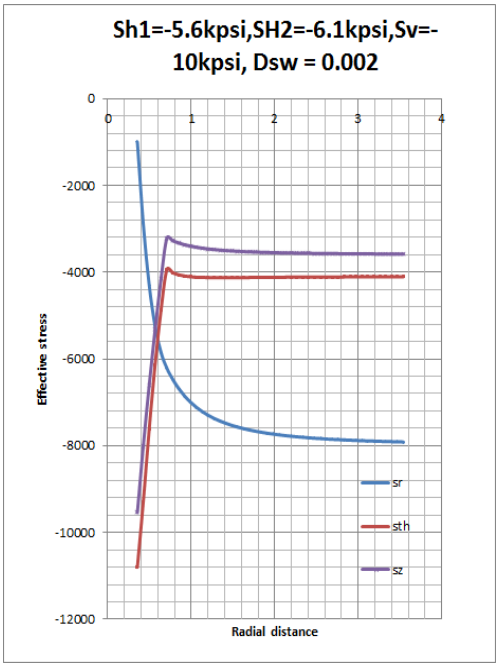

Figure II-62. Effective stress state with distance from borehole for depleted reservoir due to swelling at 0° from x axis

Orientation: 90° from x axis

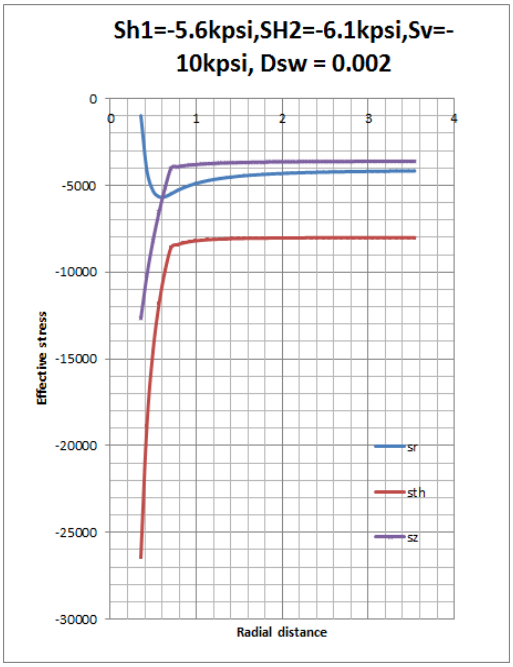

Figure II-63. Effective stress state with distance from borehole for depleted reservoir due to swelling at 90° from x axis

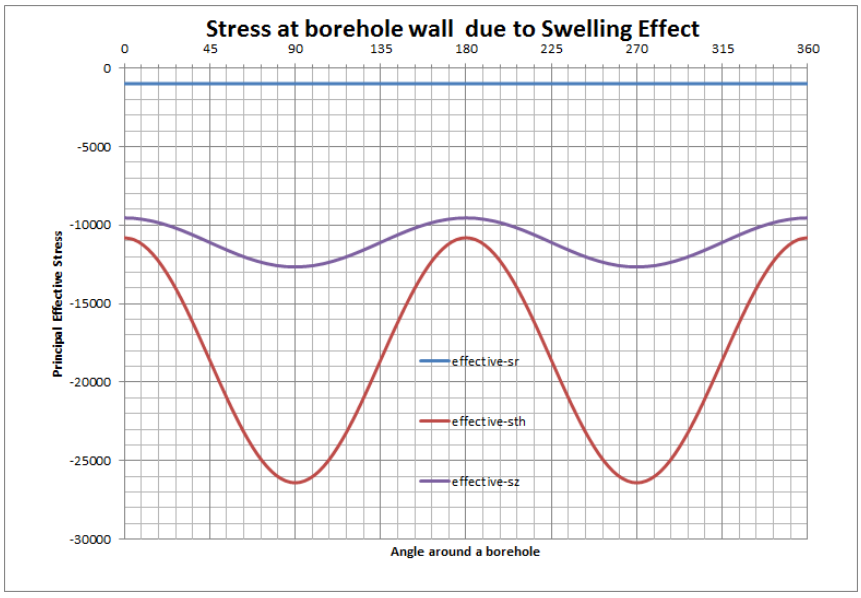

Figure II-64. Effective stress state at the borehole wall at depleted reservoir condition due to swelling

3. Stress state around borehole under the depleted reservoir condition with temperature effect

Assume that 50ºC temperature change occurs under reservoir conditions within the radius of 0.7 ft. The linear expansion coefficient is given as 1.e-5 1/°C. As shown in Fig. II-65 to Fig. II-67, a temperature change of 50 °C inside horizontal well in a depleted reservoir condtion also casues a change of stress state at and near borehole. The increase in tangiential and overburden stress is also observed.

Orientation: 0° from x axis

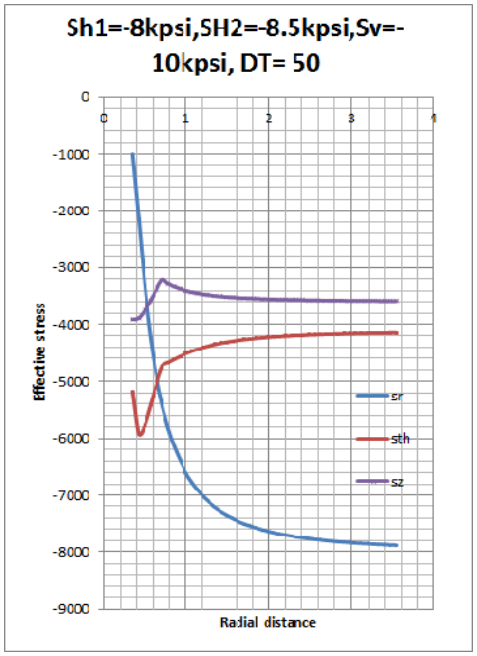

Figure II-65. Effective stress state with distance from borehole for depleted reservoir due to temperature change at 0° from x axis

Orientation: 90° from x axis

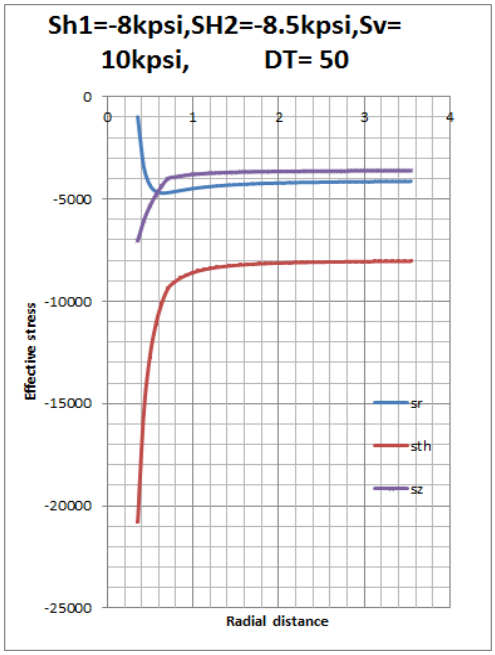

Figure II-66. Effective stress state with distance from borehole for depleted reservoir due to temperature change at 90° from x axis

Stress at borehole wall

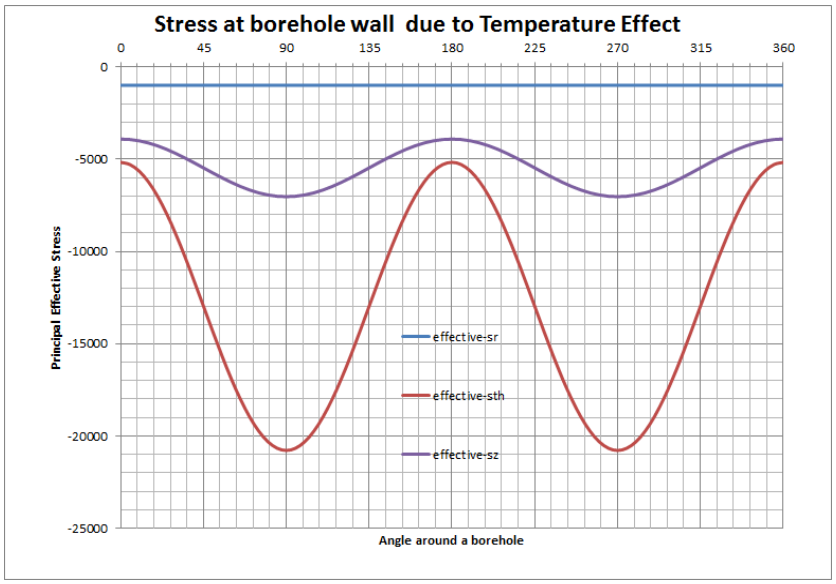

Figure II-67. Effective stress state at the borehole wall at depleted reservoir condition due to temperature change

4. Stress state around borehole under the depleted reservoir condition with drawdown effect

Assume that the pore pressure change due to drawdown is – 500 psi and the radius r_p of pressure drop is equal to 2 ft. As shown in Fig. II-68 to Fig. II-70, pore presseure change due to drawdown also increases the tangiential stress at and near the borehole wall for horizontal well in depleted reservoir condtions that can cause borehole instability. Furethermore, the radial stress decreases to 0 due to the pore pressure change, which causes the large difference between the radial stress and tangiential stress.

Orientation: 0° from x axis

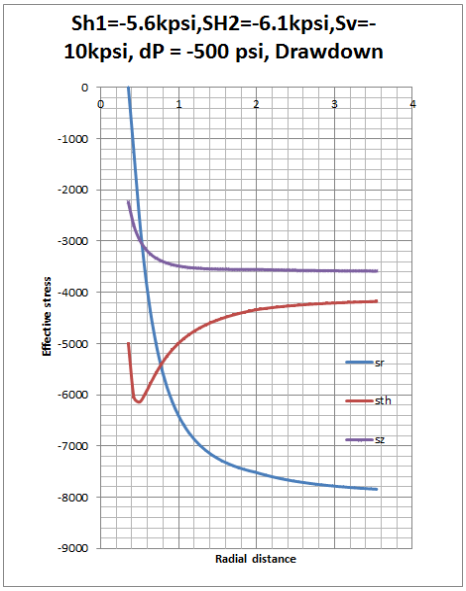

Figure II-68. Effective stress state with distance from borehole for depleted reservoir due to drawdown at 0° from x axis

Orientation: 90° from x axis

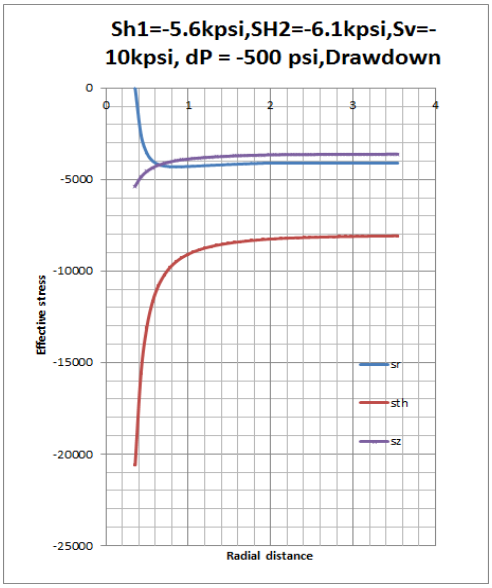

Figure II-69. Effective stress state with distance from borehole for depleted reservoir due to drawdown at 90° from x axis

Stress at borehole wall

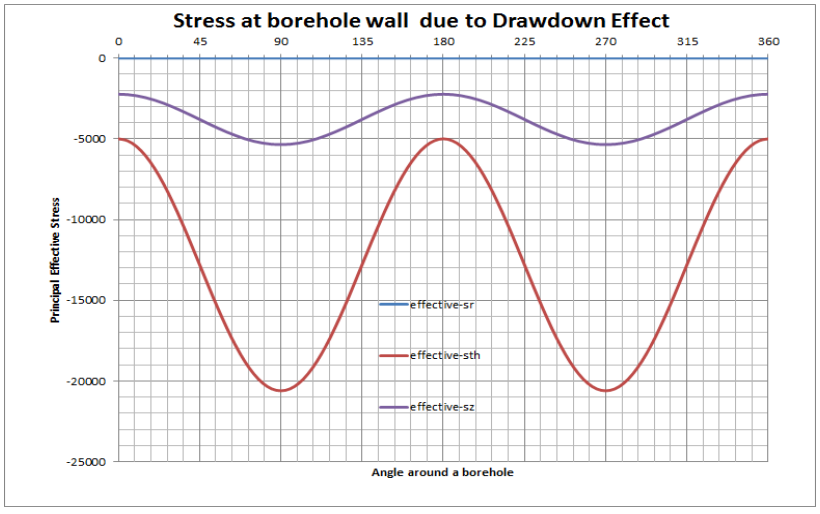

Figure II-70. Effective stress state at the borehole wall at depleted reservoir condition for depleted reservoir due to drawdown

5. **Stress state around borehole under the depleted reservoir condition with osmosis effect**

In this case, we assume the formation surface pressure drop behind the cake is -500 psi due to osmosis effect. The radius r_p of the pressure drop is assume to be 2 ft. The wellbore pressure is maitained with 500 psi overbalance. As shown in Fig.II-71 to Fig. II-73, the osmosis due to water potential difference does not significantly affect the tangiential and overburden stresses at borehole and the stresses at far distance from borehole compared with the base condition without osmsis. However, due to the osmosis effect, the raida effective stress increases to 1500 psi from 1000 psi at borhole wall, which will stabilize the borehole.

Orientation: 0° from x axis

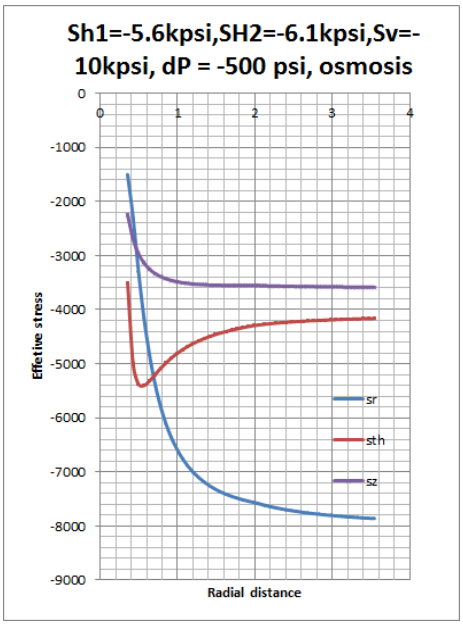

Figure II-71. Effective stress state with distance from borehole for depleted reservoir due to osmosis at 0° from x axis

Orientation: 90° from x axis

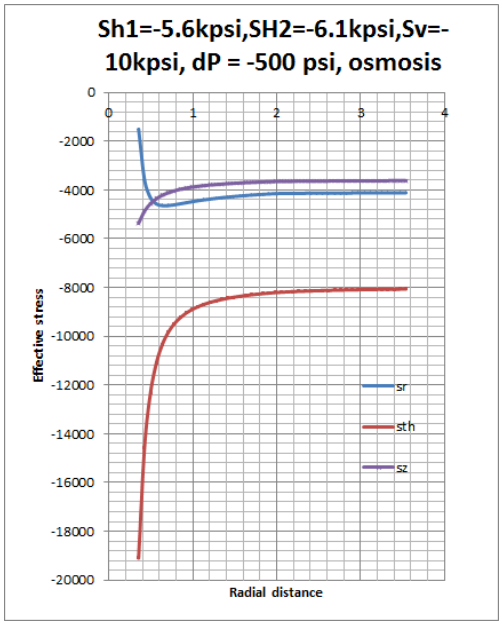

Figure II-72. Effective stress state with distance from borehole for depleted reservoir due to osmosis at 90° from x axis

Stress at borehole wall

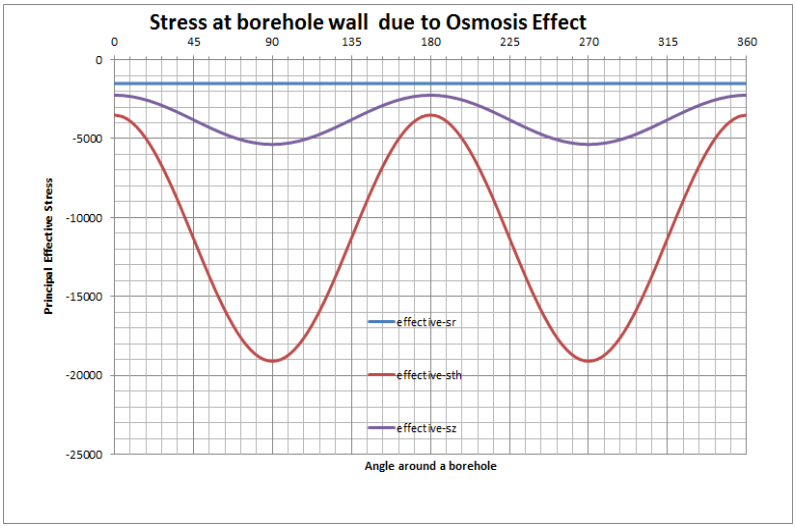

Figure II-73. Effective stress state at the borehole wall at depleted reservoir condition for depleted reservoir due to osmosis

6. Stress state around a borehole under the depleted reservoir condition with overbalance effect

Assume wellbore pressure to increase to 3500 psi from the original reservoir conditions, that is, the overbalance for this condition will be 1500 psi. As shown in Fig. II-74 to Fig.II-76, the increase in overbalance increases the effective radial stress from 1000 psi to 1500 psi and decreases the tangiential stress at borehole wall, which stabilizes the borehole.

Orientation: 0° from x axis

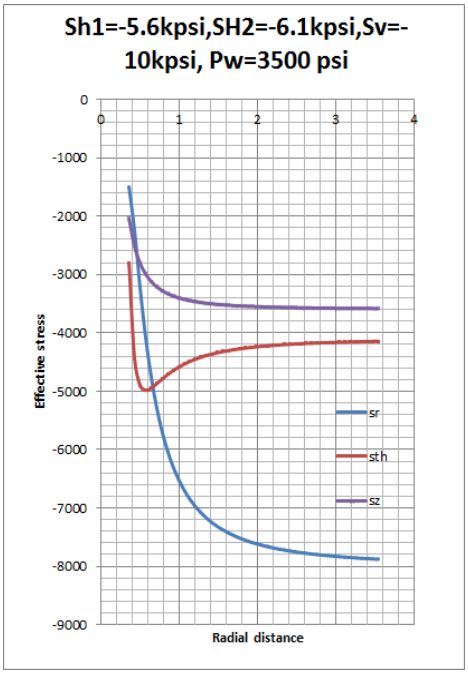

Figure II-74. Effective stress state with distance from borehole for depleted reservoir due to overbalance at 0° from x axis

Orientation: 90° from x axis

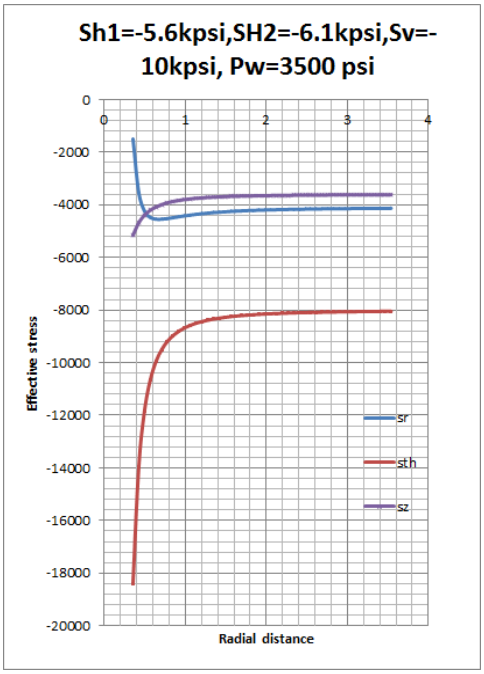

Figure II-75. Effective stress state with distance from borehole for depleted reservoir due to overbalance at 90° from x axis

Stress at borehole wall

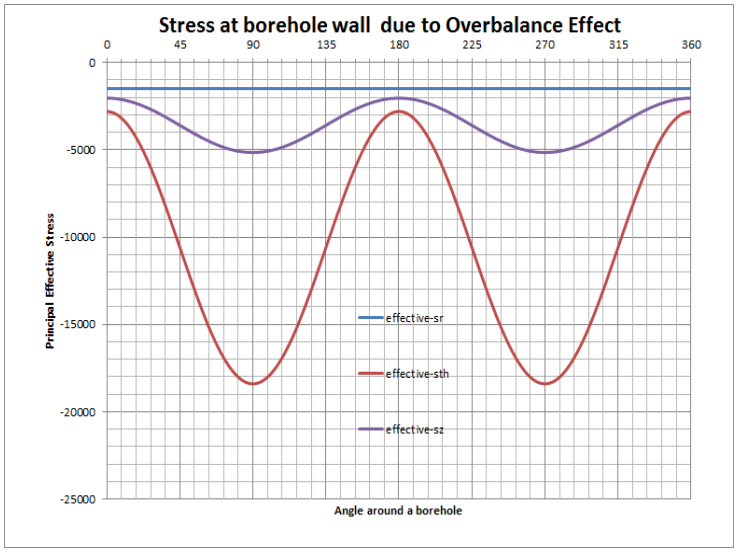

Figure II-76. Effective stress state at the borehole wall at depleted reservoir condition for depleted reservoir due to overbalance

7. Stress state around borehole under the depleted reservoir condition with sandstone non-linearity effect

Fig.II-77 shows the non-linear stress strain obtained from the core in a UK reservoir. Since $E = 3 \times 10^6$ *psi* is used for the parameter studies in this section, the rock with a similar Young's modulus is selected.

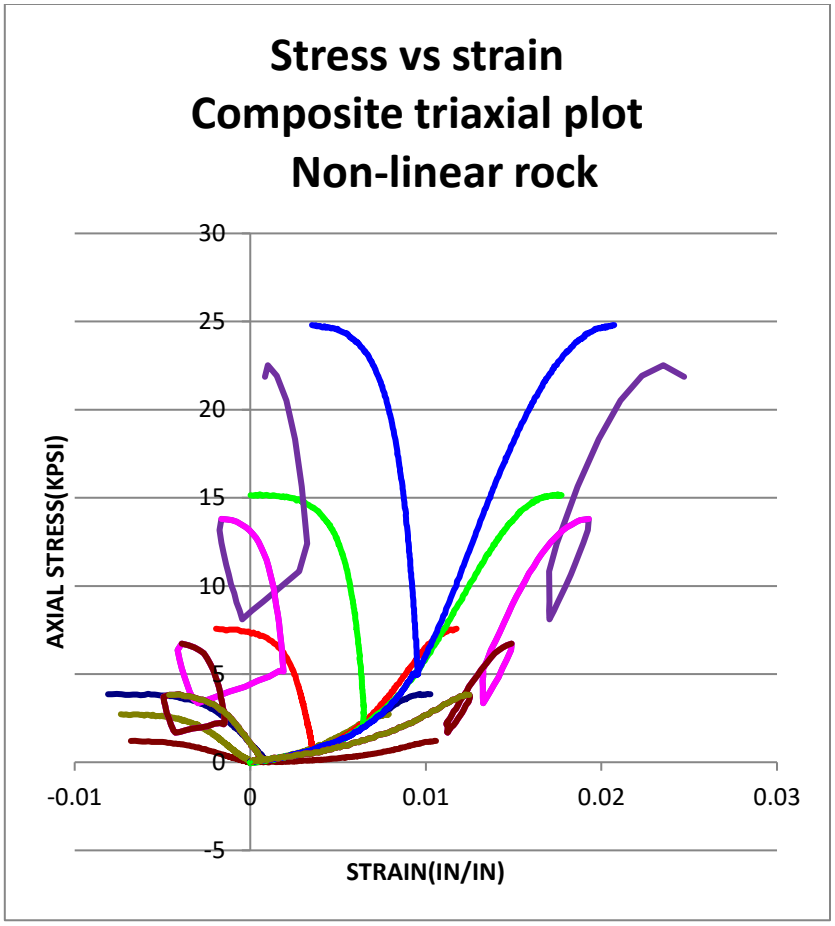

Figure II-77 Non-linear stress strain curve used for the calculation (the rock is from UK reservoir with E close to $E = 3 \times 10^6 \ psi$

As shown in Figs.II-78 to Figs.II-80, the magnitude of radial, tangential and overburden stresses at and near wellbore decreases a lot in the non-linearity sandstone formation, which illustrates a more stable borehole environment.

Orientation: 0° from x axis

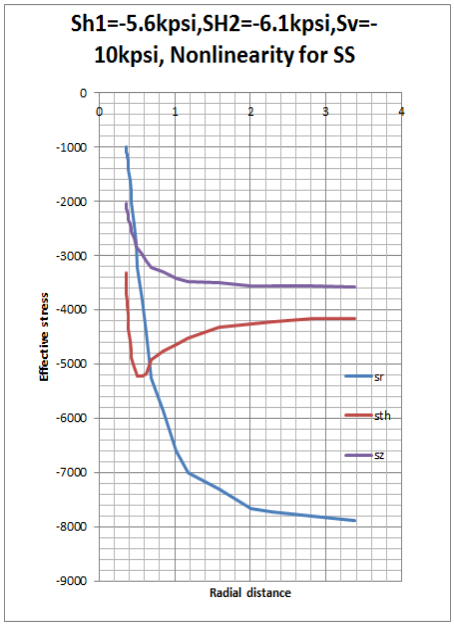

Figure II-78. Effective stress state with distance from borehole for depleted reservoir due to non-linearity at 0° from x axis

Orientation: 90° from x axis

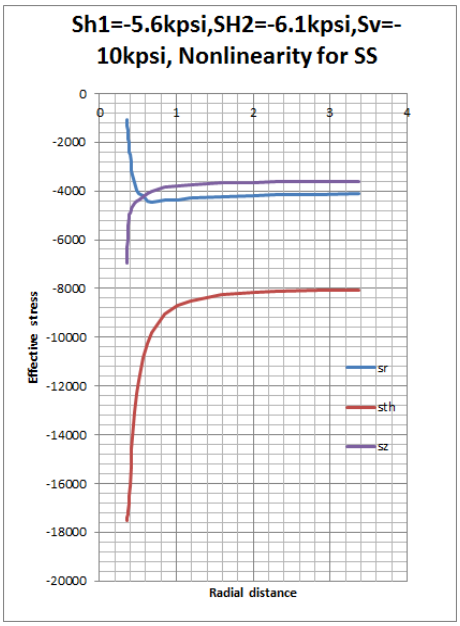

Figure II-79. Effective stress state with distance from borehole for depleted reservoir due to non-linearity at 0° from x axis

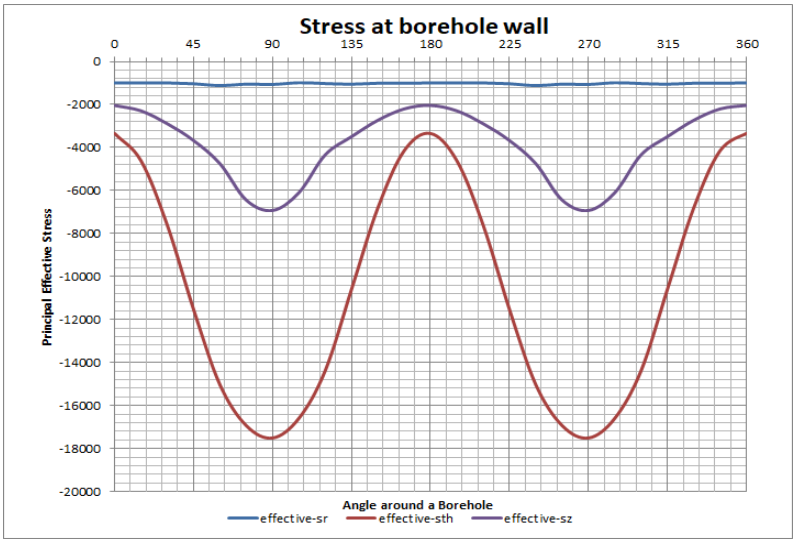

Figure II-80. Effective stress state at the borehole wall at depleted reservoir condition for depleted reservoir due to non-linearity

2.3 Conclusion

The results of the parameter effect on the stress around a vertical wellbore in the base reservoir condition and a horizontal wellbore in the depleted reservoir condition can be summarized as folllows:

1) The stresses change at and near borehole while they tend to converge to stable in-situ stresses at far field. In addition, the controllable parameters also do not effect the stress state at far field, which only contribute with certain distance near borehole.
2) Shale swelling increases both the tangential and axial stresses around a borehole resulting in serious borehole instability, which requires to pay attention during the drilling and production process in the field. The temperature change is generally less effect if the formation has some permeability. However, if the shale is 100% saturated with water and the permeability is very small, the expansion of water trapped within shale may destabilize borehole if the teperature increaes at the casing shoe.
3) Temperatrue cooling at borehole bit may stabilize the borehole.
4) Pore pressure change due to osmosis and temperature change, overbalance, drawdown during drilling only change a little of the magnitiudes of stress distribution around borehole. However, the radial effective stress increase due to the overbalance, the pore pressure reduction induced by osmosis and temerature cooling stabilize the borehole.
5) Well incalination also increases the magnittidue of the stresses around borehole.

CHAPTER III

FAILURE THEORIES TO PREDICT BREAKOUT ANGLE AROUND A BOREHOLE

3.1 Introduction

The breakout angle prediction varies with the different failure criteria applied. The following failure criterions are commonly used for borehole failure problems.

- Mohr Coulomb
- Mogi
- Lade
- Drucker-Prager

3.2 Rock Failure Criteria

Mogi's failure criterion fits well for well-consolidated rocks. Lade model is originally proposed for poorly consolidated rock. However, it has been generalized such that it can be used from poorly consolidated rock to consolidated rock by introducing k-value. Mohr Coulomb failure criterion is often used for fault analyses or weathered rocks with cracks or defects. Drucker-Prager is useful for non-linear rock since non-linear rock reduces stress concentration and stabilizes borehole. Note that if borehole stresses derived assuming a linear elasticity are used, the stress concentration is larger than the real stress, therefore, Drucker-Prager failure theory, which is larger than the actual rock failure surface, predicts closely the actual failure. It is also used for a small diameter borehole since a small diameter borehole is strong due to the size effect.

3.2.1 Mohr-Coulomb

Suppose a stress state $\sigma_1 < \sigma_2 < \sigma_3$ (negative for compression) is given, a failure is induced if the shear $\bar{\tau} = \frac{1}{2}(\sigma_1 - \sigma_3)/\cos\varphi$ evaluated at mean stress $\sigma_m = \frac{1}{2}(\sigma_1 + \sigma_3)$ has the following relation where a linear Mohr-Coulomb failure theory is assumed.

$$\bar{\tau} > \tau_o + \mu\sigma_m; \qquad \mu = \tan\phi$$

where ϕ is the internal friction angle, and τ_0 is the cohesive strength. The conversion from the cohesive strength to UCS (Uniaxial compressive Strength) is given by:

$$UCS = 2\tau_0 \frac{\cos\phi}{1-\sin\phi}$$

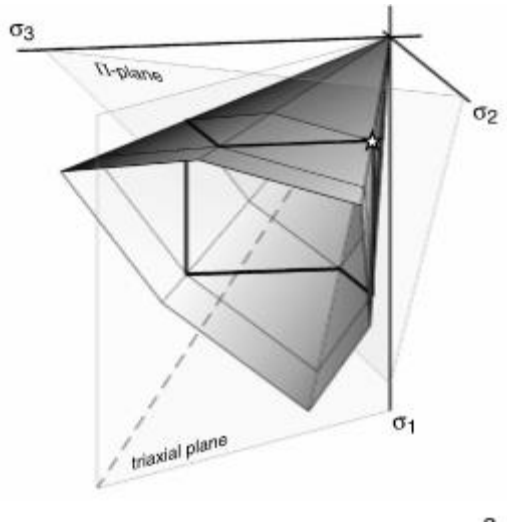

Figure III-1. Theoretical frictional sliding envelopes plotted in three-dimensional stress space and on triaxial and Π-plane graphs for Mohr-Coulomb

3.2.2 Mogi

The distance between a failure surface and a hydrostatic axis is given by the π -plane as follows:

$$\tau = \sqrt{\frac{1}{6}\left((\sigma_1 - \sigma_2)^2 + (\sigma_2 - \sigma_3)^2 + (\sigma_3 - \sigma_1)^2\right)}$$

The failure surface is given as a function of the mean stress:

$\tau = f(\sigma_m)$, where $\sigma_m = (\sigma_1 + \sigma_3)/3$

The linear Mogi failure theory is given by:

$$f = b_0 - b_1\sigma_m$$

$$b_0 = \frac{2}{\sqrt{3}}\tau_0 \cos\phi, \quad b_1 = \frac{2}{\sqrt{3}}\sin\phi$$

The failure will be induced at following condition:

$\tau > b_0 - b_1\sigma_m$ Where $\sigma_m = (\sigma_1 + \sigma_3)/2$

3.2.3 Drucker Prager

The distance between a failure surface and a hydrostatic axis is given by the π -plane as follows:

$\tau = \sqrt{\frac{1}{2}S_{ij}S_{ij}}$ 、 $S_{ij} = \sigma_{ij} - \sigma_m\delta_{ij}$

$$\tau = \sqrt{\frac{1}{6}\left((\sigma_1 - \sigma_2)^2 + (\sigma_2 - \sigma_3)^2 + (\sigma_3 - \sigma_1)^2\right)}$$

The failure surface is given as a function of the mean stress:

$\tau = f(\sigma_m)$, where $\sigma_m = (\sigma_1 + \sigma_2 + \sigma_3)/3$

If we assume the Drucker-Prager failure envelope has a corn shape which coincides with the linear Mohr coulomb failure theory under biaxial stress condition, then using ϕ and τ_o, we can express the failure envelope as follows:

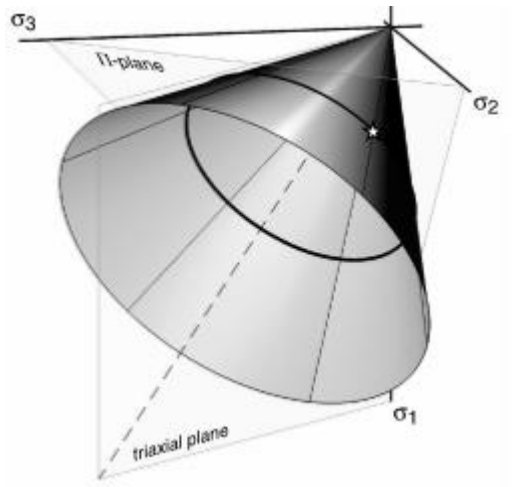

Figure III-2. Theoretical frictional sliding envelopes plotted in three-dimensional stress space and on triaxial and Π-plane graphs for Drucker-Prager

$$f = a_0 - a_1\sigma_m$$

$$a_0 = \tau_0 \frac{2\sqrt{3}\cos\phi}{3-\sin\phi} \quad , \quad a_1 = \frac{2\sqrt{3}\sin\phi}{3-\sin\phi}$$

The failure will be induced at following condition:

$$\tau > a_0 - a_1\sigma_m$$

3.2.4 Lade

Lade model is widely used by varying the value K. If K =1, Lade model has the same equations as Drucker-Prager model. As K changes smaller than 1, the equations will be different as following relationship:

$$S_{ij} = \sigma_{ij} - \sigma_m\delta_{ij}$$

$$\tau = \sqrt{\frac{1}{2} S_{ij} S_{ij}}$$

$$\tau = \sqrt{\frac{1}{6}\left((\sigma_1 - \sigma_2)^2 + (\sigma_2 - \sigma_3)^2 + (\sigma_3 - \sigma_1)^2\right)}$$

$r = (\frac{27}{2} J_3)^{1/3}$ 、 $J_3 = S_{11}S_{22}S_{33} + 2S_{12}S_{23}S_{31} - S_{11}S_{23}^2 - S_{22}S_{13}^2 - S_{33}S_{12}^2$

$t = \frac{1}{2}\tau[1 + \frac{1}{k} - (1 - \frac{1}{k})(\frac{r}{\sqrt{3}\tau})^3]$

$t = g(\sigma_m)$， $0 < K < 1$ where $\sigma_m = (\sigma_1 + \sigma_2 + \sigma_3)/3$

K=1 for Drucker-Prager

The linear Lade theory equation is:

$$g = c_0 - c_1\sigma_m$$

$$c_0 = \tau_0 \frac{2\sqrt{3}\cos\phi}{3 - \sin\phi} \quad , \quad c_1 = \frac{2\sqrt{3}\sin\phi}{3 - \sin\phi}$$

The failure will be induced at following condition:

$$\tau > c_0 - c_1\sigma_m$$

Therefore, we have the following table to summarize the four failure criteria and how to determine the failure occurrence. We assume $\emptyset = \mathbf{25}°$ and UCS=3000psi for the failure analysis as shown in Table III-1.

Table III-1 Rock Failure Criteria (assume: $\phi = 25°, UCS = 3000\ psi$)

Failure Criteria	Governing Equation	The effect of intermediate principal stress	Failure Occur
Mohr-Coulomb	$\bar{\tau} = \tau_o + \mu\sigma_m$ $UCS = 2\tau_0 \frac{\cos\phi}{1-\sin\phi}$, $\mu = \tan\phi$	No	$\bar{\tau} > \tau_o + \mu\sigma_m$
Mogi	$\tau_{oct} = b_0 - b_1\sigma_m$ $b_0 = \frac{2}{\sqrt{3}}\tau_0\cos\phi$, $b_1 = \frac{2}{\sqrt{3}}\sin\phi$	Yes	$\tau > b_0 - b_1\sigma_m$
Lade	$\tau_{oct} = c_0 - c_1\sigma_m$ $c_0 = \tau_0 \frac{2\sqrt{3}\cos\phi}{3-\sin\phi}$, $c_1 = \frac{2\sqrt{3}\sin\phi}{3-\sin\phi}$	Yes	$\tau > c_0 - c_1\sigma_m$
Drucker-Prager	$\tau_{oct} = a_0 - a_1\sigma_m$ $a_0 = \tau_0 \frac{2\sqrt{3}\cos\phi}{3-\sin\phi}$, $a_1 = \frac{2\sqrt{3}\sin\phi}{3-\sin\phi}$	Yes	$\tau > a_0 - a_1\sigma_m$

3.3 Failure Function to Predict Breakout Angle with Various Controllable Parameters

Failure condition and breakout angle are varied if the well condition changes according to the parameters study with typical field conditions. Therefore, the four rock failure criteria will be applied for all the parameters for a vertical well in the base reservoir condition and horizontal well in depleted reservoir condition to predict the breakout angle.

Assumption of the breakout angle: It is assumed that breakout occurs at the interface where the failure condition is satisfied. For example, for the Mohr-Coulomb failure criterion, the failure function is given by :

$$f = \bar{\tau} - (\tau_o + \mu\sigma_m)$$

Then, it is assumed that the breakout angle is the angle which satisfies f > 0. Many previous works are available for discussing this assumption. Field and laboratory results have confirmed this assumption approximately holds.

3.3.1 Breakout angle predicted by the four rock failure criteria of vertical well in the base reservoir conditions

3.3.1.1 The base reservoir Condition

Here we use the base reservoir condition shown in Table II-1:

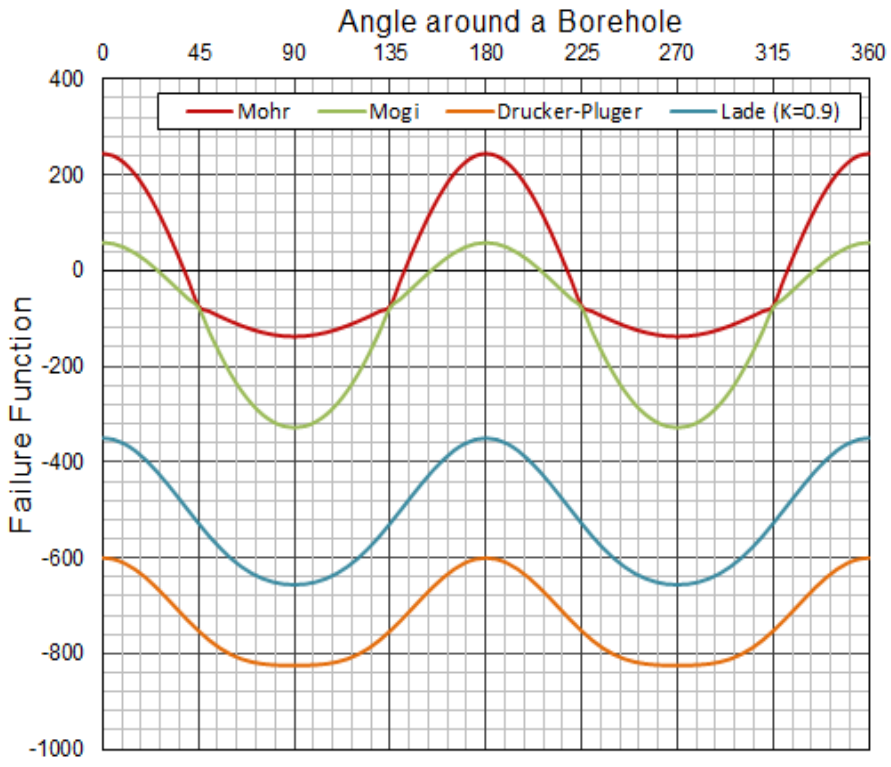

Figure III-3 Breakout prediction around borehole in the base reservoir condition

Table III-2 Breakout angle predicted by failure criteria in the base reservoir condition

Failure Criteria	Breakout Angle
Mohr	76°
Mogi	54°
Lade	No Failure
Drucker-Prager	No Failure

Fig. III-3 illustrates calculated failure function ($\tau - f(\sigma_m)$) versus angle around the wellbore in the base reservoir condition, which ranges from 0° to 360°. As Table III-1 shows, when the stress is greater than the failure surface, borehole breakout occurs, which means $\tau - f(\sigma_m)$>0. Therefore, as shown in the failure curve in Fig. III-3, the angle of two points above 0 ($\tau - f(\sigma_m)$>0) is the breakout angle. All the four failure criteria curves behave like a cosine function, which is symmetric with the axis of 180°. From Table III-2, Mohr-coulomb gives the largest breakout angle as 76°and Mogi shows the breakout angle is 54°; however, there is no breakout according to the Drucker-Prager and Lade failure criteria.

Therefore, it can conclude that Mohr-coulomb and Mogi can estimate higher breakout value than Drucker-Prager and Lade model.

3.3.1.2 Well Inclination Effect

In this case, the well inclination is set at 0 º, 30º, 60 º, 90º at the given reservoir conditions.

Well azimuth = 0 °, well angle = 30°

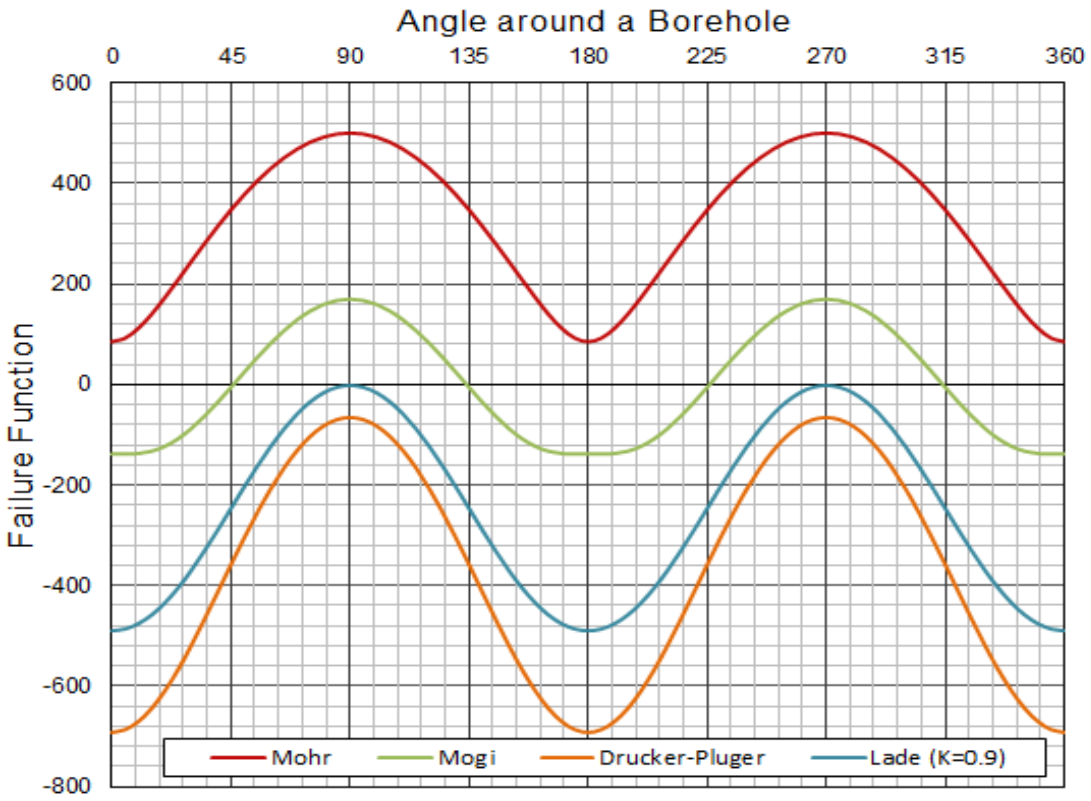

Figure III-4. Breakout prediction around borehole (Well azimuth = 0°, and Well angle = 30°)

Table III-3.Breakout angle predicted by failure criteria (Well azimuth = 0°, and Well angle = 30°)

Failure Criteria	Breakout Angle
Mohr	All Failure
Mogi	90°
Lade	No Failure
Drucker-Prager	No Failure

Fig. III-4 is the calculated failure function ($\tau - f(\sigma_m)$) versus angle around the wellbore in the base reservoir condition, which ranges from 0° to 360° at well angle = 30° and well azimuth = 0°. As shown in the figure, all the failure function curves move

up to the vertical direction. In addition, the results in Table III-3 demonstrate that Mohr-Coulomb failure criterion indicates all failure around the borehole and the Mogi's criterion predicts the breakout angle as 90°, in contrast, Drucker-Prager and Lade still show no failure around borehole. Based on the results, we may find the wellbore become more unstable due to the well inclination, which agrees with the results of stress state around borehole in chapter 2.

Well azimuth = 0 °, well angle = 60°

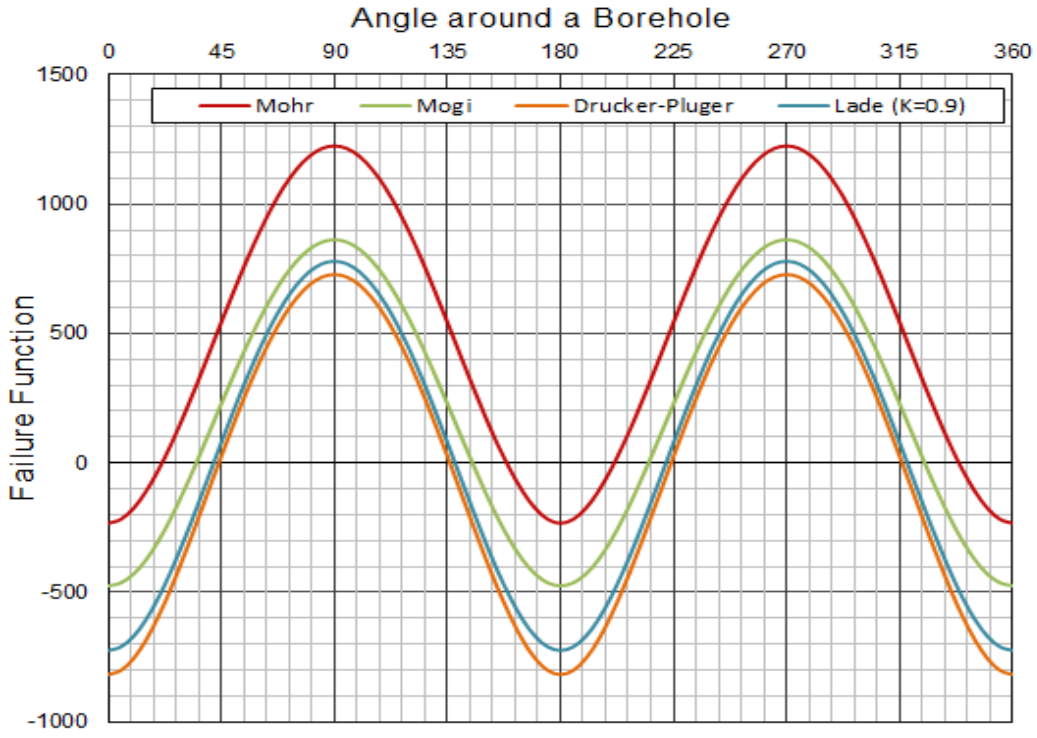

Figure III-5. Breakout prediction around borehole (Well azimuth = 0°, and Well angle = 60°)

Table III-4. Breakout angle predicted by failure criteria (Well azimuth = 0°, and Well angle = 60°)

Failure Criteria	Breakout Angle
Mohr	138°
Mogi	110°
Lade	98°
Drucker-Prager	90°

Fig. III-5 is the results of calculated failure function ($\tau - f(\sigma_m)$) versus angle around the wellbore in the base reservoir condition, which ranges from 0° to 360° at well angle = 60° and well azimuth = 0°. It should be pointed out that all the failure function curves move up to the vertical direction and make the borehole unstable. The results in Table III-3 demonstrate that breakout angle predicted by the four failure criteria is much larger than the value of the base condition.

Well azimuth = 0 °, well angle = 90°

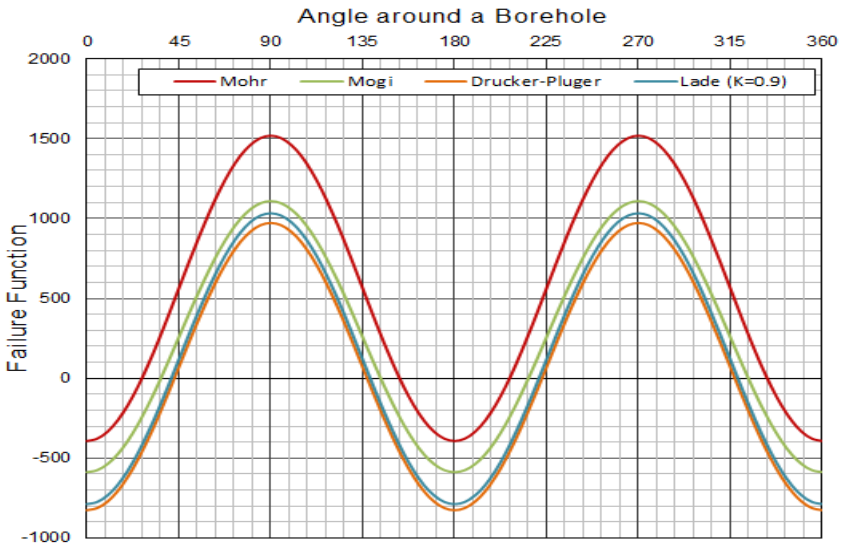

Figure III-6. Breakout prediction around borehole (Well azimuth = 0°, and Well angle = 90°)

Table III-5. Breakout angle predicted by failure criteria (Well azimuth = 0°, and Well angle = 90°)

Failure Criteria	Breakout Angle
Mohr	136°
Mogi	108°
Lade	100°
Drucker-Prager	94°

Fig. III-6 shows the calculated failure function ($\tau - f(\sigma_m)$) versus angle around the wellbore in the base reservoir condition, which ranges from 0° to 360° at well angle = 90° and well azimuth = 0°. All the failure function curves move up to the vertical direction and make the borehole unstable. The results in Table III-5 demonstrate that breakout angles predicted by the four failure criteria continue to become larger than the value of the base condition.

Well azimuth = 90 °, well angle = 30°

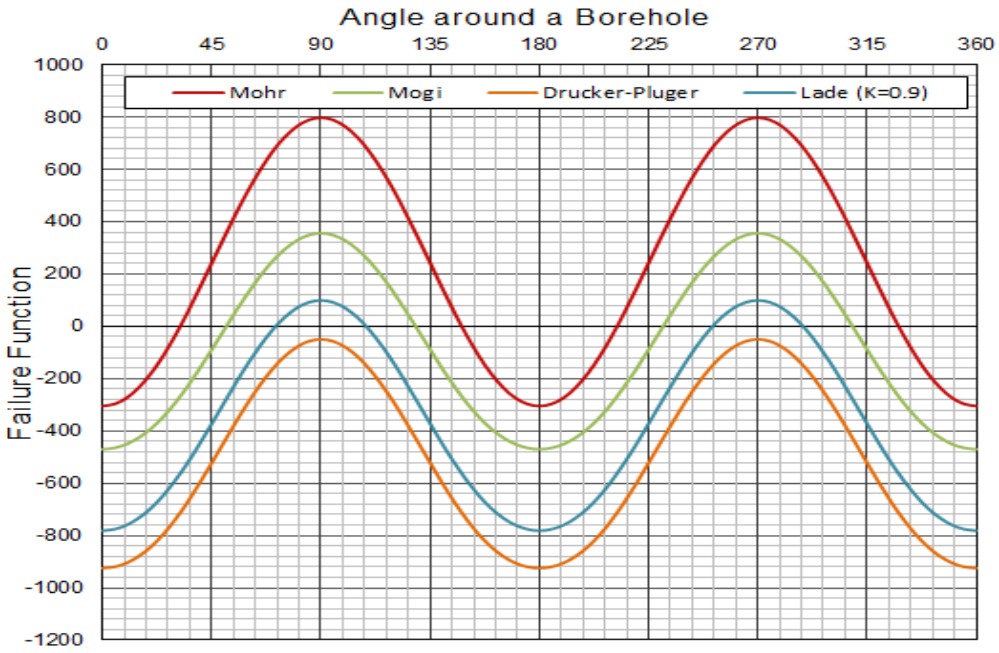

Figure III-7. Breakout prediction around borehole (Well azimuth = 90°, and Well angle = 30°)

Table III-6. Breakout angle predicted by failure criteria (Well azimuth =90°, and Well angle = 30°)

Failure Criteria	Breakout Angle
Mohr	114°
Mogi	88°
Lade	36°
Drucker-Prager	No Failure

Well azimuth = 90 °, well angle = 60°

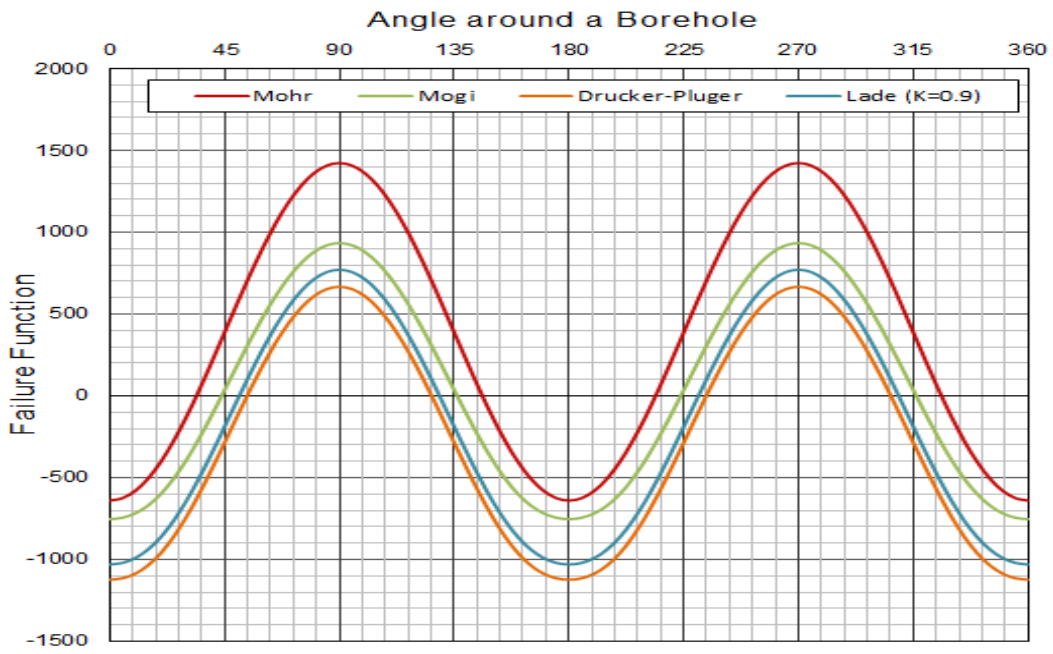

Figure III-8. Breakout prediction around borehole (Well azimuth = 90°, and Well angle = 60°)

Table III-7. Breakout angle predicted by failure criteria (Well azimuth = 90°, and Well angle = 60°)

Failure Criteria	Breakout Angle
Mohr	112°
Mogi	94°
Lade	78°
Lade Drucker-Prager	72°

Well azimuth = 90 °, well angle = 90°

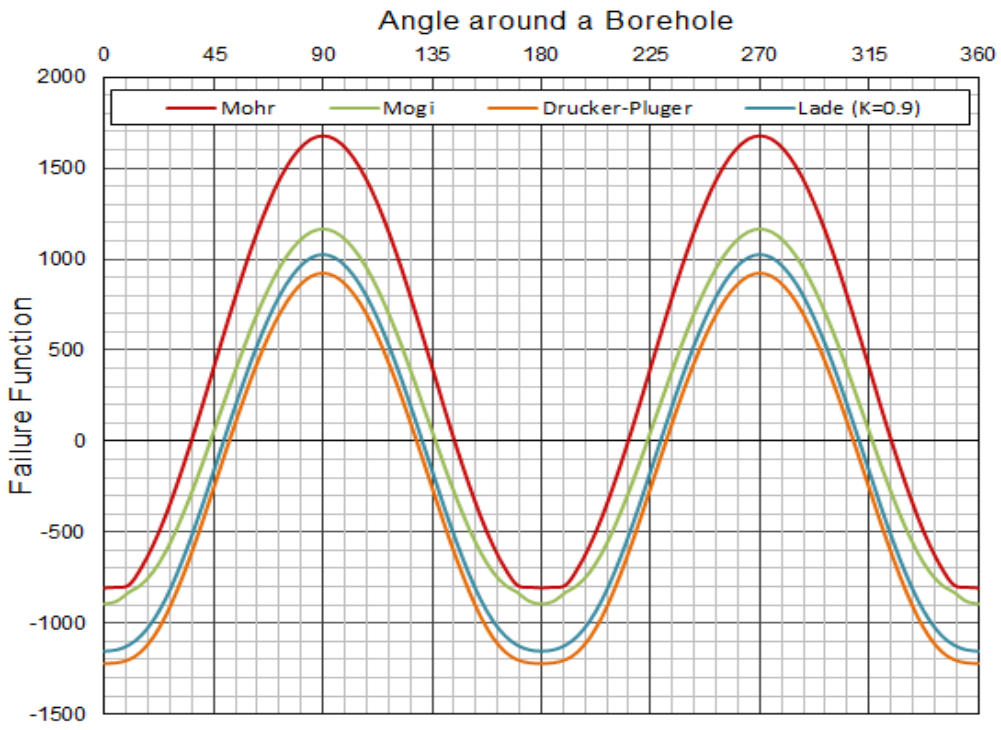

Figure III-9. Breakout prediction around borehole (Well azimuth =90°, and Well angle = 90°)

Table III-8. Breakout angle predicted by failure criteria (Well azimuth = 90°, and Well angle = 90°)

Failure Criteria	Breakout Angle
Mohr	108°
Mogi	92°
Lade	82°
Drucker-Prager	78°

Fig.III-7- Fig. III-9 show calculated failure function ($\tau - f(\sigma_m)$) versus angle around the wellbore in the base reservoir condition, which ranges from 0° to 360° at well azimuth= 90°. By comparing these results of breakout angle predicted by different

failure at well azimuth= 90° condition with the results at well azimuth=0° condition, it shows the predicted breakout angle is much larger at well azimuth=0°, which means the azimuth of well also affects borehole stability for inclined wells.

3.3.1.3 Osmosis Effect

Osmosis is caused by water potential difference. Therefore, the osmosis is always considered together with shale swelling. However, even the novel drilling fluids additives can reduce the magnitude of shale swelling, while the osmosis will not be controlled. Therefore, in this research, pore pressure change due to osmosis is discussed separately with shale swelling.

In this case, the surface pressure drop of -500 psi is given due to osmosis effect. The radius of the pressure drop is assumed to be 2 ft. The wellbore pressure is maintained 500 psi overbalance.

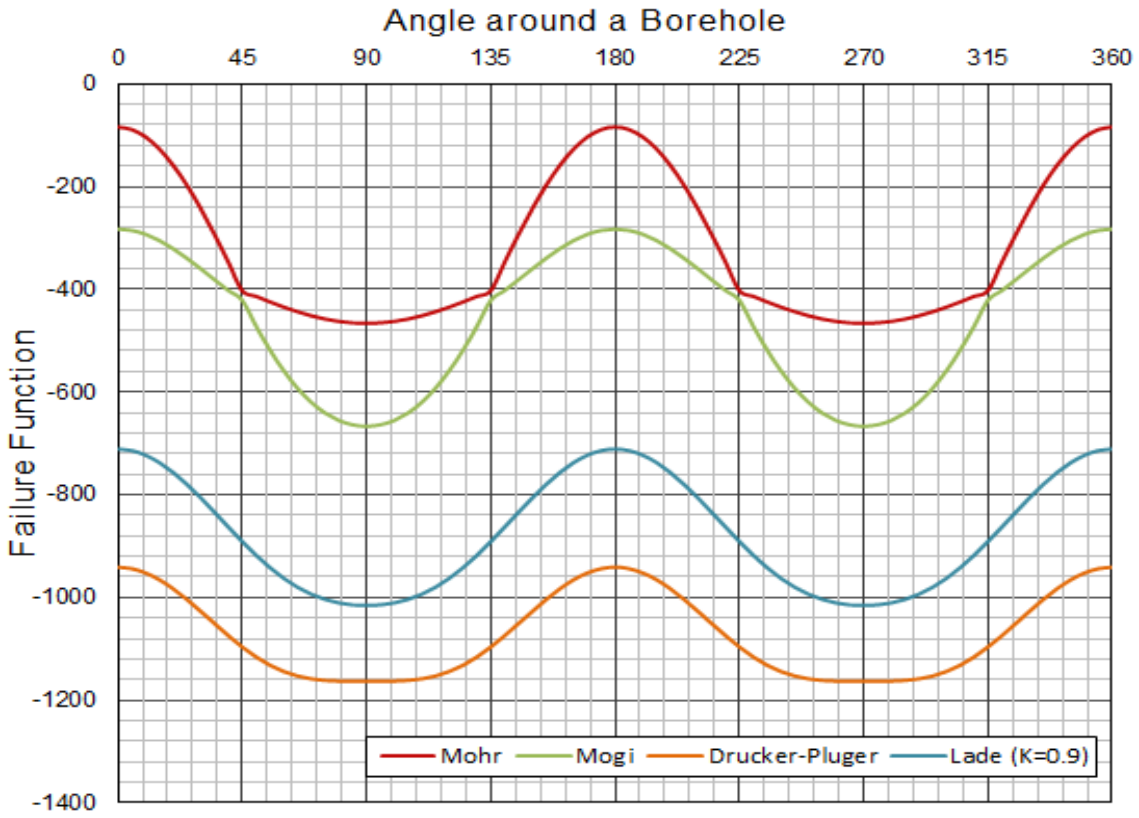

Figure III-10. Breakout prediction around borehole with effect of osmosis

Table III-9. Breakout angle predicted by failure criteria in the base condition with the effect of osmosis

Failure Criteria	Breakout Angle
Mohr	No Failure
Mogi	No Failure
Lade	No Failure
Drucker-Prager	No Failure

Fig.III-10 shows calculated failure function ($\tau - f(\sigma_m)$) versus angle around the wellbore in the base reservoir condition. The effect of osmosis is small, but it shows no

breakout around wellbore for all failure criteria. It is important to highlight that stress changes around borehole due to osmosis will make the borehole more stable, which can reduce the effect in the well environment that can leads to borehole instability including swelling, temperature, etc.

3.3.1.4 Swelling Effect

0.2 % swelling is assumed at the wellbore surface (ΔS) and the swelling radius (rs) is 0.7 ft. This is the most significant parameter that we need to estimate.

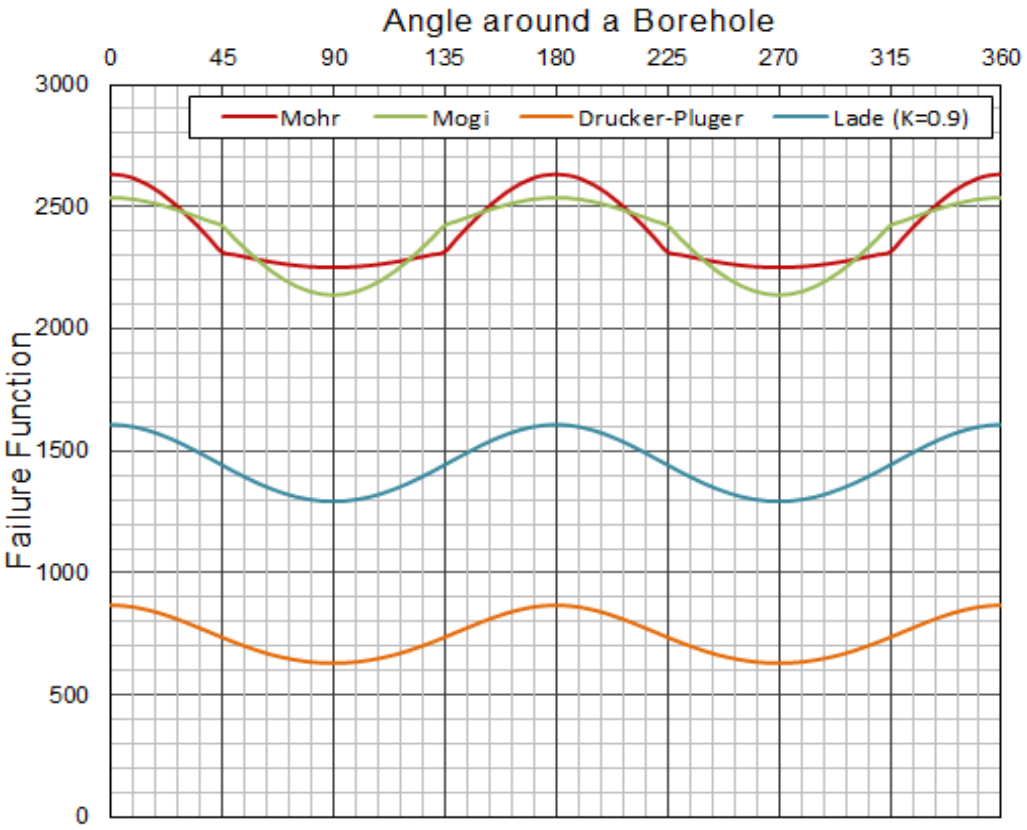

Figure III-11. Breakout prediction around borehole with effect of shale swelling

Table III-10. Breakout angle predicted by failure criteria in the base condition with the effect of shale swelling

Failure Criteria	Breakout Angle
Mohr	All Failure
Mogi	All Failure
Lade	All Failure
Drucker-Prager	All Failure

Fig.III-11 shows calculated failure function ($\tau - f(\sigma_m)$) versus angle around the wellbore in the base reservoir condition, which ranges from 0° to 360° with the effect of shale swelling. The results illustrate that, with the effect of shale swelling, the borehole failure is predicted by all the failure criteria. This supports the conclusion in previous study where shale swelling significantly affects the stress state around borehole and leads to borehole instability problems. The borehole stability depends on the magnitude of $\{E/(1-\nu)\}(\mathrm{S}+\alpha\Delta\mathrm{T})$. Therefore, the shale swelling effect is significant if $\{E/(1-\nu)\}$ is large.

3.3.1.5 Temperature Effect

A temperature change of 50°C is considered for the reservoir conditions within the radius of 0.7 ft. The linear expansion coefficient is given as 1.e-5 1/ºC.

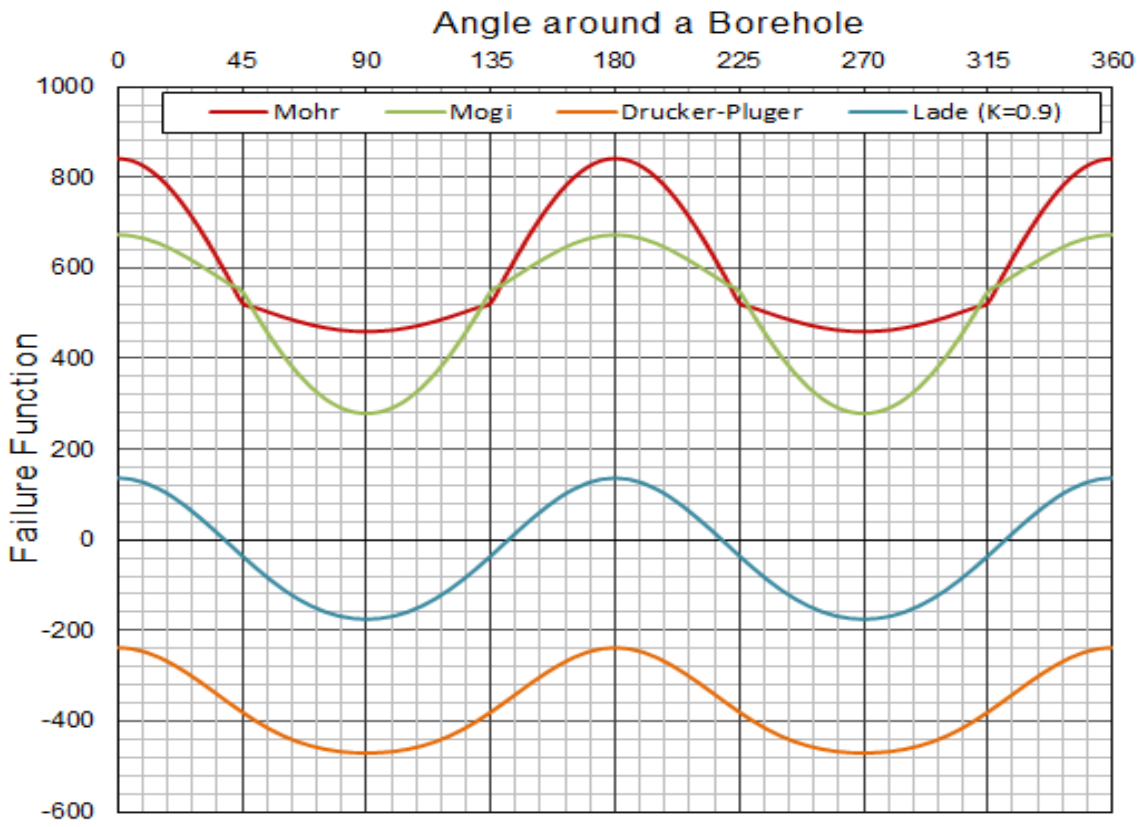

Figure III-12. Breakout prediction around borehole with effect of temperature

Table III-11. Breakout angle predicted by failure criteria in the base condition with the effect of temperature

Failure Criteria	Breakout Angle
Mohr	All Failure
Mogi	All Failure
Lade	76°
Drucker-Prager	No Failure

Fig.III-12 shows calculated failure function ($\tau - f(\sigma_m)$) versus angle around the wellbore in the base reservoir condition, which ranges from 0° to 360° with the effect of

temperature. The results illustrate the effect of temperature. The borehole is all failure predicted by Mohr-Coulomb and Mogi, and Lade model also predicts the breakout angle 76°. This is consistent with the observation from stress state with effect of temperature in previous study, where temperature change lead to borehole instability. The temperature affects the borehole stability with $\{E/(1-\nu)\}(S+\alpha\Delta T)$. Normally, $\alpha\Delta T$ is significantly smaller than swelling effct S. However, if shale is 100% saturated with water and the permeability is small, the expansion of water trapped in shale results in shale volume increase, which may induce valume expansion equivalent to shale swelling.

3.3.1.6 Overbalance Effect

Assume overbalance occurs during the drilling, wellbore pressure is assumed to increase to 7000 psi at the original reservoir conditions.

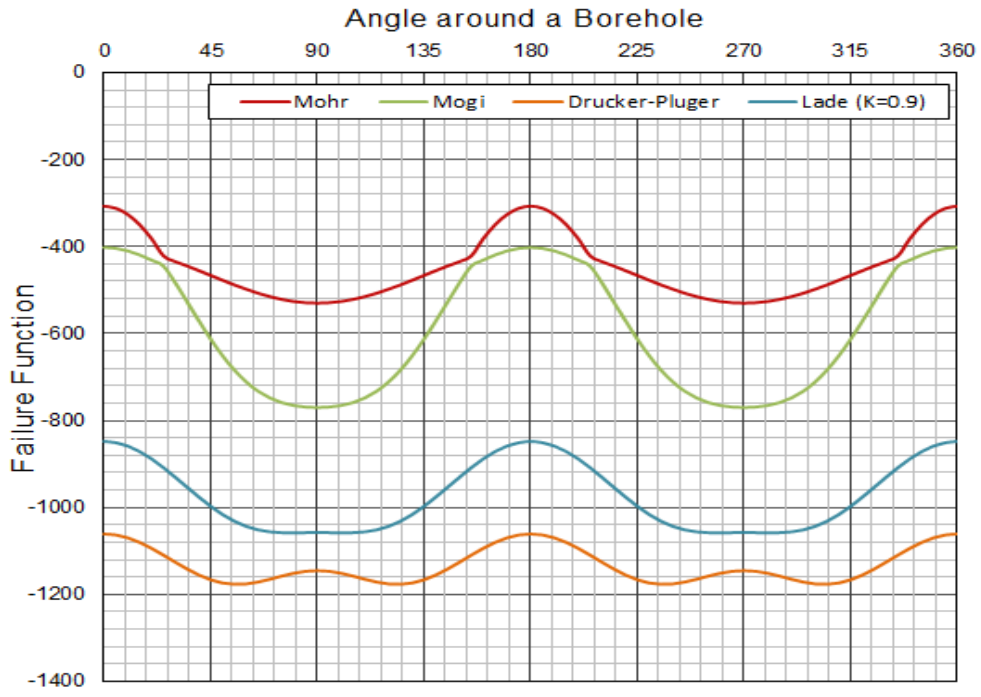

Figure III-13. Breakout prediction around borehole with effect of overbalance

Table III-12. Breakout angle predicted by failure criteria in the base condition with the effect of overbalance

Failure Criteria	Breakout Angle
Mohr	No Failure
Mogi	No Failure
Lade	No Failure
Drucker-Prager	No Failure

Fig.III-13 shows calculated failure function ($\tau - f(\sigma_m)$) versus angle around the wellbore in the base reservoir condition, which ranges from 0° to 360° with the effect of overbalance. It shows no breakout around wellbore for all failure criteria. Although overbalance has a little effect on the total stress state around a borehole, it can make the borehole more stable due to the effective stress change.

3.3.1.7 Drawdown Effect

In this case, the pore pressure change due to drawdown is – 500 psi and the radius of pressure drop is equal to 2 ft.

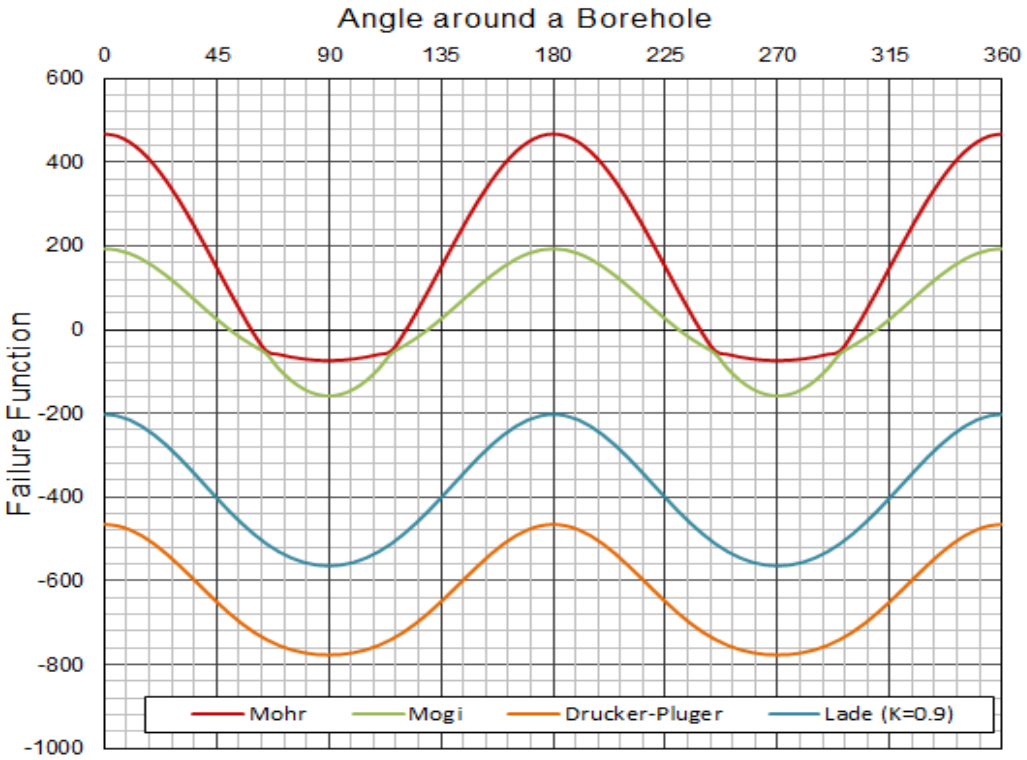

Figure III-14. Breakout prediction around borehole with effect of drawdown

Table III-13. Breakout angle predicted by failure criteria in the base condition with the effect of drawdown

Failure Criteria	Breakout Angle
Mohr	120°
Mogi	104°
Lade	No Failure
Drucker-Prager	No Failure

Fig.III-14 shows calculated failure function ($\tau - f(\sigma_m)$) versus angle around the wellbore in the base reservoir condition, which ranges from 0° to 360° with the effect of drawdown. It predicts a lager breakout angle than at the base condition. Therefore, the drawdown can also cause borehole instability although it is not significant.

3.3.1.8 Hard Bedding Layer

In this case, a hard bedding layer is considered above and below the target layer, which has 6×10^6 psi Young's modulus, two times as that of the target layer.

Hard bedding layer (γ=0°)

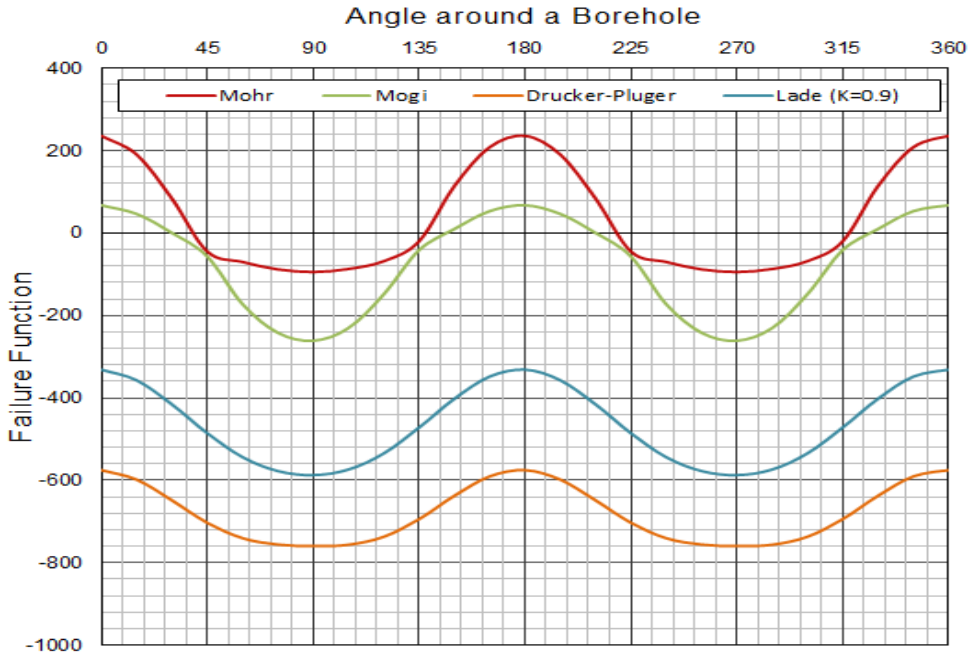

Figure III-15. Breakout prediction around borehole with effect of hard bedding layer (γ=0°)

Table III-14. Breakout angle predicted by failure criteria in the base condition with the effect of hard bedding layer(γ=0°)

Failure Criteria	Breakout Angle
Mohr	76°
Mogi	60°
Lade	No Failure
Drucker-Prager	No Failure

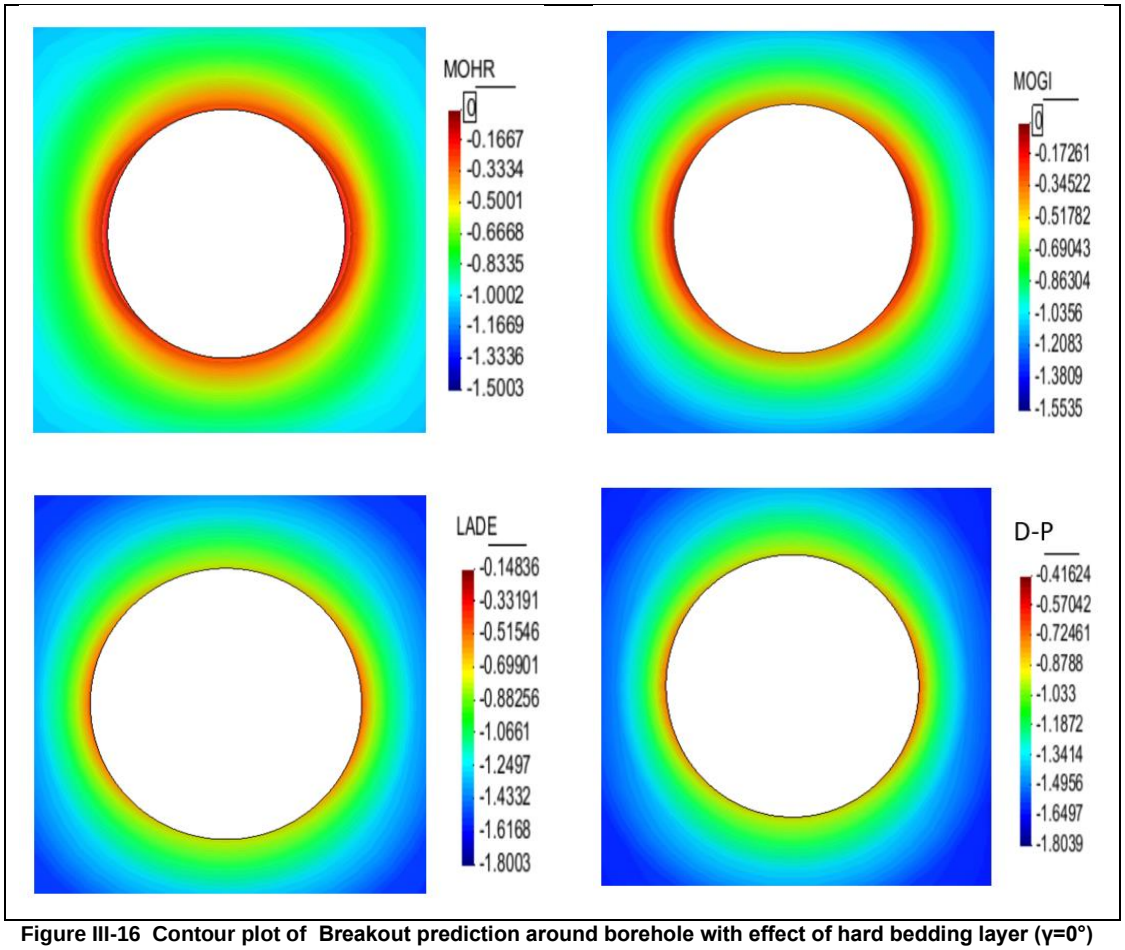

Figure III-16 Contour plot of Breakout prediction around borehole with effect of hard bedding layer (γ=0°)

Hard bedding layer (γ=60°)

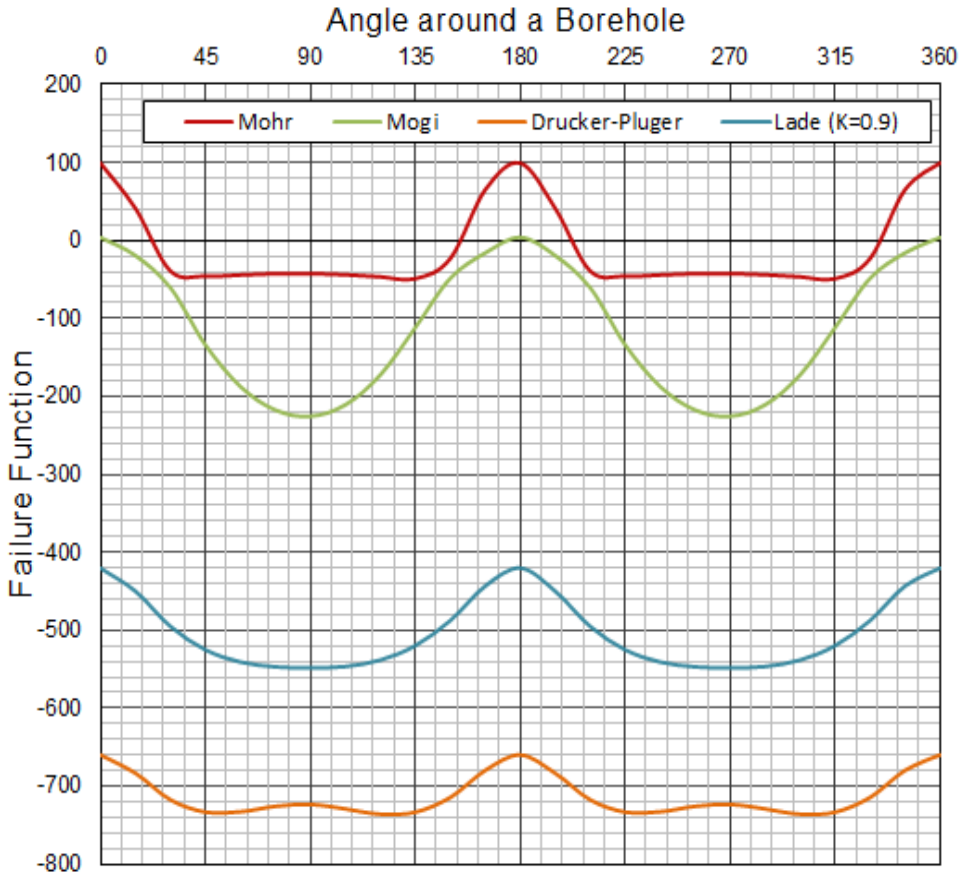

Figure III-17. Breakout prediction around borehole with effect of hard bedding layer (γ=60°)

Table III-15. Breakout angle predicted by failure criteria in the base condition with the effect of hard bedding layer(γ=60°)

Failure Criteria	Breakout Angle
Mohr	48°
Mogi	6°
Lade	No Failure
Drucker-Prager	No Failure

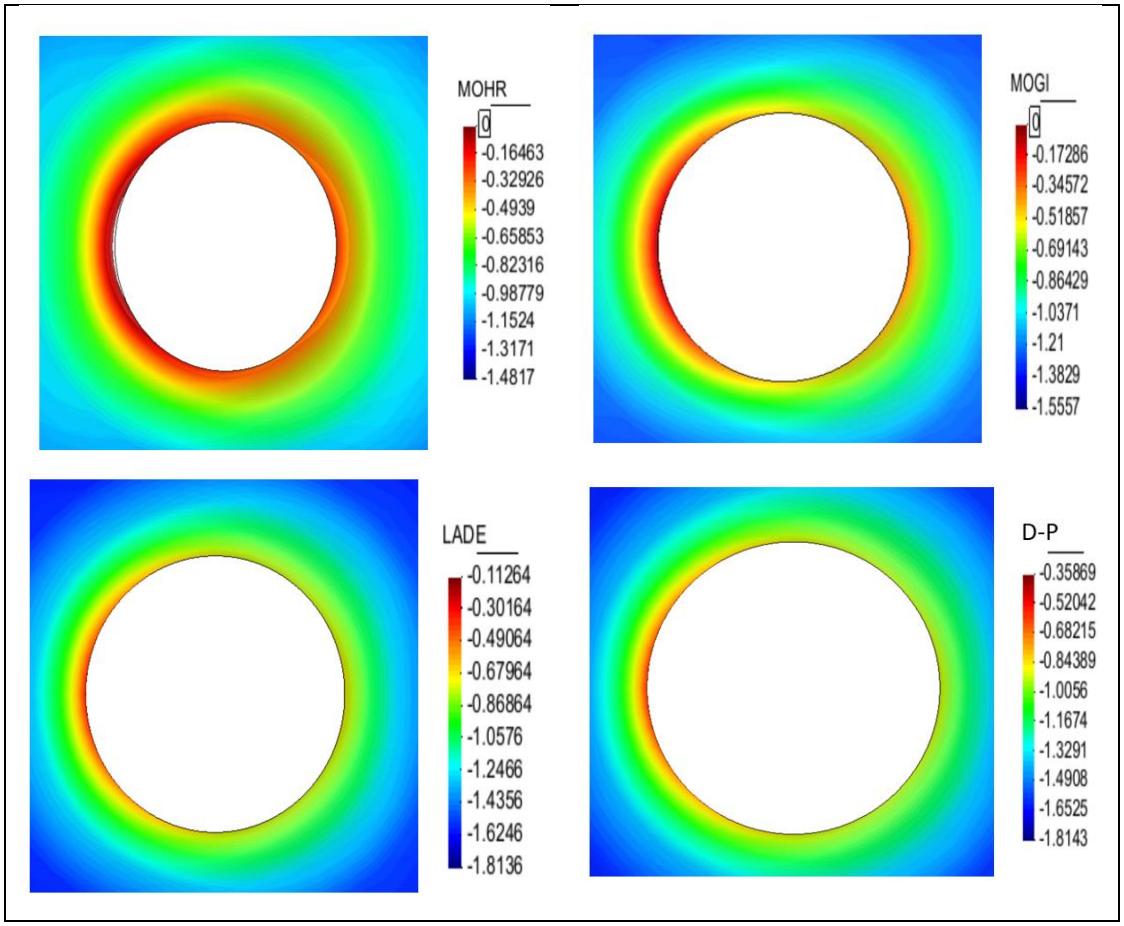

Figure III-18 Contour plot of Breakout prediction around borehole with effect of hard bedding layer (γ=60°)

According to the results shown in Figs. III 15 to18, the hard bedding layer with orientation of 0° has the same breakout angle without bedding plane, whereas the predicted breakout angle of the effect of hard bedding layer with orientation of 60° is smaller. The hard layers support the soft layer resulting in a higher stability of the soft formation.

3.3.1.9 Soft Bedding Layer

In this case, a soft bedding layer is considered above the target layer, which has the young's modulus of 1.5×10^{6} psi as half as that of the target layer.

Soft Bedding Layer (γ=0°)

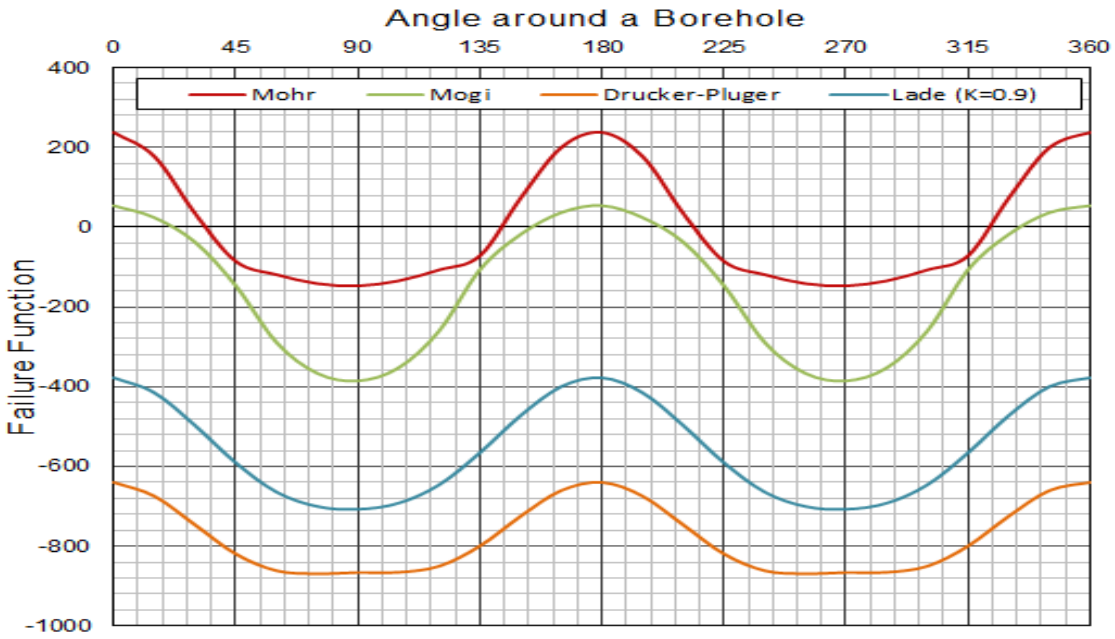

Figure III-19. Breakout prediction around borehole with effect of soft bedding layer (γ=0°)

Table III-16. Breakout angle predicted by failure criteria in the base condition with the effect of soft bedding layer(γ=0°)

Failure Criteria	Breakout Angle
Mohr	70°
Mogi	40°
Lade	No Failure
Drucker-Prager	No Failure

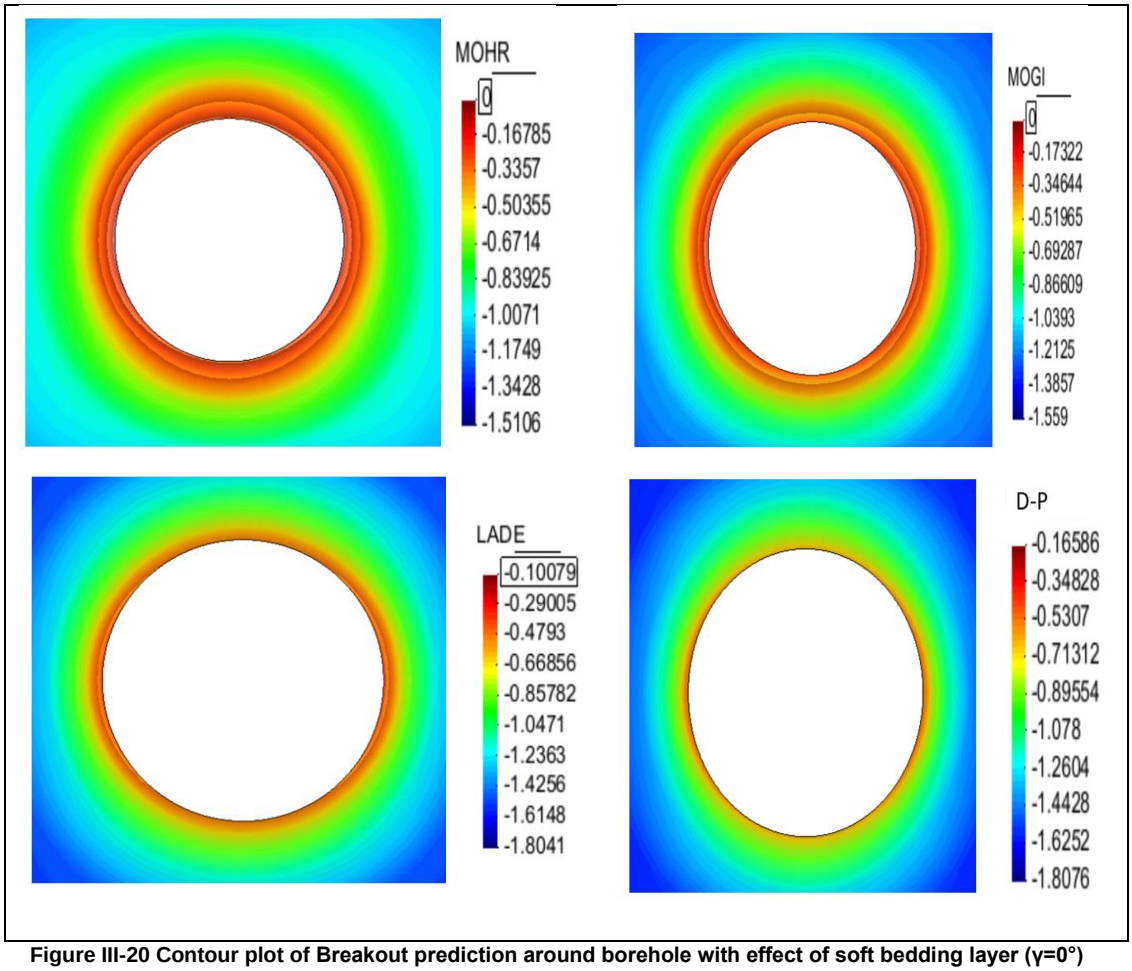

Figure III-20 Contour plot of Breakout prediction around borehole with effect of soft bedding layer (γ=0°)

Soft Bedding Layer (γ=60°)

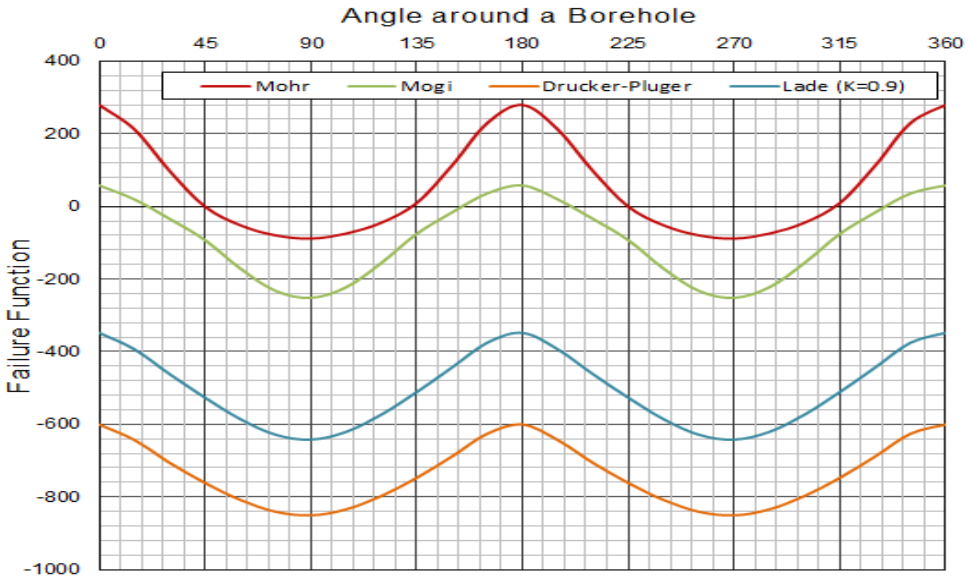

Figure III-21. Breakout prediction around borehole with effect of soft bedding layer (γ=60°)

Table III-17. Breakout angle predicted by failure criteria in the base condition with the effect of soft bedding layer(γ=60°)

Failure Criteria	Breakout Angle
Mohr	90°
Mogi	45°
Lade	No Failure
Drucker-Prager	No Failure

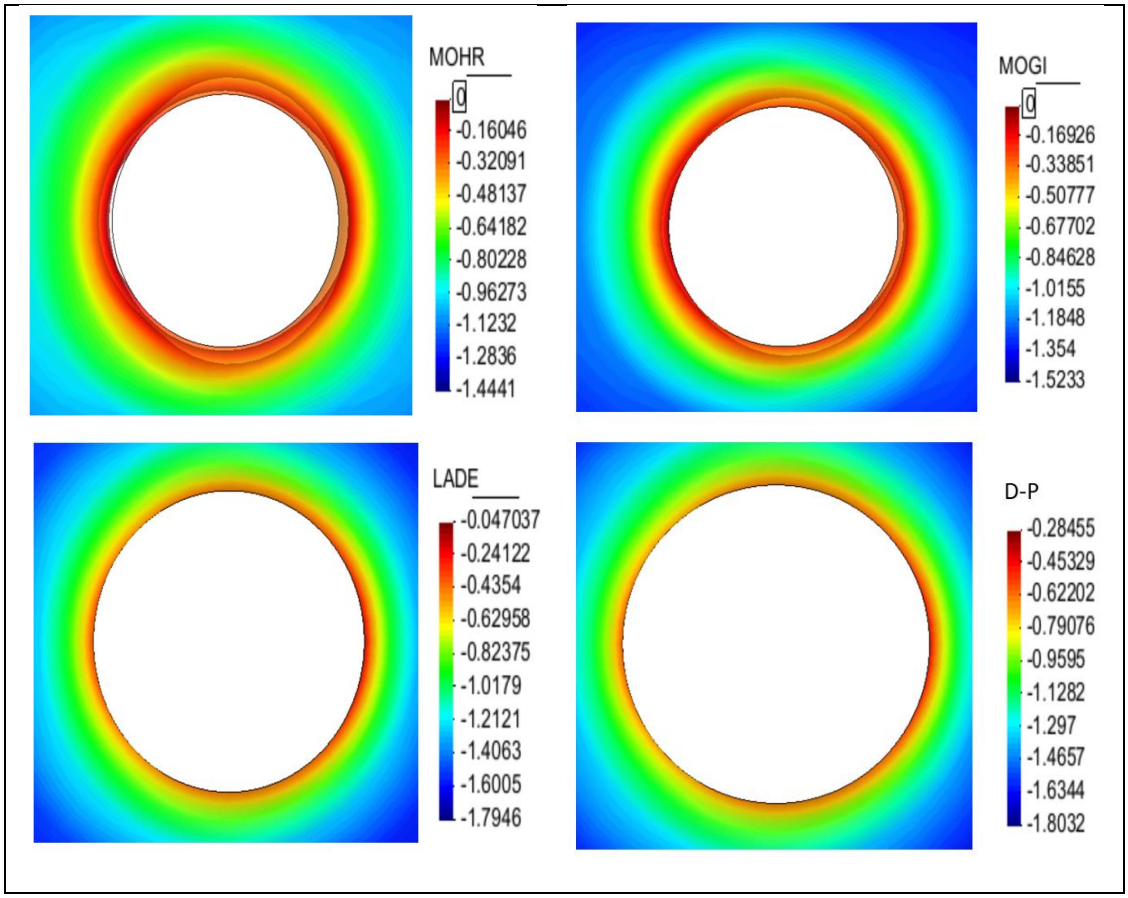

Figure III-22 Contour plot of Breakout prediction around borehole with effect of soft bedding layer (γ=60°)

According to the results shown in Fig. III 17-22, the soft bedding layer with orientation of 0° has almost the same predicted breakout angle without bedding layer, whereas the predicted breakout angle of the effect of soft bedding layer with orientation of 60° is a little larger for Mohr Coulomb and a little smaller for Mogi.

3.3.1.10 Formation with Transversely Isotropic Elastic Material

Shale formation is laminated with mud and shale layers. The elastic property may be approximated by a transversely isotropic material. The magnitude of orthotropy is $E_{vertical}/E_{horizontal}=1/2$ which is reasonable from all rock data available to me. As shown in Fig. III-23to Fig. III-24, the predicted breakout angles almost do not change with the effect of formation with transversely isotropic elastic material for a vertical well compared with the results for a well for the base case. The shape of the failure function is irregular for anisotropic rock. However, the breakout angle remains similar, although it may not be the case if the magnitude of anisotropy is larger.

Figs.III-25 to 30 show the results for inclined wells. The breakout angles significantly increase with well angle resulting in instability of borehole.

a. Well angle= 0°

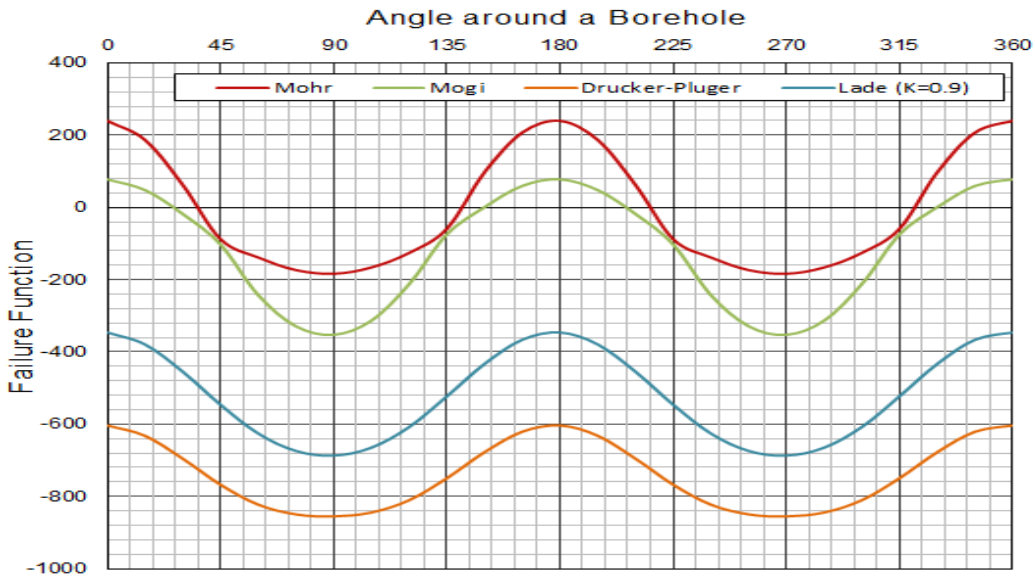

Figure III-23. Breakout prediction around borehole with effect of formation with transversely isotropic elastic material (well angle = 0°)

Table III-18. Breakout angle predicted by failure criteria in the base condition with the effect of formation with transversely isotropic elastic material (well angle = 0°)

Failure Criteria	Breakout Angle
Mohr	72°
Mogi	54°
Lade	No Failure
Drucker-Prager	No Failure

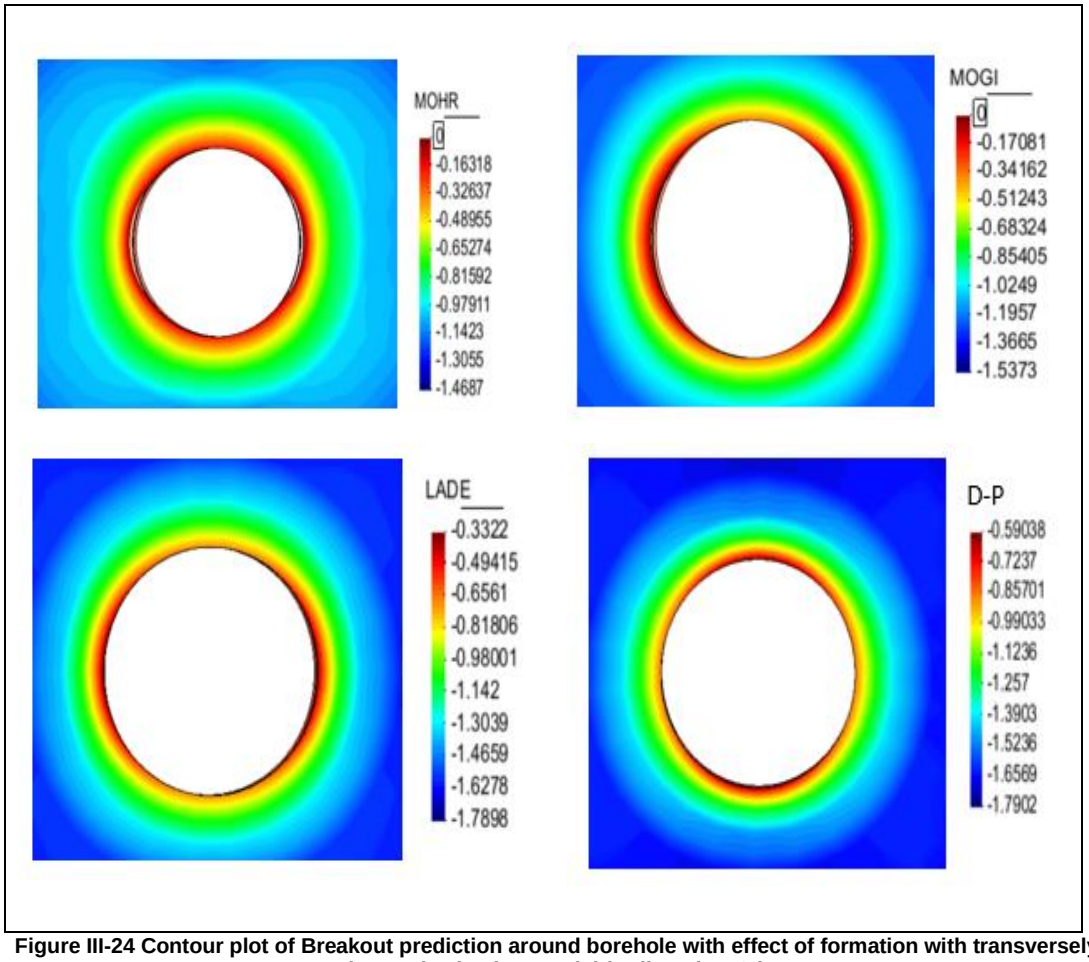

Figure III-24 Contour plot of Breakout prediction around borehole with effect of formation with transversely isotropic elastic material (well angle = 0°)

b. Well angle =30°

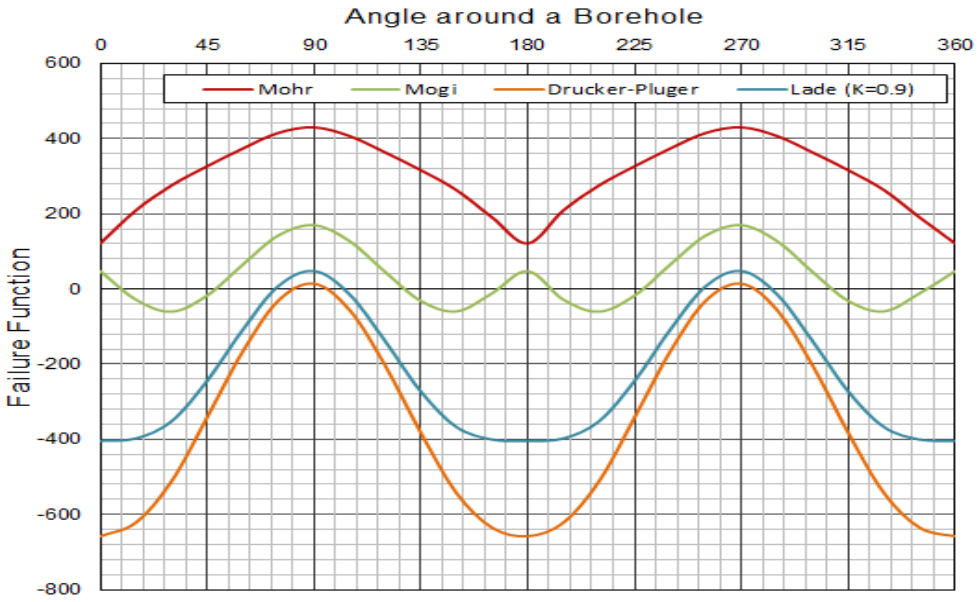

Figure III-25. Breakout prediction around borehole with effect of formation with transversely isotropic elastic material (well angle = 30°)

Table III-19. Breakout angle predicted by failure criteria in the base condition with the effect of formation with transversely isotropic elastic material (well angle = 30°)

Failure Criteria	Breakout Angle
Mohr	All Failure
Mogi	94°
Lade	32°
Drucker-Prager	18°

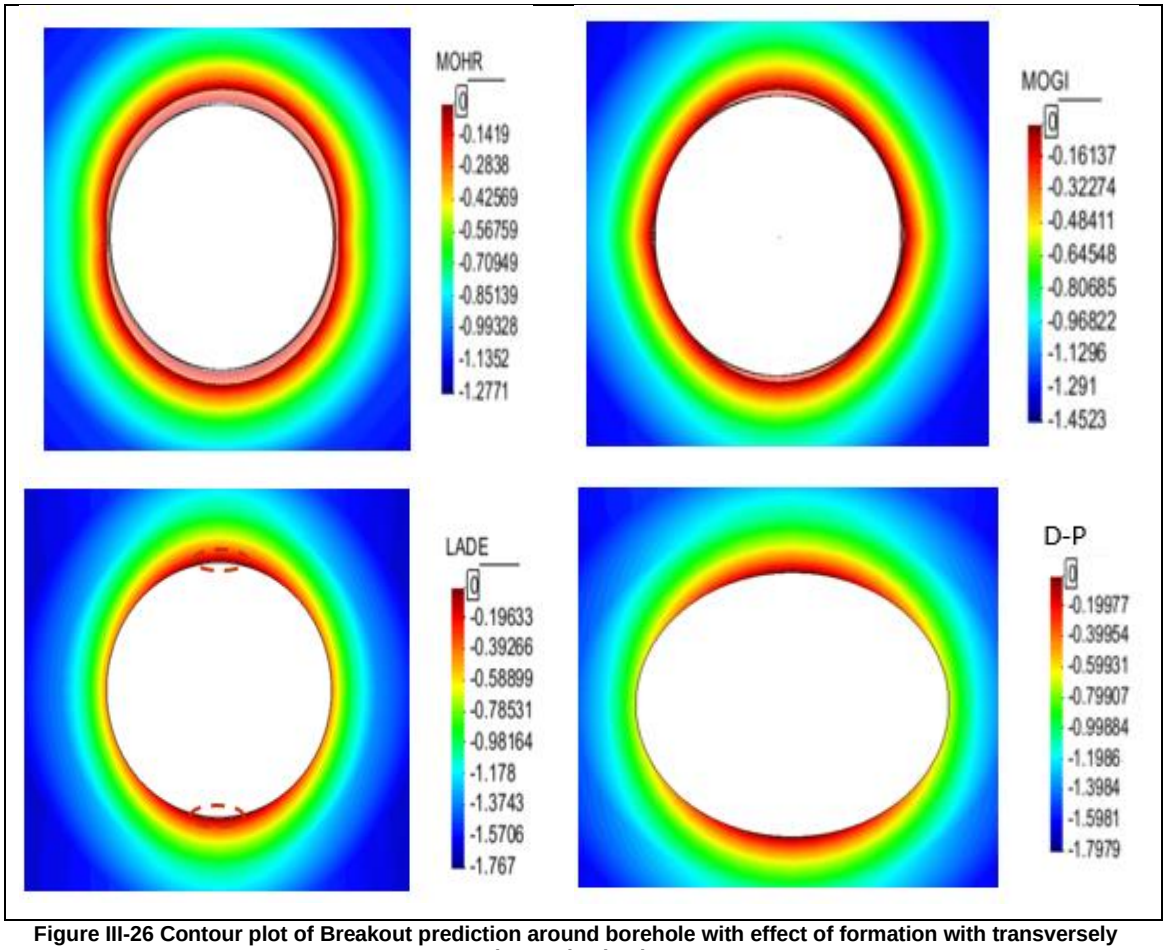

Figure III-26 Contour plot of Breakout prediction around borehole with effect of formation with transversely isotropic elastic

c. Well angle= 60°

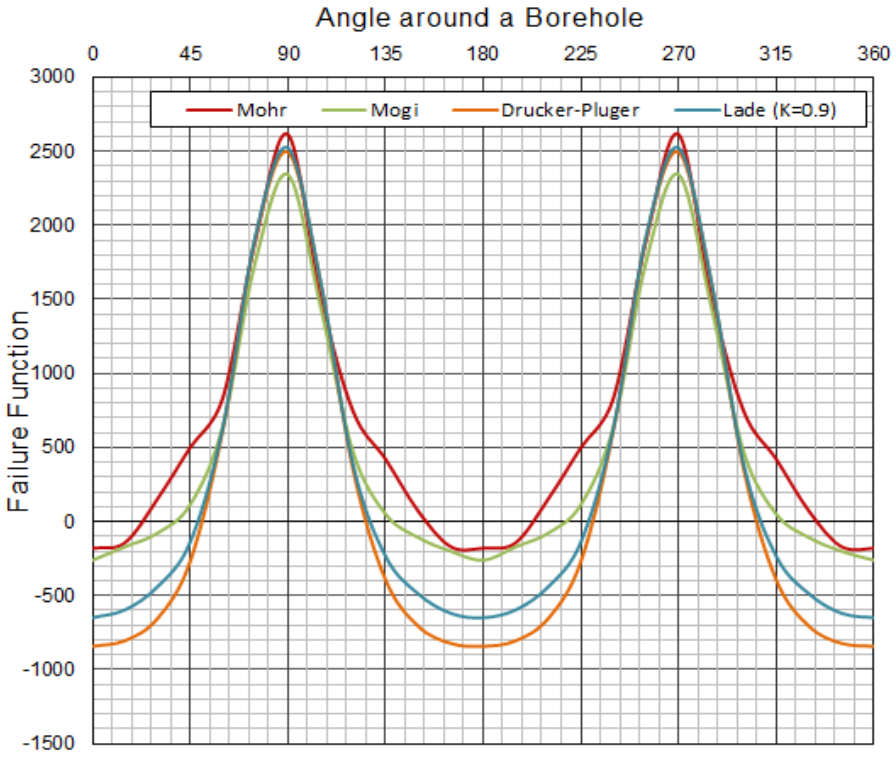

Figure III-27. Breakout prediction around borehole with effect of formation with transversely isotropic elastic material (well angle = 60°)

Table III-20. Breakout angle predicted by failure criteria in the base condition with the effect of formation with transversely isotropic elastic material (well angle = 60°)

Failure Criteria	Breakout Angle
Mohr	132°
Mogi	106°
Lade	94°
Drucker-Prager	80°

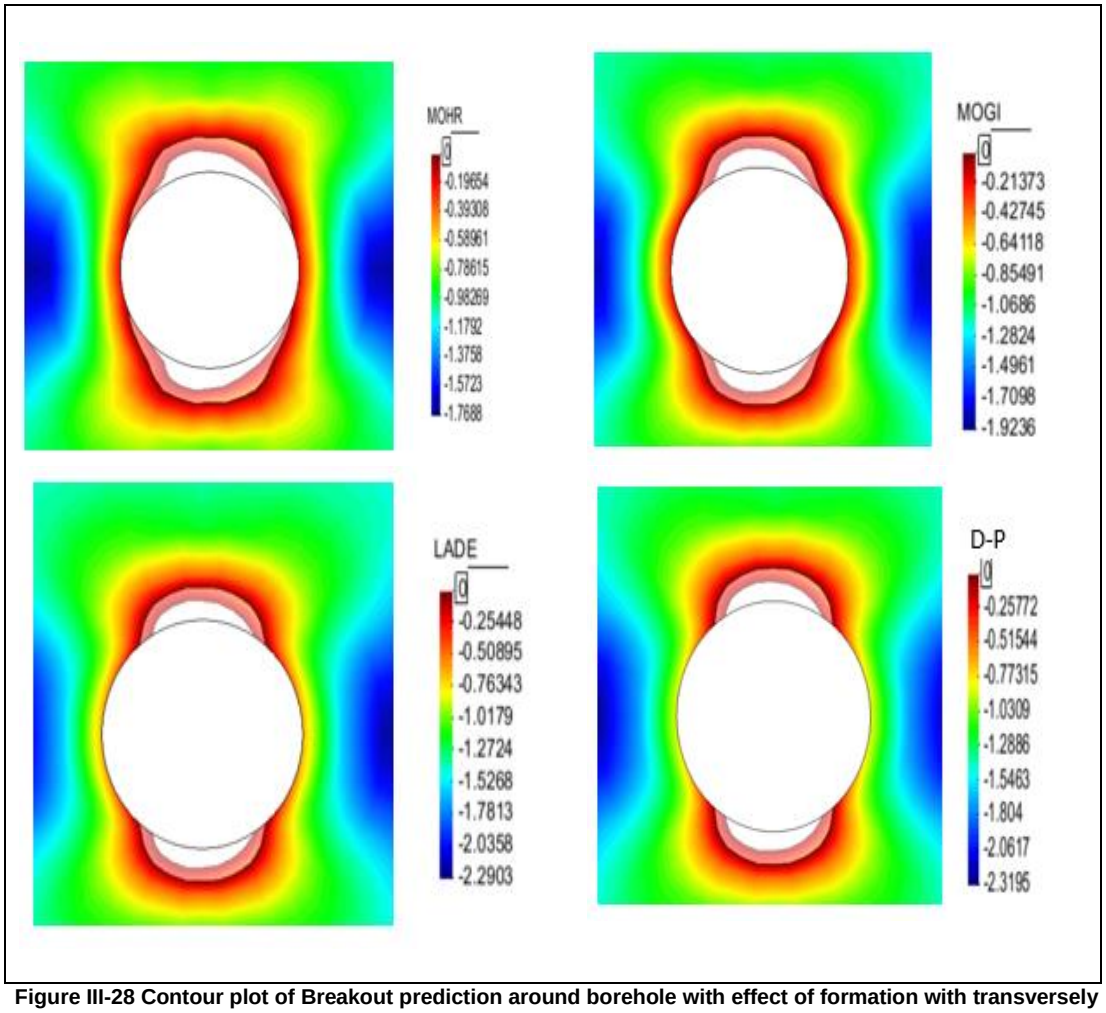

Figure III-28 Contour plot of Breakout prediction around borehole with effect of formation with transversely isotropic elastic material (well angle = 60°)

d. Well angle =90

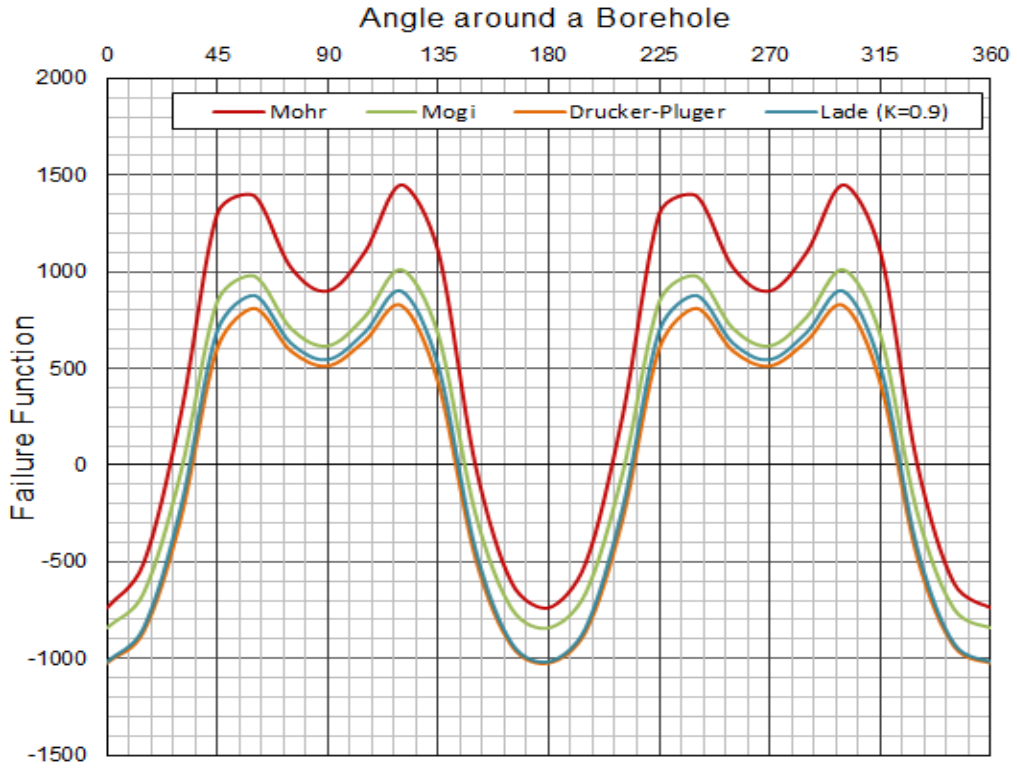

Figure III-29. Breakout prediction around borehole with effect of formation with transversely isotropic elastic material (well angle =90°)

Table III-21. Breakout angle predicted by failure criteria in the base condition with the effect of formation with transversely isotropic elastic material (well angle = 90°)

Failure Criteria	Breakout Angle
Mohr	126°
Mogi	100°
Lade	114°
Drucker-Prager	110°

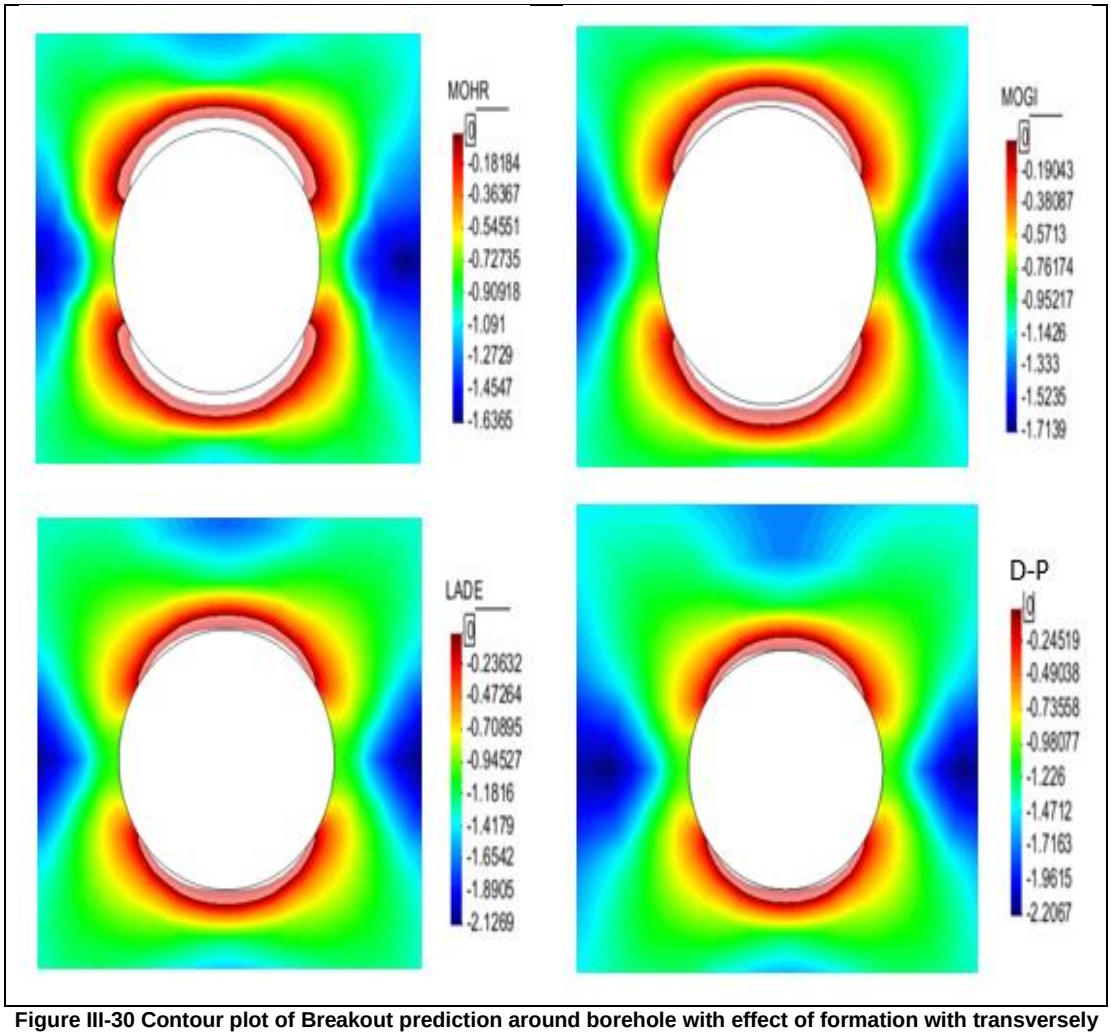

Figure III-30 Contour plot of Breakout prediction around borehole with effect of formation with transversely isotropic elastic material (well angle =90°)

3.3.2 Breakout angle predicted by the four rock failure criteria of horizontal well in depleted reservoir condition

3.3.2.1 Depleted Reservoir Condition

All the failure calculations are based on the results from the stress state around a borehole for horizontal well in depleted reservoir condition in Table II-2.

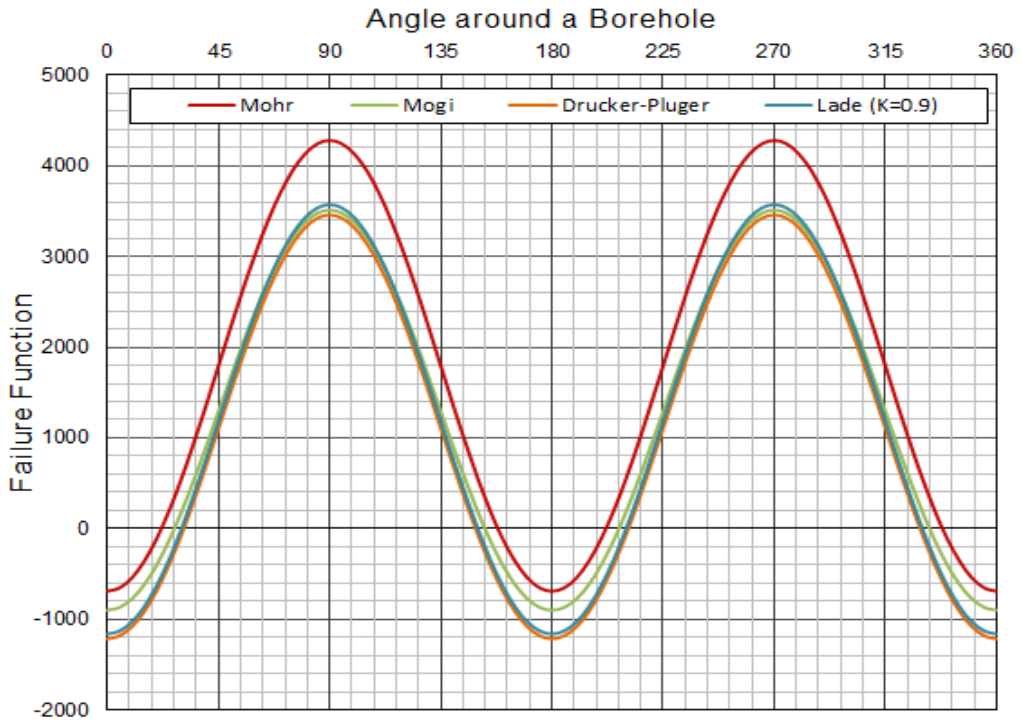

Figure III-31. Breakout prediction around borehole in depleted reservoir condition

Table III-22. Breakout angle predicted by failure criteria in depleted reservoir condition

Failure Criteria	Breakout Angle
Mohr	138°
Mogi	126°
Lade	118°
Drucker-Prager	116°

Fig. III-31 illustrates calculated failure function ($\tau - f(\sigma_m)$) versus angle around the wellbore in depleted reservoir condition. In this condition, all the failure criteria show a large value of breakout, as shown in the Table III-22. Therefore, the borehole will be unstable after the depletion of reservoir.

3.3.2.2 Osmosis Effect

In this case, we assume the borehole surface pore pressure has dropped by -500 psi behind the cake due to osmosis effect. The radius of the pressure drop is assumed to be 2 ft. The wellbore pressure is maintained with 500 psi overbalance.

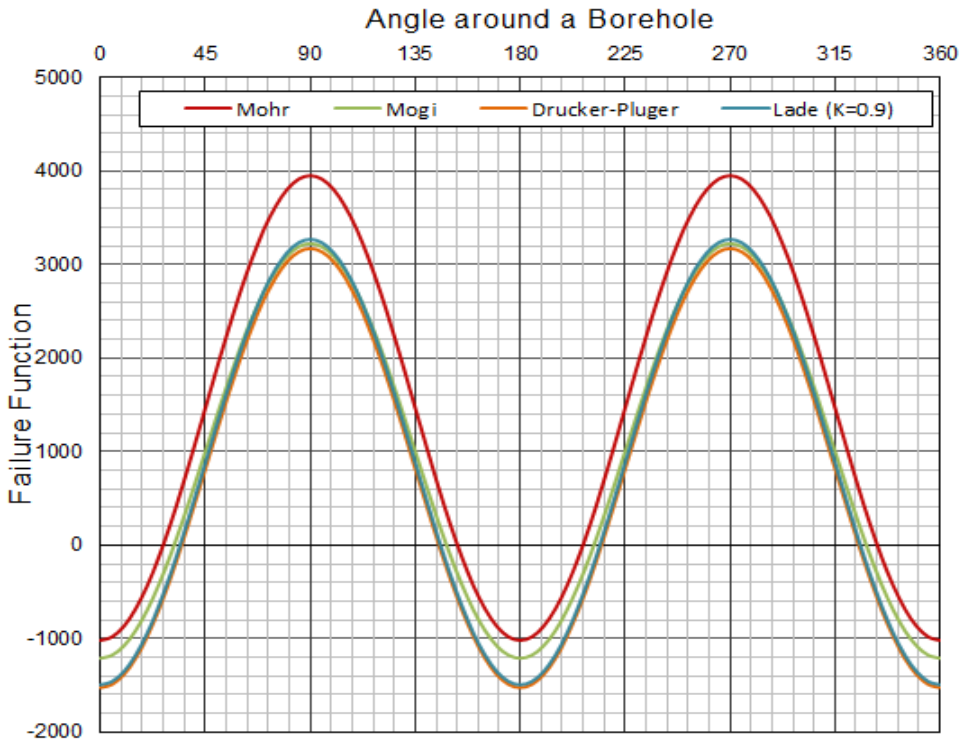

Figure III-32. Breakout prediction around borehole in depleted reservoir condition with the effect of osmosis

Table III-23. Breakout angle predicted by failure criteria in depleted reservoir condition with the effect of osmosis

Failure Criteria	Breakout Angle
Mohr	126°
Mogi	116°
Lade	112°
Drucker-Prager	108°

As the results shown in Fig. III-32 and Table III-23, with the effect of osmosis, the breakout angle is also reduced compared with the depleted condition without any effect.

3.3.2.3 Swelling Effect

0.2 % swelling is assumed at the wellbore surface (ΔS) and the swelling radius (rs) is 0.7 ft.

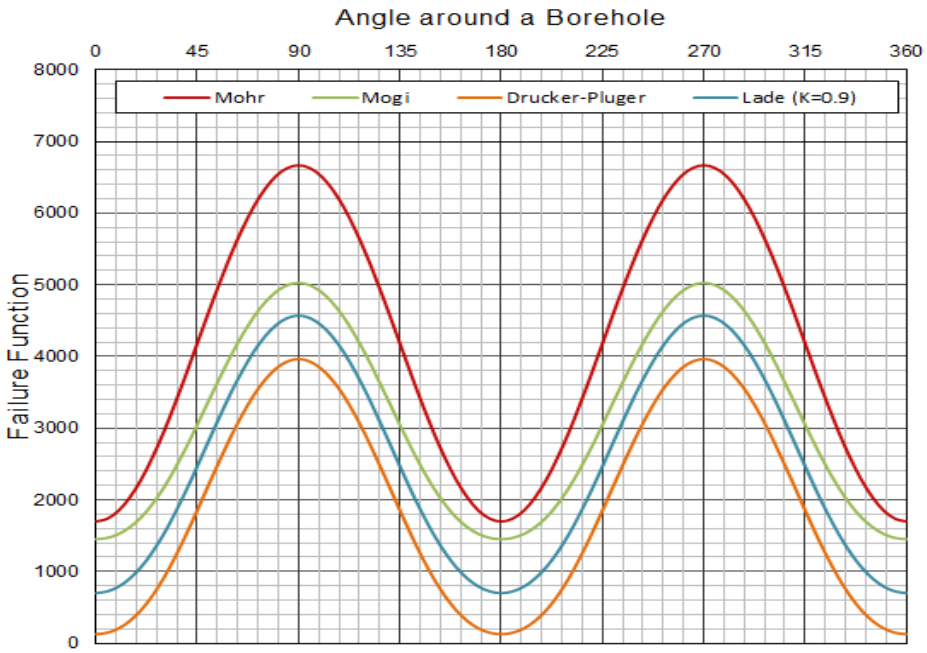

Figure III-33. Breakout prediction around borehole in depleted reservoir condition with the effect of shale swelling

Table III-24. Breakout angle predicted by failure criteria in depleted reservoir condition with the effect of shale swelling

Failure Criteria	Breakout Angle
Mohr	All Failure
Mogi	All Failure
Lade	All Failure
Drucker-Prager	All Failure

As the results shown in Fig. III-33 and Table III-24, with the effect of shale swelling, the borehole shows in all failure condition, which proves the significant effect of shale swelling on borehole stability.

3.3.2.4 Temperature Effect

Assume that a temperature change of 50°C occurs within the radius of 0.7 ft. The linear expansion coefficient is given as 1.e-5 1/ºC.

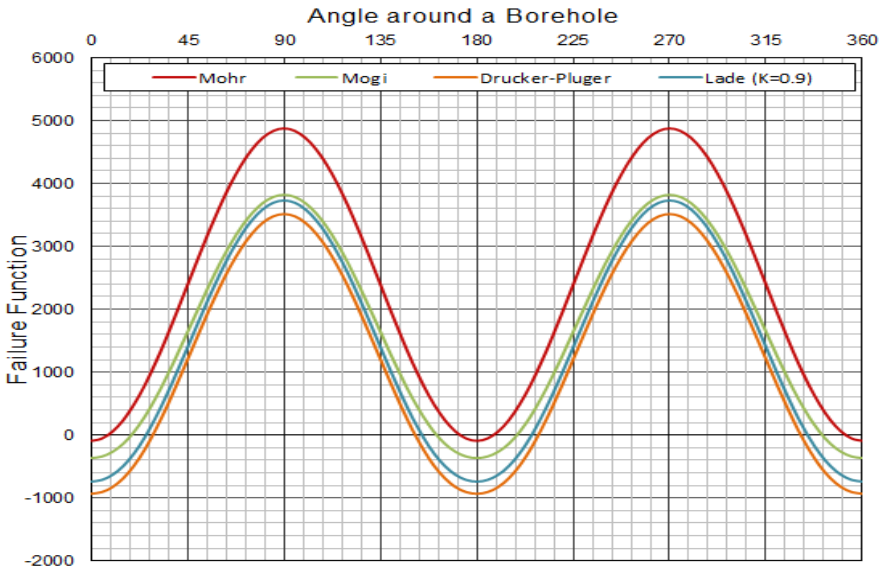

Figure III-34. Breakout prediction around borehole in depleted reservoir condition with the effect of temperature

Table III-25. Breakout angle predicted by failure criteria in depleted reservoir condition with the effect of temperature

Failure Criteria	Breakout Angle
Mohr	162°
Mogi	144°
Lade	128°
Drucker-Prager	122°

As the results shown in Fig. III-34 and Table III-25, the temperature change also leads to very large breakout angles that cause borehole instability, although the magnitude is smaller compared with welling.

3.3.2.5 Overbalance Effect

Assume wellbore pressure to increase to 3500 psi at the original reservoir conditions. It means the overbalance for this condition will be 1500 psi.

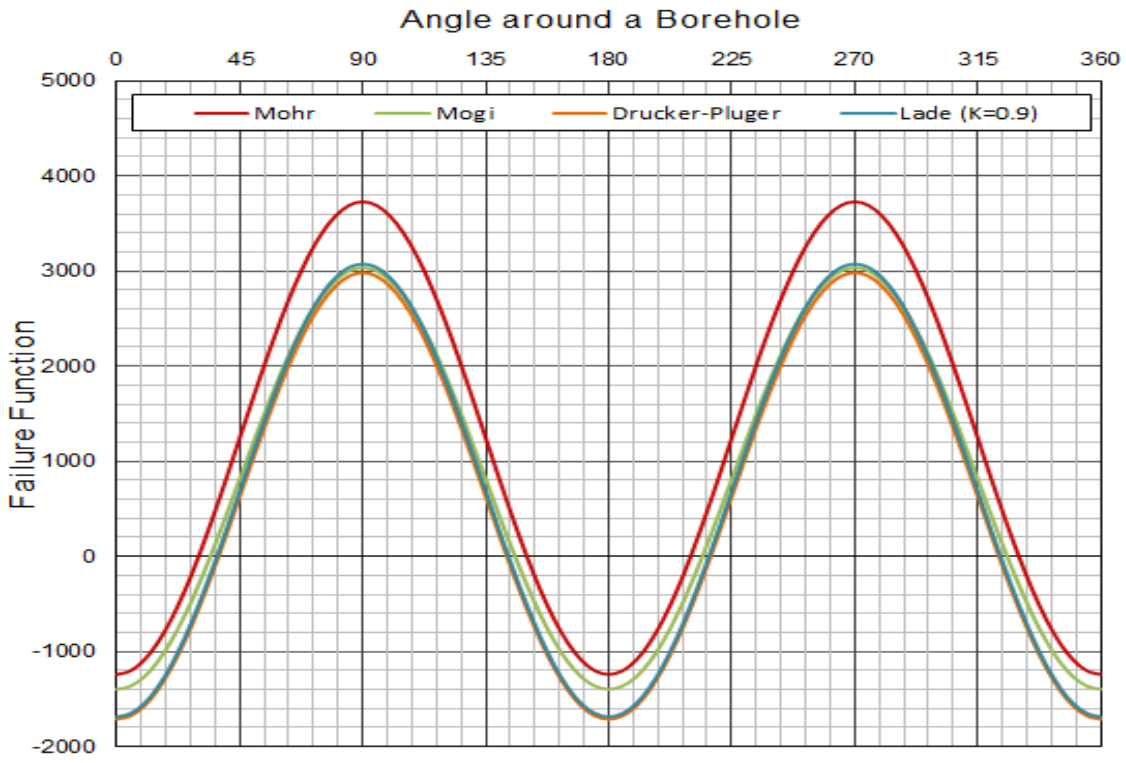

Figure III-35. Breakout prediction around borehole in depleted reservoir condition with the effect of overbalance

Table III-26. Breakout angle predicted by failure criteria in depleted reservoir condition with the effect of overbalance

Failure Criteria	Breakout Angle
Mohr	120°
Mogi	112°
Lade	106°
Drucker-Prager	104°

As the results shown in Fig. III-35 and Table III-26, with the effect of overbalance, the breakout angle is also reduced compared with the depleted condition without any effect, however, the breakout angles are too large, which result in absolute instability of the borehole.

3.3.2.6 Drawdown Effect

Assume that the pore pressure change due to drawdown is – 500 psi and the radius of pressure drop is equal to 2 ft.

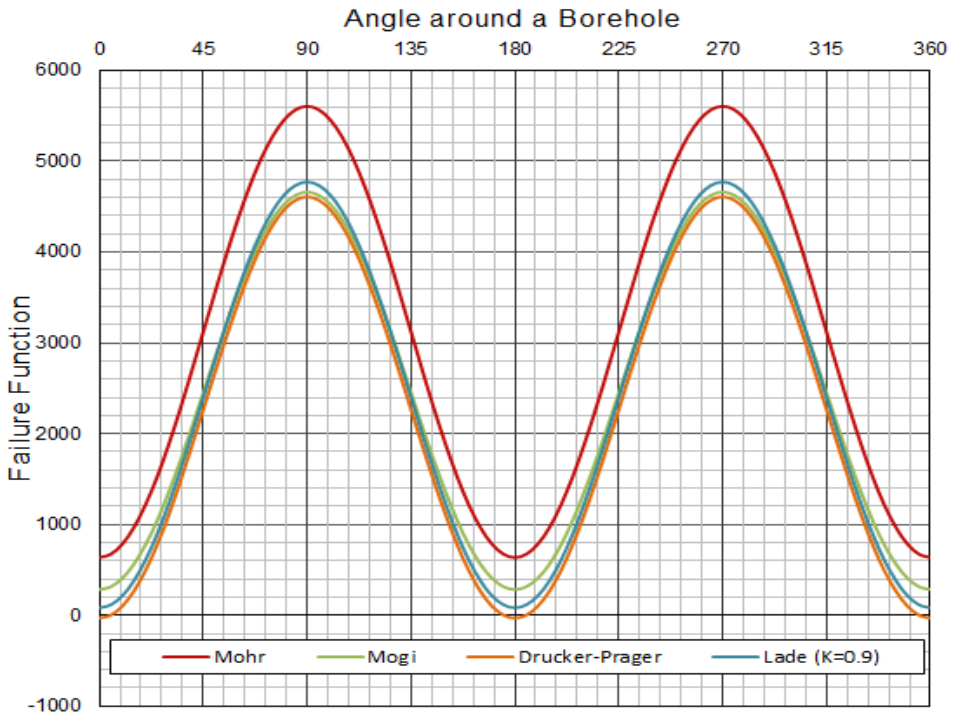

Figure III-36. Breakout prediction around borehole in depleted reservoir condition with the effect of drawdown

Table III-27. Breakout angle predicted by failure criteria in depleted reservoir condition with the effect of drawdown

Failure Criteria	Breakout Angle
Mohr	All Failure
Mogi	All Failure
Lade	All Failure
Drucker-Prager	168°

As the results shown in Fig. III-36 and Table III-27, in the depleted reservoir condition for the horizontal well, the pressure drawdown also enlarges the breakout angle around borehole.

3.3.2.7 Sandstone Non-Linearity Effect

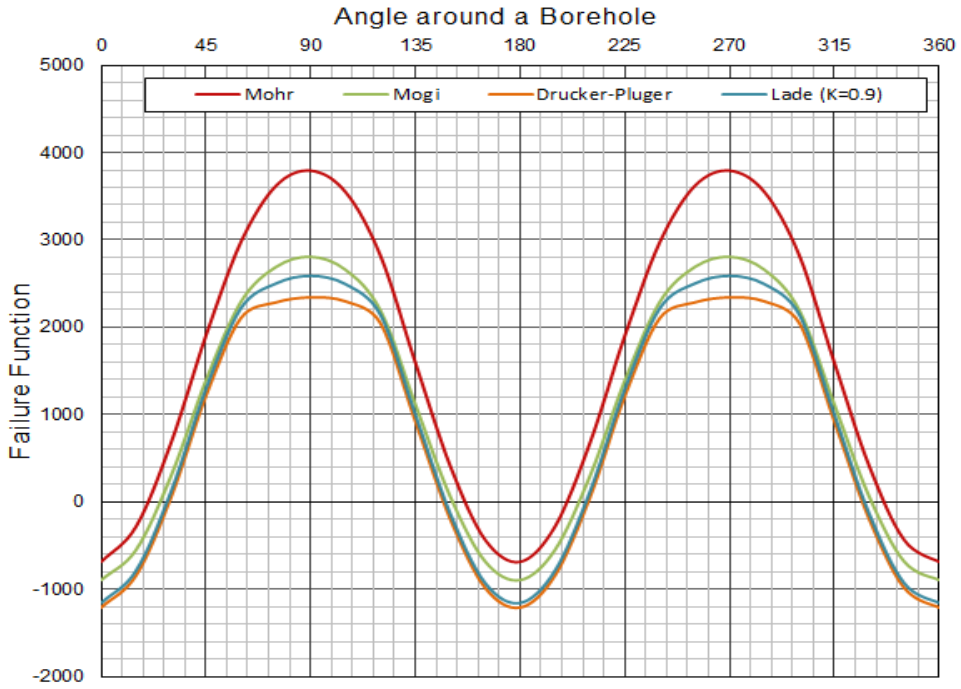

Figure III-37. Breakout prediction around borehole in depleted reservoir condition with the effect of sandstone non-linearity

Table III-28. Breakout angle predicted by failure criteria in depleted reservoir condition with the effect of sandstone non-linearity

Failure Criteria	Breakout Angle
Mohr	134°
Mogi	126°
Lade	117°
Drucker-Prager	116°

As shown in Fig. III-37 and Table III-28, with the effect of non-linearity sandstone formation, the breakout angle is a little reduced compared with the depleted condition without any effect.

3.4 Conclusion

It is straightforward that Mohr and Mogi failure model predicts a relatively large breakout width, while Drucker-Prager and Lade predicts a relatively small value. Tables III-29 to III-32 are the summary of the results. The peak of each failure function and breakout angle are used as the quantitative indicators of the wellbore stability. The difference of the function peaks between the current parameter and the base case indicates the qualitative sensitivity of the parameter to borehole failure. The negative value indicates the improvement of the stability and the positive value indicates the higher instability. For example, the largest value is for shale swelling. Note that the effect of the shale swelling is proportional to $E/(1-\nu)$ so that the difference from the base case will reduce if E is smaller than 3×10^6 psi. The parameters in red ink show de-stabilization factors, while those in green show stabilization factors. The temperature is a de-stabilization factor if warming while it is a stabilization factor if cooling.

Table III-29 Changes in peak of the failure function and the difference from the base case

	Peak of failure function				Difference from the base case			
	Mohr	Mogi	Lade	Drucker	Mohr	Mogi	Lade	Drucker
The base case	240	70	-355	-580	0	0	0	0
Inclination 30º Azimuth=0	500	165	0	-70	260	95	355	510
Inclination 60º Azimuth=0	1220	870	780	720	980	800	1135	1300
Inclination 90º Azimuth=0	1510	1100	1020	980	1270	1030	1375	1560
Inclination 30º Azimuth=90	800	360	100	-50	560	290	455	530
Inclination 60º Azimuth=90	1410	920	780	660	1170	850	1135	1240
Inclination 90º Azimuth=90	1680	1170	1010	910	1440	1100	1365	1490
Swelling 0.2%	2620	2530	1600	875	2380	2460	1955	1455
Osmosis -500psi	-85	-280	-720	-940	-325	-350	-365	-360
Temperature 50ºC	840	670	135	-240	600	600	490	340
Overbalance 500psi	-310	-400	-845	-1060	-550	-470	-490	-480
Drawdown -500psi	470	195	-200	-470	230	125	155	110
Layer(adjacent E= 6×10^6 psi),0º	240	70	-355	-580	0	0	0	0
Layer(adjacent E= 6×10^6 psi) ,60º	95	0	-420	-660	-145	-70	-65	-80
Layer (adjacent E= 1.5×10^6 psi),0º	240	50	-380	-640	0	-20	-25	-60
Layer (adjacent E= 1.5×10^6 psi),60º	280	50	-375	-600	-40	-20	-20	-20
Orthotropic $\theta = 0^o$	240	75	-350	-605	0	5	5	25
Orthotropic $\theta = 30^o$	430	170	40	10	190	100	395	590
Orthotropic $\theta = 60^o$	2600	2330	2510	2500	2360	2260	2865	3080
Orthotropic $\theta = 90^o$	1400	995	890	800	1160	925	1245	1380

Table III-30 Breakout angle

	Breakout angle (º)			
	Mohr	Mogi	Lade	Drucker
The base case	76	54	0	0
Inclination 30º Azimuth=0	360	90	0	0
Inclination 60º Azimuth=0	138	110	98	90
Inclination 90º Azimuth=0	136	108	100	94
Inclination 30º Azimuth=90	114	88	36	0
Inclination 60º Azimuth=90	112	94	78	72
Inclination 90º Azimuth=90	108	92	82	78
Swelling 0.2%	360	360	360	360
Osmosis -500psi	0	0	0	0
Temperature 50ºC	360	360	76	0
Overbalance 500psi	0	0	0	0
Drawdown -500psi	120	104	0	0
Layer(adjacent E 6×10^6 psi),0º	76	60	0	0
Layer(adjacen tE 6×10^6 psi) ,60º	48	6	0	0
Layer (adjacent E=1.5×10^6 psi),0º	70	40	0	0
Layer (adjacent E=1.5×10^6 psi),60º	90	40	0	0
Orthotropic $\theta = 0^o$	72	54	0	0
Orthotropic $\theta = 30^o$	360	94	32	18
Orthotropic $\theta = 60^o$	132	106	94	80
Orthotropic $\theta = 90^o$	126	100	114	110

Table III-31 Changes in peak of the failure function and breakout angle for deplete reservoir

	Peak of failure function				Difference from the base case			
	Mohr	Mogi	Lade	Drucker	Mohr	Mogi	Lade	Drucker
The base case	4025	3500	3600	3450	0	0	0	0
Swelling 0.2%	6610	5000	4600	4000	2585	1500	1000	550
Osmosis -500psi	3950	3200	3250	3190	-75	-300	-350	-260
Temperature 50ºC	4830	3800	3760	3500	355	300	160	150
Overbalance 500psi	3710	3040	3050	3000	-315	-460	-550	-450
Drawdown -500psi	5600	4650	4800	4600	1575	1150	1200	1150
Non-linear	3800	2800	2600	2350	-225	-700	-1000	-1100

Table III-32 Breakout angle for deplete reservoir

	Breakout angle (º)			
	Mohr	Mogi	Lade	Drucker
The base case	138º	126º	118º	116º
Swelling 0.2%	360	360	360	360
Osmosis -500psi	126	115	112	108
Temperature 50ºC	162	144	128	122
Overbalance 500psi	120	112	106	104
Drawdown -500psi	360	360	360	168
Non-linear	134	126	117	116

Comparing the results from various controllable parameters, it should be pointed out that:

Factors destabilizing borehole

1) Swelling effect seriously affects the borehole stability, which easily cause borehole total failure.
2) Well inclination also significantly affects the borehole stability.
3) Temperature increase is the secondary factor to de-stabilize borehole

4) Layering of heterogeneous formations and orthotropic formation do not affect the stability of borehole if it is a vertical hole. If the formation angle becomes higher, the borehole becomes unstable as the isotropic and non-heterogeneous formation. However, if the degree of heterogeneity or anisotropy is less than 2, the instability is not so serious, although it may not be the case if it is large.

Factors stabilizing borehole

1) Eliminating the shale swelling is the most important factor to stabilizing borehole.
2) Non-linearity of rock, overbalance and pore pressure reduction due to osmosis are the factors stabilizing borehole and they are equally important.
3) Effect of the overbalance, pore pressure, shale welling, pore pressure change, and temperature change on well stability are independently expressed in this work to separate each effect. However, all thee parameters are actually dependent on each other.
   (A) If some overbalance is added, it reduces the tangential effective stress and increase the radial effective stress. The increase of the radial effective stress significantly reduces shale swelling according to the laboratory experiments on shale swelling with confining stresses. With these two effects, borehole stability significantly improves.
   (B) Some shale inhibitors reduce swelling and pore pressure due to osmosis. The pore pressure reduction reduces the swelling and reduction of swelling reduces the pore pressure, resulting in wellbore stability.
   (C) Temperature cooling reduces the tangential stress around a borehole by shrinking the formation. In addition, if the permeability of shale is close to zero, it also reduces the volume of the water trapped in shale since the water thermal expansion coefficient is significantly larger the formation thermal expansion coefficient.
   (D) Therefore, when borehole instability problem occurs due to shale swelling, it is important to consider interaction of all the parameters to stabilize borehole.

We can observe that results are consistent with the conclusion from the previous analysis of parameter effect on the stress state around a borehole in chapter 2.

CHAPTER IV

EFFECT OF CONTROLLABLE PARAMETERS ON SAFE MUD WINDOW DESIGN

4.1 Introduction of safe mud weight window

Wellbore instability is still one of the main problems that petroleum engineers need to concern during drilling. The controllable parameters that affect drilling of a hole are mud weight and wellbore azimuth and inclination. (Masoud Aslannezhad, 2016). Using a proper mud with shale swelling inhibitor is also important when the shale swelling is the problem. Therefore, the way to prevent wellbore instability is to choose optimal mud weight, well trajectory and selection of mud type.

From the mechanical perspective, wellbore instability is caused by stress concentration around a wellbore, resulting in shear and tensile failure. Therefore, the critical mud weight should be considered before drilling to reduce the stress concentration. Numerous drilling engineers tried to predicted wellbore breakout using different failure criteria and analyzed the stress state around borehole to obtain optimal safe mud weight window for successful drilling process.

The traditional safe mud weight window is determined by only considering well inclination and azimuth effect with in-situ stress. However, from the study of controllable parameters on stresses around borehole in chapter 2 and 3, comprehensive safe mud weight window should be designed in consistence with the effect of controllable parameters on stresses around borehole, including swelling, temperature, bedding layers, non-linearity and anisotropic shales. Therefore, the objective of this

chapter is to perform comprehensive examination of the instability of the wellbore using the Geo3D model. The results lead to designing comprehensive and optimal mud weight window and favorable drilling direction to improve drilling planning. In the section, we use both Mohr-Coulomb and Mogi criteria to determine the polar diagram of critical mud weight.

The polar diagrams of critical mud weight are plotted based on the safe mud weights versus well inclination (radial direction) and azimuth (circumferential direction). The field experiences indicate that during drilling process, vertical wells usually induce shallow and wide breakouts which do not cause the borehole instability, while the breakout of horizontal well is usually deep so that even a 30 º breakout angle can lead the borehole to unstable conditions. Furthermore, since the cuttings transport is not a problem near vertical wells, stuck pipe does not occur with a larger number of cuttings with wider breakouts. On the other hand, the low capability of cuttings transport in horizontal well section usually causes the problem that may accumulate a stationary bed. It causes stuck pipe. Therefore, we assume the following equation to compute the minimum safe mud weight. The equation gives the critical breakout angle to maintain well instability and to minimize drill pipe stuck problems, which is derived from field experiences.

$$\theta_{safe} < \theta_{critical} = 90° - 60° \sin \gamma$$

where

$\theta_{critical}$: Critical breakout angle

γ : Well inclination

For all the polar diagrams of safe mud weight, the maximum horizontal in-situ stress is oriented East-West and the minimum horizontal in-situ stress is oriented in the North-South direction in this work

4.2 Optimal Safe Mud Weight Window Design with Various Controllable Parameters

1. Polar Diagram of Safe Mud Window in the Base reservoir Condition

In this section, we use the reservoir condition shown in Table II-1 to specify the safe mud weight. The borehole stability problems are different for the three stress state regimes shown in Fig.IV-1. Therefore, the in-situ stress conditions are set into three cases shown in Table IV-1. The maximum in-situ stress $\sigma_{h\max}$ is oriented in West-East for all polar diagrams.

Table IV-1. Various in-situ stress conditions

$\sigma_v > \sigma_{h\max} > \sigma_{h\min}$	$\sigma_{h\max} > \sigma_v > \sigma_{h\min}$	$\sigma_{h\max} > \sigma_{h\min} > \sigma_v$
$\sigma_v = 10000\,psi$	$\sigma_v = 10000\,psi$	$\sigma_v = 10000\,psi$
$\sigma_{h\max} = 8500\,psi$	$\sigma_{h\max} = 11500\,psi$	$\sigma_{h\max} = 12500\,psi$
$\sigma_{h\min} = 8000\,psi$	$\sigma_{h\min} = 9000\,psi$	$\sigma_{h\min} = 12000\,psi$

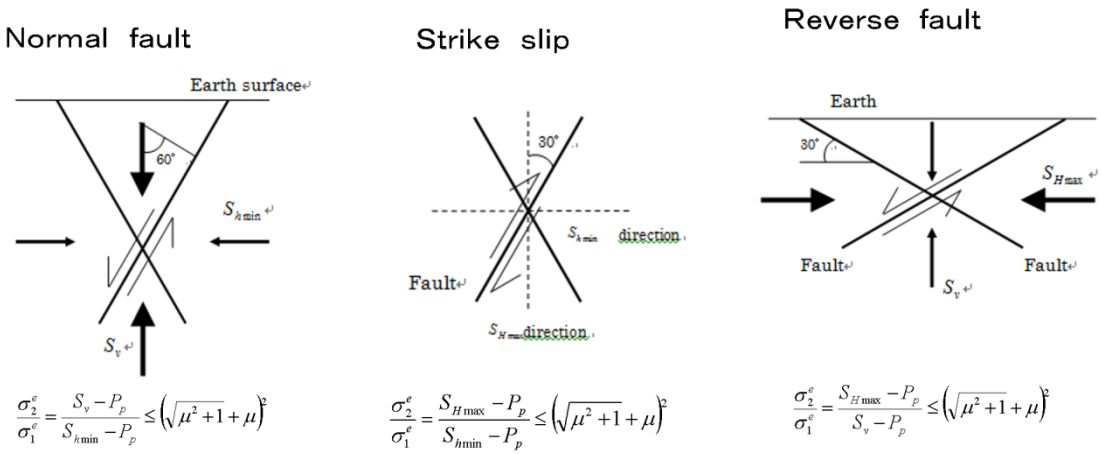

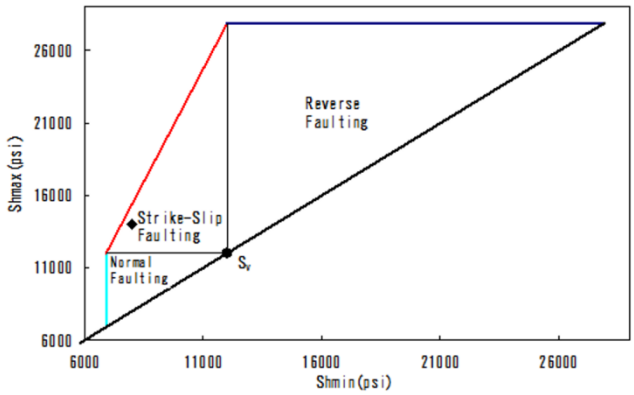

Figure IV-1 Three stress state regimes of the earth crust

The base reservoir condition without any other effect except for the normal faulting regime.

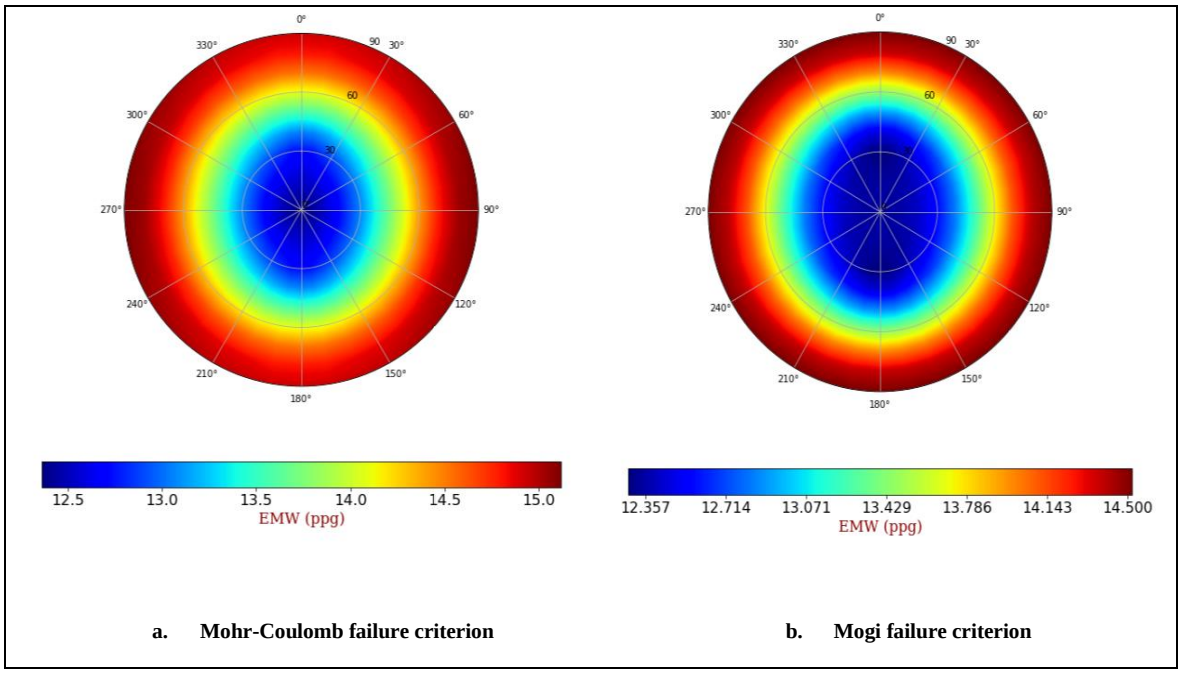

a. Mohr-Coulomb failure criterion

b. Mogi failure criterion

Figure IV-2. Minimum mud weight to avoid shear collapse for an inclined well in the base field condition without any under the normal faulting regime. The center of the polar diagram stands for vertical wells and the outer ring corresponds to horizontal wells.

From Fig. IV-2, the minimum mud weight ranges from 12.5 ppg to 15.5 ppg predicted by Mohr-Coulomb failure criteria for an inclined well in the base reservoir condition, while the Mogi failure criteria shows the minimum mud weight ranges from 12 ppg to 14.5 ppg. The difference is that Mogi's failure criteria takes into account the effect of intermediate principal stress so that the safe mud weight is less and the well orientation effect is also less. For the normal in-situ stress regime, the polar diagram shows the wells oriented along the minimum horizontal direction (North-South direction) is more stable with a lower mud weight than those oriented in the maximum horizontal in-situ stress direction (West-East) although the difference is small.

The base reservoir condition without any other effect under the strike-slip faulting regime.

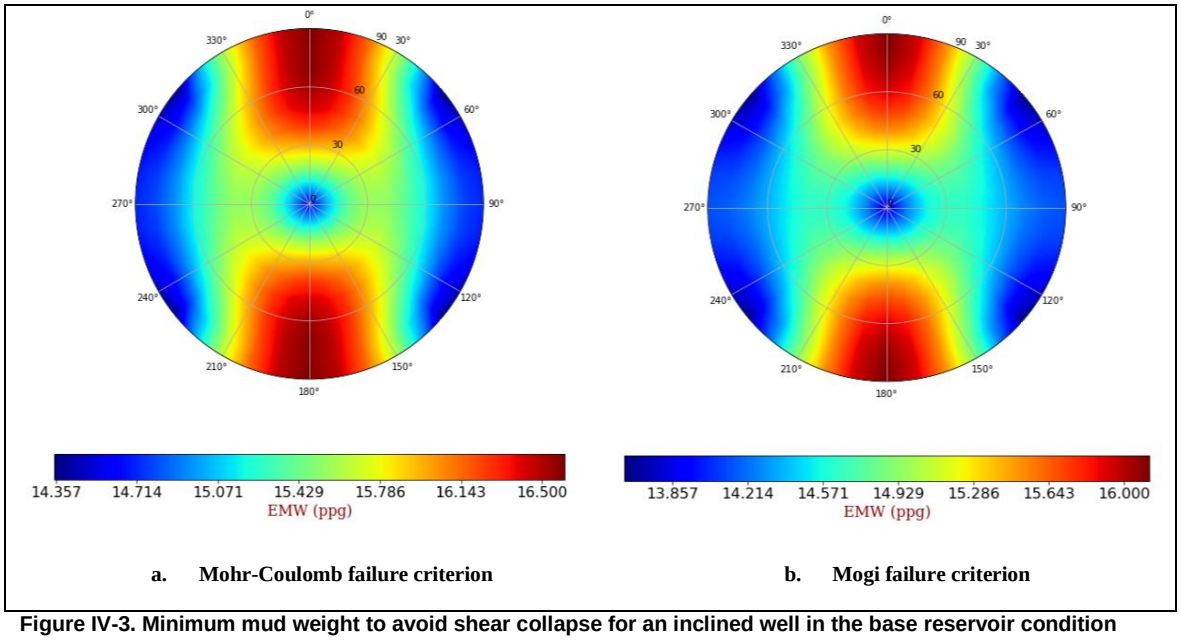

a. Mohr-Coulomb failure criterion **b. Mogi failure criterion**

Figure IV-3. Minimum mud weight to avoid shear collapse for an inclined well in the base reservoir condition without any effect under the strike-slip faulting regime. The center of the polar diagram stands for vertical wells and the outer ring correspond to horizontal wells.

From Fig. IV-3, the minimum mud weight ranges from 14 ppg to 17 ppg predicted by Mohr-Coulomb failure criteria for an inclined well in the base reservoir condition without any effect and the Mogi failure criteria shows the minimum mud weight ranges from 13.5 ppg to 16.5 ppg. In addition, under the strike-slip faulting regime, it is less mud weight to drilling in the maximum horizontal in-situ stress direction (West-East), which behaves totally different with the drilling in the normal fault regime. Therefore, it concludes that in-situ stress condition can significantly affect the drilling direction and well trajectory.

The base reservoir condition without any other effect under the reverse faulting regime.

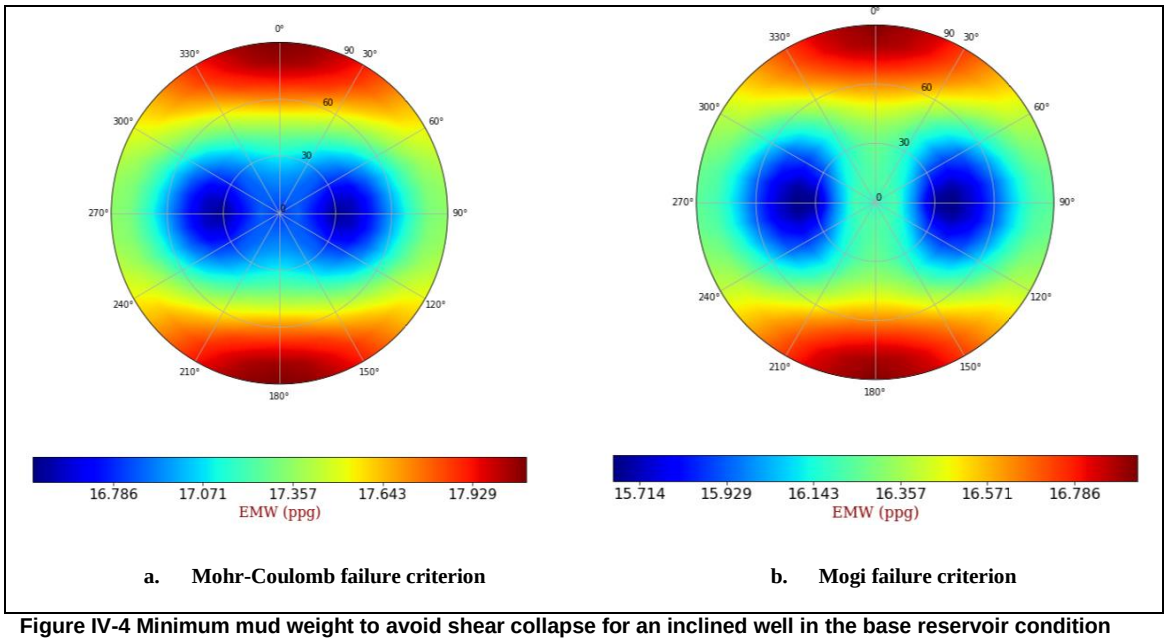

a. Mohr-Coulomb failure criterion **b. Mogi failure criterion**

Figure IV-4 Minimum mud weight to avoid shear collapse for an inclined well in the base reservoir condition without any effect under the revere faulting regime. The center of the polar diagram stands for vertical wells and the outer ring correspond to horizontal wells.

From Fig. IV-4, the minimum mud weight ranges from 16.5 ppg to 18.4 ppg predicted by Mohr-Coulomb failure criteria for an inclined well in the base reservoir condition without any effect and the Mogi failure criteria shows the minimum mud weight ranges from 15.6 ppg to 17.0 ppg. In addition, under the reverse faulting regime, it is less mud weight to drilling in the maximum horizontal in-situ stress direction (West-East), which behaves totally different compared with the drilling in the normal fault regime. Therefore, it concludes that in-situ stress condition can significantly affect the drilling direction and well trajectory.

2. Critical mud weight polar diagram for Shale Swelling

Based on previous study, we know shale swelling significantly affects the stress state around borehole and causes serious borehole instability problems. Therefore, we assume 0.1%, 0.2%, 0.3% shale swelling to occur at the wellbore surface (ΔS) and the swelling radius (rs) to be 0.7 ft to calculate the critical mud weight polar diagram. The critical mud weight polar diagrams for 0.1%, 0.2%, 0.3% shale swelling with Mohr-Coulomb failure criteria are used to evaluate how the change of shale swelling affects the range of safe mud weight.

In addition, we also plot the polar diagram of critical mud weight in the strike-slip faulting and the reverse faulting regimes with 0.2% shale swelling.

0.2% shale swelling under the normal faulting regime:

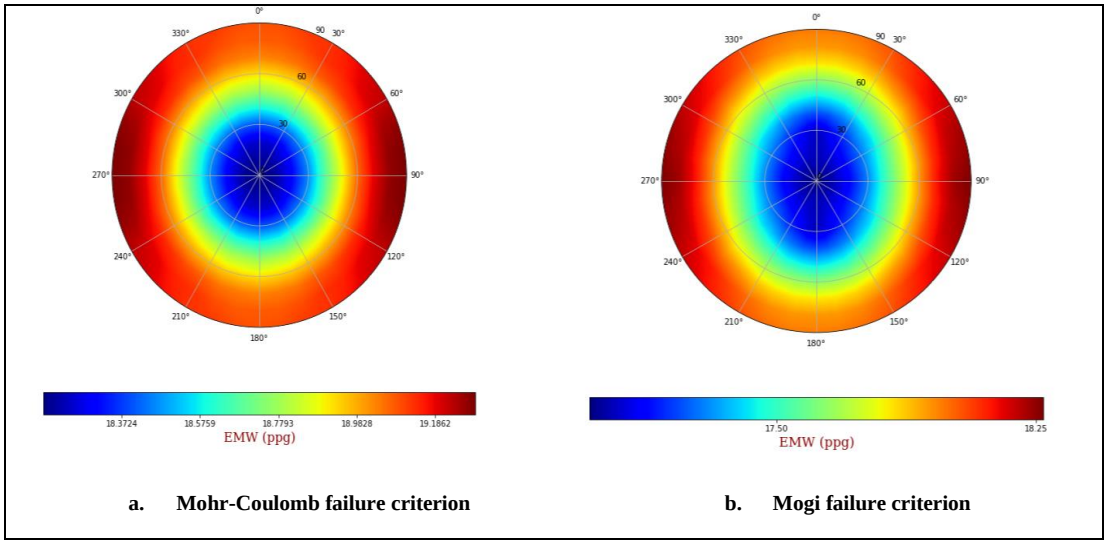

a. Mohr-Coulomb failure criterion

b. Mogi failure criterion

Figure -IV-5 Minimum mud weight to avoid shear collapse for an inclined well in the base field condition due to effect of 0.2% shale swelling under the normal faulting regime. The center of the polar diagram stands for vertical wells and the outer ring correspond to horizontal wells. The drilling azimuthal direction is measured from North (top), in the clockwise direction.

From Fig. IV-5, the minimum mud weight ranges from 18 ppg to 19.5 ppg predicted by Mohr-Coulomb failure criteria for an inclined well in the base reservoir condition with 0.2% shale swelling and the Mogi failure criteria shows the minimum mud weight ranges from 17 ppg to 18.3 ppg. From the results, we can easily find that it is consistent with the conclusion we obtain in the previous sections that shale swelling causes serious borehole instability problem and it requires larger mud weight to prevent borehole failure. In addition, in the normal faulting regime, it also indicates that it is easier to drill along the direction of North-South (NS), although the difference of the safe mud weight between North-South and East-West is trivial.

0.1% shale swelling under the normal faulting regime

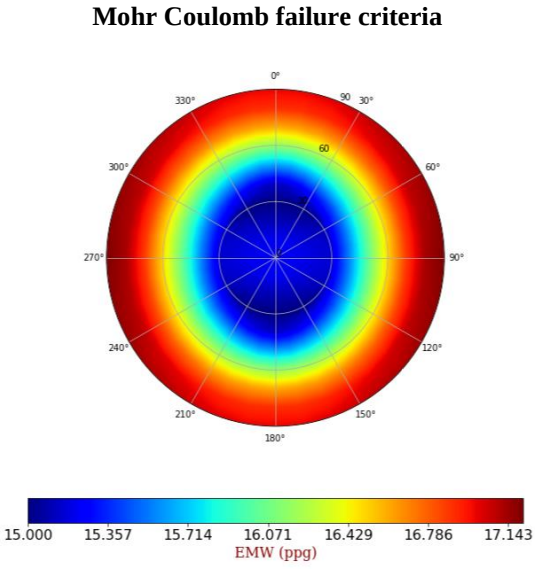

Figure IV-6.Minimum mud weight to avoid shear collapse for an inclined well in the base field condition due to effect of 0.1% shale swelling. The center of the polar diagram stands for vertical wells and the outer ring correspond to horizontal wells.

0.3% shale swelling under the normal faulting regime

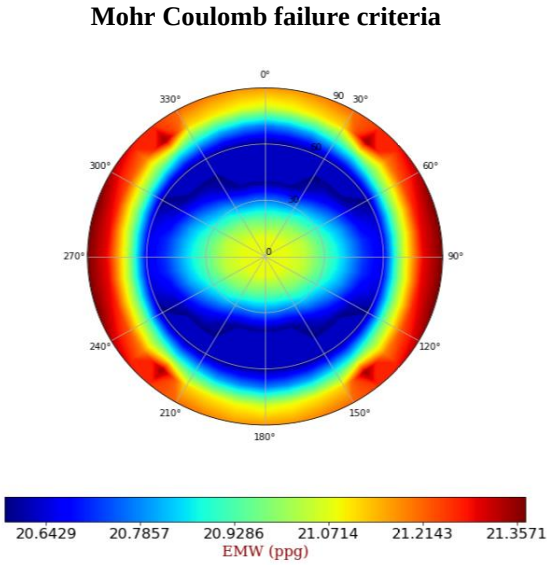

Figure IV-7. Minimum mud weight to avoid shear collapse for an inclined well in the base field condition due to effect of 0.3% shale swelling. The center of the polar diagram stands for vertical wells and the outer ring correspond to horizontal wells.

As shown in Fig. IV-6 and Fig. IV-7, the 0.1% shale swelling requires the mud weight ranging from 15 to 17 ppg and the 0.3 % shale swelling requires a larger range of mud weight as large as 20 to 21.5 ppg. Note that the mud weight 19.2 ppg creates 1psi/ft, therefore, the mud weight exceeding 19.2 may induce a lost circulation problem with a horizontal fracture. Therefore, according to the sensitivity analysis of shale swelling, the change in the magnitude of shale swelling heavily affects the mud weight, that is, even only 0.1% change in shale swelling can cause the mud weight increase or decrease.

0.2% shale swelling under the strike-slip faulting regime

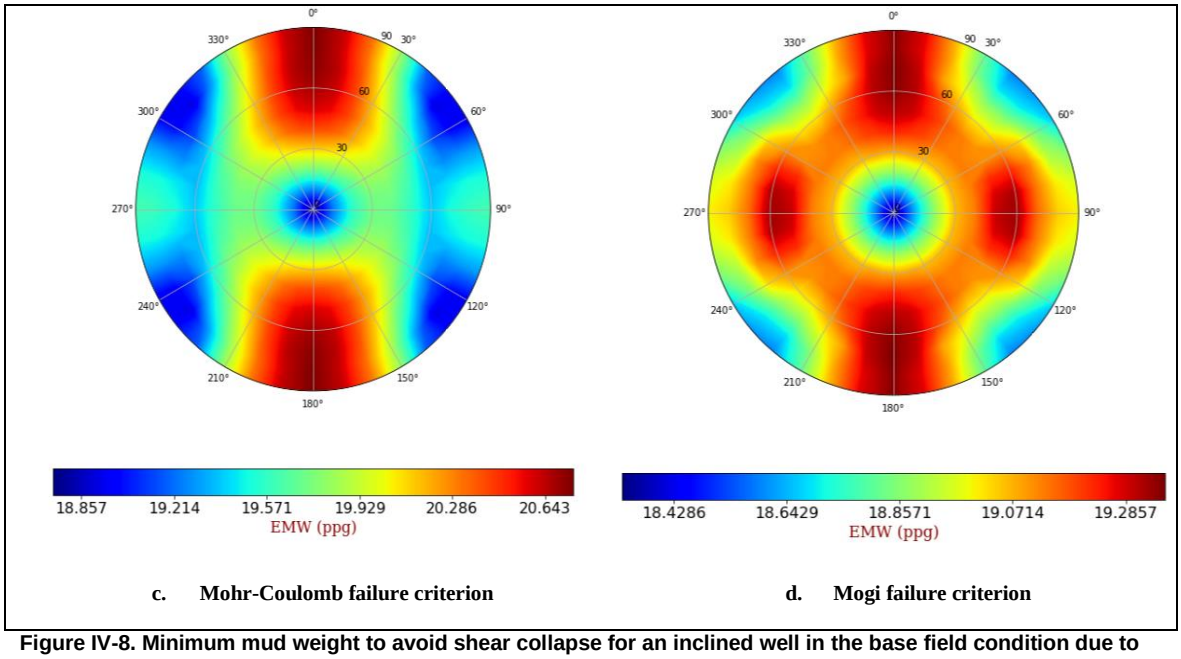

c. **Mohr-Coulomb failure criterion** d. **Mogi failure criterion**

Figure IV-8. Minimum mud weight to avoid shear collapse for an inclined well in the base field condition due to effect of 0.2% shale swelling under the strike-slip faulting regime. The center of the polar diagram stands for vertical wells and the outer ring correspond to horizontal wells.

As shown in Fig. IV-8, by comparing the result from Fig. IV-5, it demonstrates that it is safer drilling in the direction of WEST-EAST (WE) under the strike-slip faulting regime with Mohr-Coulomb failure criterion while the difference of the safe mud weight between North-South and East-West is trivial for Mogi's failure theory. It is important to emphasize that the effect of in-situ stress becomes less under the condition of shale swelling.

0.2% shale swelling under the reverse faulting regime

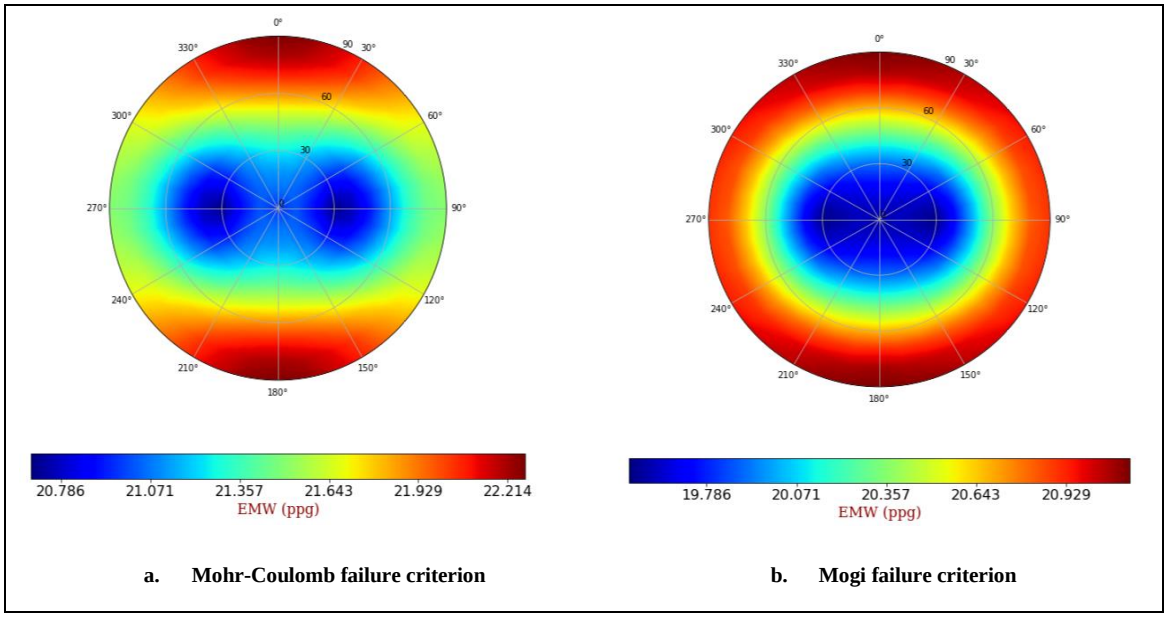

a. Mohr-Coulomb failure criterion **b. Mogi failure criterion**

Figure IV-9 Minimum mud weight to avoid shear collapse for an inclined well in the base field condition due to effect of 0.2% shale swelling at in-situ stress condition of $\sigma_h > \sigma_v$. The center of the polar diagram stands for vertical wells and the outer ring correspond to horizontal wells.

As shown in Fig. IV-9, by comparing the result from Fig. IV-5, it also demonstrates that it is easier drilling in the direction of WEST-EAST (WE) under Mohr-Coulomb since the safe mud weights between West-East and North-South are significantly different.

3. Safe Mud Weight Window due to Temperature Effect

A temperature increases in 50°C is considered within the radius of 0.7 ft. The linear expansion coefficient is given by 1.e-5 1/ºC.

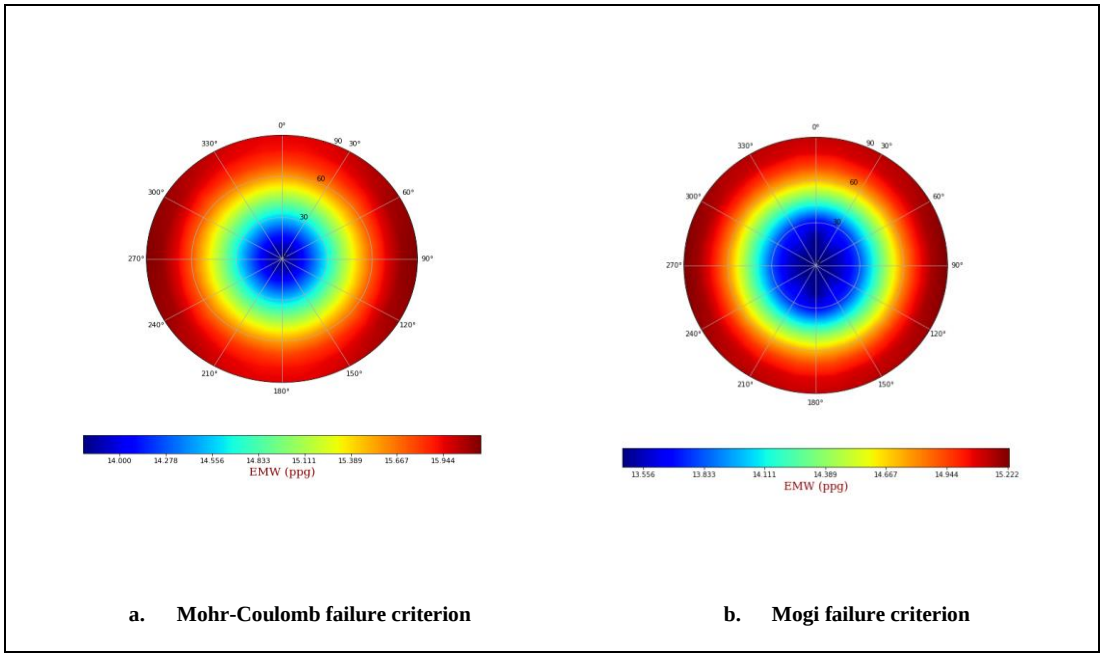

a. Mohr-Coulomb failure criterion **b. Mogi failure criterion**

Figure IV-10.Minimum mud weight to avoid shear collapse for an inclined well in the base field condition due to effect of temperature change of 50 °C. The center of the polar diagram stands for vertical wells and the outer ring correspond to horizontal wells. The drilling azimuthal direction is measured from north (top), in the clockwise direction.

.

Fig. IV-10 shows the safe mud weight with the temperature increase in 50 ºC: the minimum mud weight ranges from 13.5 ppg to 16 ppg with Mohr-Coulomb failure criteria and the Mogi failure criteria shows the minimum mud weight ranges from 13 ppg to 15.3 ppg. From the results, it confirms that temperature increase causes borehole instability problem and it required larger mud weight to prevent borehole failure although it is not as serious as shale swelling. In addition, under the normal faulting regime, it also indicates that it is safer to drill along the direction of North-South (NS), and East-West is trivial.

4. Safe Mud Weight Window due to Hard Bedding Layer Effect

Chapter 3 shows that for a vertical well, the wellbore stability is not affected by formation bedding with different elastic moduli. For inclined wells, the borehole becomes unstable with well inclination. However, if the ratio of Young's modulus of alternating layers is less than 2, the stability slightly improves since the formation of larger Young's modulus takes more load and the stress concentration of the weaker formation with less Young's modulus becomes smaller. For example, Fig.IV-11 shows the critical mud weight polar diagram for a formation which is sandwiched by two layers with a higher Young's modulus. The stress becomes smaller than a uniform formation since the adjacent two layers take the load. The orientation of the critical mud weight disappears since the well angle with respect to the formation determines the stress state around a well.

Hard bedding layer with inclination (γ=0°)

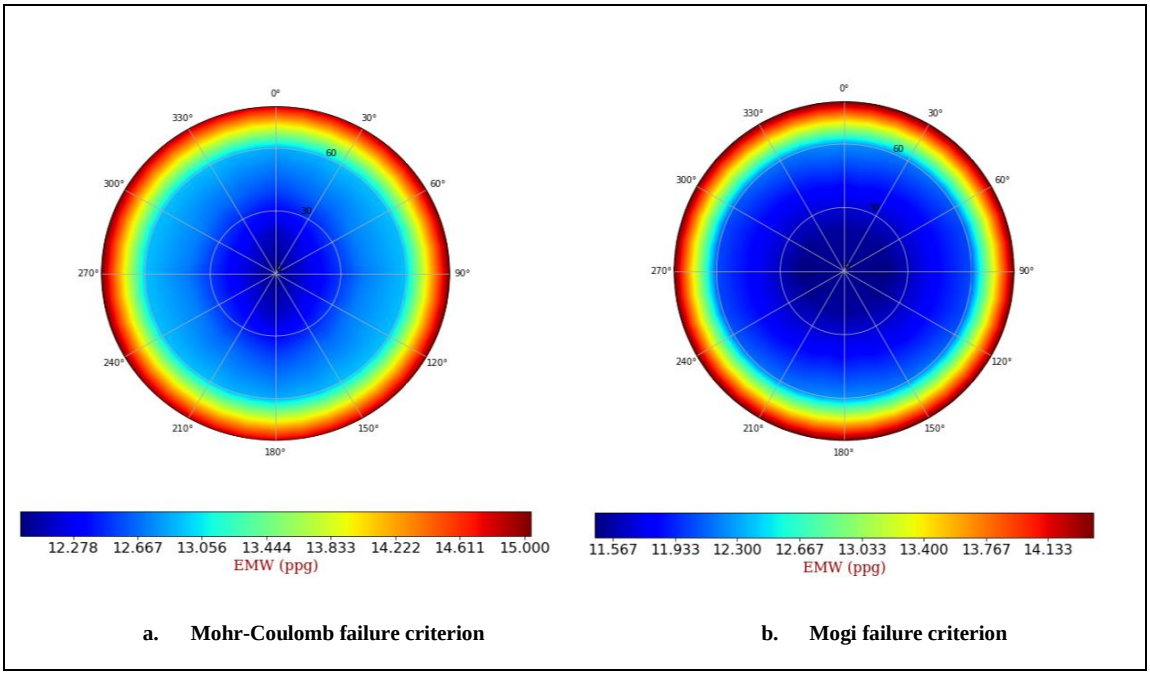

a. **Mohr-Coulomb failure criterion** b. **Mogi failure criterion**

Figure IV-11 Minimum mud weight to avoid shear collapse for an inclined well in the base field condition due to effect of hard bedding layer. The center of the polar diagram stands for vertical wells and the outer ring correspond to horizontal wells. The drilling azimuthal direction is measured from north (top), in the clockwise direction. Note: when bedding layer exists, the result of well inclination above 60 ° is not accurate and it shows the tendency that from 60 ° to 90 °

5. Safe Mud Weight Window due to Soft Bedding Layer Effect

Fig.IV-12 shows the critical mud weight polar diagram for a formation which is sandwiched by two layers with a lower Young's modulus. The stress becomes larger than a uniform formation since the adjacent two layers take less load. The orientation of the critical mud weight disappears since the well angle with respect to the formation determines the stress state around a well; therefore, the in-situ stress orientation has less effect on the orientation of the critical mud weight polar diagram.

Soft bedding layer with inclination (γ=0°)

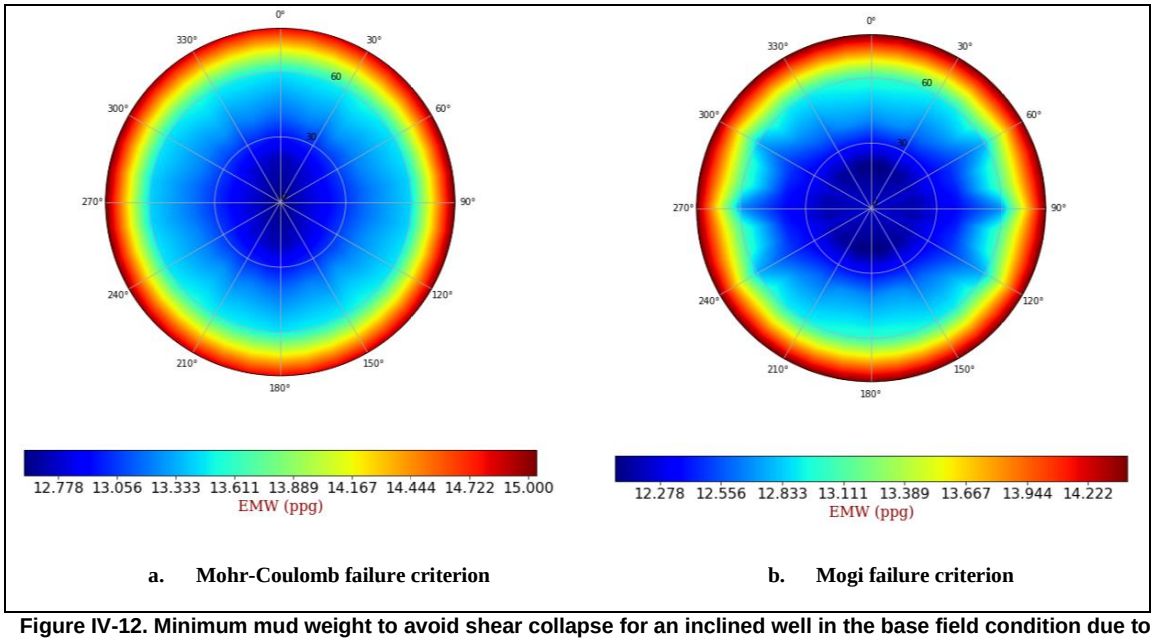

a. Mohr-Coulomb failure criterion

b. Mogi failure criterion

Figure IV-12. Minimum mud weight to avoid shear collapse for an inclined well in the base field condition due to effect of soft bedding layer. The center of the polar diagram stands for vertical wells and the outer ring correspond to horizontal wells. The drilling azimuthal direction is measured from north (top), in the clockwise direction. Note: when bedding layer exists, the result of well inclination above 60 ° is not accurate and it shows the tendency that from 60 ° to 90 °.

6. Safe Mud Weight Window due to Formation with Transversely Isotropic Elastic Material Effect

Shale formation is laminated with mud and shale layers. The elastic property may be approximated by a transversely isotropic material given by the five elastic coefficients in Table II-9 descrived in Chapter II. As shown in Table II-9, the elastic modulus along a plane is as large as two times of the elastic modulus in vertical plane. As shown in Figs.IV-13, the breakout angles become large with the borehole inclination. Comparing with Fig.IV-2 for isotropic formation, the mud weight must be increased more for 20-60º wells for anisotropic formation. However, comparing with 90º well (horizontal well), the safe mud weight is not significantly different between isotropic and

orthotropic case. These calculations show that as long as the degree of anisotropy is less than 2, the safe mud weight for inclined wells are not significantly different.

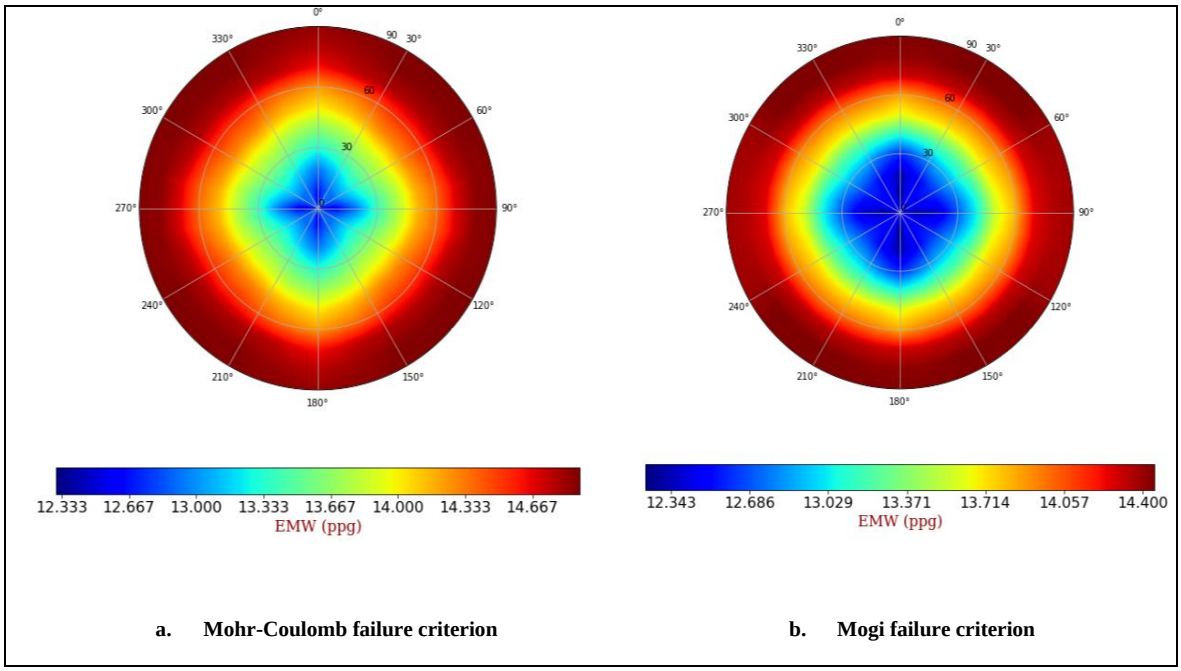

a. **Mohr-Coulomb failure criterion** b. **Mogi failure criterion**

Figure IV-13 Minimum mud weight to avoid shear collapse for an inclined well in the base field condition due to effect of soft bedding layer. The center of the polar diagram stands for vertical wells and the outer ring correspond to horizontal wells. The drilling azimuthal direction is measured from north (top), in the clockwise direction.

4.3 Conclusion

- The polar diagrams of safe mud weight show that the safe mud weight significantly increases with well angle. In the in-situ stress under the normal faulting regime, the safe mud weight is slightly higher if the borehole is oriented in the minimum horizontal in-situ stress direction North-South) assuming the maximum horizontal in-situ stress direction is oriented in East-West, although the difference of safe mud weight between East-West and North-South well azimuths is small. Under the strike-slip faulting regime, the well oriented in the maximum horizontal in-situ stress direction (East-West) can be drilled with

smaller mud weight compared with the well oriented in North-South assuming the maximum horizontal in-situ stress is oriented in East-West direction. Under the reverse faulting regime, the safe mud weight gives the similar trend as the strike-slip faulting regime.

- A significantly higher mud weight is required to suppress the borehole instability induced by shale swelling. The mud weight may exceed 19.2ppg, which is approximately the vertical stress gradient. Since a high overbalance may cause a differential sticking problem or a lost circulation, the swelling must be reduced as small as possible. When the shale swelling is the problem of borehole instability, the borehole orientation affects less according to the polar diagram of safe mud weight.
- Since the formation expansion is moderate with the temperature increase than with the shale swelling, a slight mud weight increase can suppress the borehole instability due to the temperature increase.
- For layered formation and for orthotropic formation, the breakout angle is not significantly different if the ratio of the orthotropy or heterogeneity is less than 2.
- General trend is that the polar diagrams for safe mud weight produced with Mohr-Coulomb failure criterion is more sensitive to the well orientation than those by Mogi's criterion.

CHAPTER V

CONCLUSIONS

1. Shale swelling increases both the tangential and axial stresses around a borehole resulting in serious borehole instability, which need to pay more attention during the drilling and production process in the field. The temperature change is generally less effect if the formation has some permeability. However, if the shale is 100% saturated with water and the permeability is very small, the expansion of water trapped within shale may destabilize borehole if the teperature increaes at the caing shoe.
2. Temperatrue cooling at borehole bit may stabilizes the borehole.
3. Pore pressure change due to osmosis and temperature change, overbalance, drawdown during drilling and hard and soft bedding layer only change a little of the magnitiude of stress distribution around borehole. However, the radial effective stress increase due to the overbalance and the pore pressure reduction induced by osmosis and temerature stabilize the borehole.
4. Well incalination also increases the stress magnitudes around borehole.
5. Following is the summary of each parameter effect.

   Factors destabilizing borehole

   - Swelling seriously affects the borehole stability.
   - Well inclination also significantly affects the borehole stability.
   - Temperature increase is the secondary factor to de-stabilize borehole
   - Layering of heterogeneous formations and orthotropic formation do not affect the stability of borehole if it is a vertical hole. If the formation angle becomes higher, the borehole becomes unstable. However, if the degree of heterogeneity and anisotropy is less than 2, the instability

caused by anisotropy or layering is not significantly different from isotropic formation.

Factors stabilizing borehole

- Eliminating the shale swelling is the most important factor to stabilize borehole.
- Non-linearity of rock, overbalance and pore pressure reduction due to osmosis are the factors stabilizing borehole and they are equally important.
- Effect of the overbalance, pore pressure, shale welling, pore pressure change, and temperature change on well stability are independently expressed in this work to separate each effect. However, all these parameters are actually dependent on each other.
    a. If some overbalance is added, it reduces the tangential effective stress and increase the radial effective stress. The increase of the radial effective stress significantly reduces shale swelling according to the laboratory experiments on shale swelling with confining stresses. With these two effects, borehole stability significantly improves.
    b. Some shale inhibitors reduce swelling and pore pressure due to osmosis. The pore pressure reduction reduces the swelling and reduction of swelling reduces the pore pressure, resulting in wellbore stability.
    c. Temperature cooling reduces the tangential stress around a borehole by shrinking the formation. In addition, if the permeability of shale is close to zero, it also reduces the volume of the water trapped in shale since the water thermal expansion coefficient is significantly larger the formation thermal expansion coefficient.
    d. Therefore, when borehole instability problem occurs due to shale swelling, it is important to use all the methods to stabilize borehole.

6. The polar diagrams of safe mud weight show that the safe mud weight significantly increases with well angle. In the in-situ stress under the normal faulting regime, the safe mud weight is slightly lower if the borehole is drilled in the minimum in-situ stress direction (North-South), although the difference between East-West and North-South well azimuths is small. Under the strike-slip

faulting regime, the well oriented in the maximum horizontal in-situ stress direction (East-West) can be drilled with a small mud weight compared with the well oriented in North-South. Under the reverse faulting regime, the safe mud weight gives the similar trend as the strike-slip faulting regime.

7. A significantly higher mud weight is required to suppress the borehole instability induced by shale swelling. The mud weight may exceed 19.2ppg, which is approximately the vertical stress gradient. Since a high overbalance may cause a differential sticking problem or a lost circulation, the swelling must be reduced as small as possible. When the shale swelling is the problem of borehole instability, the borehole orientation affects less for the polar diagram of safe mud weight.
8. Since the formation expansion is moderate with the temperature increase than with the shale swelling, a slight mud weight increase can suppress the borehole instability induced by the temperature increase.
9. For layered formation and for orthotropic formation, if the Young's modulus in a plane is as small as two times than that in vertical direction or if the Young's modulus varies two times in alternate bedding planes, the safe mud weight is not significantly different with respect to well inclination from the isotropic formation. However, if the degree of anisotropy or heterogeneity is more than 2, the safe mud weight significantly varies depending on the combinations of layer thickness and modulus contrast, which requires constructing a polar diagram of safe mud weight by changing each parameter.

10. General trend is that the polar diagrams for safe mud weight produced with Mohr-Coulomb failure criterion is more sensitive to the well orientation than those by Mogi's criterion.

REFERENCES

Al Saedi, A. Q., Flori, R. E., & Kabir, C. S. (2019). Influence of Frictional or Rotational Kinetic Energy on Wellbore-Fluid/Temperature Profiles During Drilling Operations. *SPE Drilling & Completion*, *34*(02), 128-142.

Bol, G. M., Wong, S. W., Davidson, C. J., & Woodland, D. C. (1994). Borehole stability in shales. *SPE Drilling & Completion*, *9*(02), 87-94.

Khan, K., Halim, A., Hamid, A., & Al-Anazi, H. A. (2016, January). Optimum Mud Overbalance and ROP Limits for Managing Wellbore Stability in Horizontal Wells in a Carbonate Gas Reservoir. In *SPE/IADC Middle East Drilling Technology Conference and Exhibition*. Society of Petroleum Engineers.

Likrama, F., & Diaz, A. (2015, November). A Practical Log-Based Approach on Assessing and Preventing Wellbore Instability Considering Both Mechanical and Shale Swelling Effects. In *49th US Rock Mechanics/Geomechanics Symposium*. American Rock Mechanics Association.

Morita, N. (2004, January). Well orientation effect on borehole stability. In *SPE Annual Technical Conference and Exhibition*. Society of Petroleum Engineers.

Morita, N., & Nagano, Y. (2016, September). Comparative Analysis of Various Failure Theories for Borehole Breakout Predictions. In *SPE Annual Technical Conference and Exhibition*. Society of Petroleum Engineers.

McLean, M. R., & Addis, M. A. (1990, January). Wellbore stability: the effect of strength criteria on mud weight recommendations. In *SPE annual technical conference and exhibition*. Society of Petroleum Engineers.

McLellan, P., & Hawkes, C. (2001). Borehole stability analysis for underbalanced drilling. *Journal of Canadian Petroleum Technology*, *40*(05).

Pellegrino, A., Sulem, J., & Barla, G. (1994, January). Nonlinear effects in the study of borehole stability. In *Rock Mechanics in Petroleum Engineering*. Society of Petroleum Engineers.

Santarelli, F. J., Chenevert, M. E., & Osisanya, S. O. (1992, January). On the Stability of Shales and its consequences in terms of swelling and wellbore stability. In *SPE/IADC Drilling Conference*. Society of Petroleum Engineers.

Takuma,K.(2019) Development of high performance water base mud and estimation of downhole swelling (Doctoral dissertation)

Wang, Y., Papamichos, E., & Dusseault, M. B. (1996). Thermal stresses and borehole stability. In *Proc. 2nd NARMS Conference, Balkema, Rotterdam* (pp. 1121-1131).

Xue, F., Zhang, N., & Feng, X. (2014). The estimation method of the borehole stability based on unified strength criterion. *Electronic Journal of Geotechnical Engineering*, *19*, 19065-19078.

Yuan, J., Deng, J., Luo, Y., Guo, S., Zhang, H., Tan, Q., ... & Hu, L. (2013). The research on borehole stability in depleted reservoir and caprock: using the geophysics logging data. *The Scientific World Journal*, *2013*.

Zhou, S. (1992). In search of evidence for protostellar collapse-A systematic study of line formation in low-mass dense cores. *the Astrophysical Journal*, *394*, 204-216.

APPENDIX A

DERIVATION OF STRESS EQUATION AROUND AN INCLINED WELL WITH SWELLING AND TEMPERATURE

Solution for axisymmetric problems

If the pore pressure effect is considered, the axisymmetric solution for poro-elasticity problem can be superposed. Then,

Equation of equilibrium

$$\partial\sigma_v / \partial r + (1/r)\partial\tau_{re}\rho\partial\theta + \partial\tau_{Tz} / \partial z + \left(\sigma_r - \sigma_\theta\right)/r + \rho R = 0$$

$$\partial\tau_{re} / \partial r + (1/r)\partial\sigma_\theta / \partial\theta + \partial\tau\theta z / \partial z + 2\tau_{r\theta} / r + \rho\Theta = 0$$

$$\partial\tau_{ra} / \partial r + (1/r)\partial\tau_{\theta_2} / \partial\theta + \partial\sigma_z / \partial z + \tau_{rz} / r + \rho Z = 0$$

Setting $\tau_{11} = 0$ for $i \neq j$, and using $\partial\sigma_\theta / \partial\theta = 0$ and $\partial\sigma_z / \partial z = 0$, the equilibrium equation for axially symmetric problems is reduced to the following equation.

$$\partial\sigma_r / \partial r + \left(\sigma_r - \sigma_\theta\right)/r = 0$$

Stress displacement relation

$$\varepsilon_r = \partial u / \partial r$$

$$\varepsilon_\theta = (1/r)\partial v / \partial\theta + u / r$$

$$\varepsilon_z = \partial w / \partial z$$

$$\mathrm{Y}_{\theta z} = 0.5*[\partial v / \partial z + (1/r)\partial w / \partial\theta]$$

$$\mathrm{Y}_{rz} = 0.5*(\partial w / \partial r + \partial u / \partial z)$$

$$\mathrm{Y}_{r\theta} = 0.5*[(1/r)\partial u / \partial\theta + \partial v / \partial r - v / r]$$

The relation between the shear stress and strain are automatically satisfied and $\partial v / \partial\theta$ and $\partial w / \partial z$ are zero. Hence, the displacement and strain relation are reduced to the following two equations.

$$\varepsilon_r = \partial u / \partial r$$

$$\varepsilon_\theta = u / r$$

The following is the summary of the fundamental equations of elasticity for axisymmetric problems.

Equation of equilibrium

$$\partial\sigma_r / \partial r + (\sigma_r - \sigma_\theta) / r = 0$$

Strain displacement relation

$$\varepsilon_r = \partial u / \partial r$$

$$\varepsilon_\theta = u / r$$

Temperature, pore pressure and swelling effects

The following is the summary of the fundamental equations of elasticity for axisymmetric problems.

Stress strain relation (plane strain condition)

$$\varepsilon_{ij} = \frac{1+\nu}{E}\sigma_{ij} - \frac{\nu}{E}\sigma_{kk}\delta_{ij} + \frac{1-2\nu}{E}\left\{\alpha\Delta p + \frac{E}{1-2\nu}(\eta\Delta T + \Delta S)\right\}\delta_{ij}$$

$$(\alpha = 1 - \frac{3(1-2\nu_m)}{E_m} / \frac{3(1-2\nu)}{E})$$

$$\sigma_{ij} = \frac{E}{1+\nu}\left(\varepsilon_{ij} + \frac{\nu}{1-2\nu}\varepsilon_{mm}\delta_{ij}\right) - \left\{\alpha\Delta p + \frac{E}{1-2\nu}(\eta\Delta T + \Delta S)\right\}\delta_{ij}$$

For axisymmetric plane strain condition, we have

$$\sigma_r = \frac{E}{(1+\nu)(1-2\nu)}\left[(1-\nu)\varepsilon_r + \nu\varepsilon_\theta\right] - \left\{\alpha\Delta p + \frac{E}{1-2\nu}(\eta\Delta T + \Delta S)\right\}$$

$$\sigma_\theta = \frac{E}{(1+\nu)(1-2\nu)}\left[\nu\varepsilon_r + (1-\nu)\varepsilon_\theta\right] - \left\{\alpha\Delta p + \frac{E}{1-2\nu}(\eta\Delta T + \Delta S)\right\}$$

$$\sigma_z = \nu(\sigma_r + \sigma_\theta) - (1-2\nu)\left\{\alpha\Delta p + \frac{E}{(1-2\nu)}(\eta\Delta T + \Delta S)\right\}$$

then

$$\sigma_r = \frac{E}{(1+\nu)(1-2\nu)}\left[(1-\nu)\frac{\partial u}{\partial r} + \nu\frac{u}{r}\right] - \left\{\alpha\Delta p + \frac{E}{1-2\nu}(\eta\Delta T + \Delta S)\right\}$$

$$\sigma_\theta = \frac{E}{(1+\nu)(1-2\nu)}\left[\nu\frac{\partial u}{\partial r} + (1-\nu)\right]\frac{u}{r} - \left\{\alpha\Delta p + \frac{E}{1-2\nu}(\eta\Delta T + \Delta S)\right\}$$

From $\partial\sigma_r / \partial r + (\sigma_r - \sigma_\theta)/r = 0$, we have

$$\frac{E}{(1+\nu)(1-2\nu)}\left[(1-\nu)\frac{\partial^2 u}{\partial r^2} + \nu(\frac{1}{r}\frac{du}{dr} - \frac{u}{r^2})\right] - \left\{\alpha\frac{d}{dr}\Delta p + \frac{E}{1-2\nu}(\eta\frac{d}{dr}\Delta T + \frac{d}{dr}\Delta S)\right\}$$
$$+\frac{1}{r}\left[\frac{E}{(1+\nu)(1-2\nu)}\left[(1-\nu)\frac{\partial u}{\partial r} + \nu\frac{u}{r}\right] - \frac{E}{(1+\nu)(1-2\nu)}\left[\nu\frac{\partial u}{\partial r} + (1-\nu)\right]\frac{u}{r}\right]$$

Solution

The above problem is solved as follows. Eliminating the stress and strain components result in the following equation expressed with the radial displacement.

$$\frac{\partial^2 u}{\partial r^2} + \frac{1}{r}\frac{\partial u}{\partial r} - \frac{u}{r^2} = \frac{(1+\nu)}{(1-\nu)}\frac{(1-2\nu)}{E}\frac{\partial}{\partial r}\left\{\alpha\Delta p + \frac{E}{(1-2\nu)}(\eta\Delta T + \Delta S)\right\}$$

Or

$$\frac{\partial}{\partial r}\left[\frac{1}{r}\frac{\partial(ru)}{\partial r}\right] = \frac{(1+\nu)}{(1-\nu)}\frac{(1-2\nu)}{E}\frac{\partial}{\partial r}\left\{\alpha\Delta p + \frac{E}{(1-2\nu)}(\eta\Delta T + \Delta S)\right\}$$

The general solution is:

$$u = A'r + B'/r + \frac{(1+\nu)}{(1-\nu)}\frac{(1-2\nu)}{E}\frac{1}{r}\int_{r_w}^{r} r\left\{\alpha\Delta p + \frac{E}{(1-2\nu)}(\eta\Delta T + \Delta S)\right\}dr$$

where A' and B' are constants.

$$\sigma_r = \frac{E}{(1+\nu)(1-2\nu)}\left[A' - (1-2\nu)B'/r^2\right] - \frac{1-2\nu}{1-\nu}\frac{1}{r^2}\int_{r_w}^{r} r\left\{\alpha\Delta p + \frac{E}{(1-2\nu)}(\eta\Delta T + \Delta S)\right\}dr$$

$$\sigma_\theta = \frac{E}{(1+\nu)(1-2\nu)}\left[A' + (1-2\nu)B'/r^2\right] + \frac{1-2\nu}{1-\nu}\frac{1}{r^2}\int_{r_w}^{r} r\left\{\alpha\Delta p + \frac{E}{(1-2\nu)}(\eta\Delta T + \Delta S)\right\}dr$$
$$-\frac{1-2\nu}{1-\nu}\left\{\alpha\Delta p + \frac{E}{(1-2\nu)}(\eta\Delta T + \Delta S)\right\}$$

Boundary condition: $\sigma_r = -Pw$ at $r = r_w$ and $\sigma_r = \sigma_H$ at $r = \infty$.

$$\sigma_r\left(r = r_w\right) = [E/(1+\nu)(1-2\nu)]\left[A' - (1-2\nu)B' r^{-2} w\right] = -Pw$$

$$\sigma_r(r = \infty) = [E/(1+\nu)(1-2\nu)]A' = \sigma_H$$

Therefore $A' = \dfrac{(1+\nu)(1-2\nu)}{E}\sigma_H$, and $B' = \dfrac{(1+\nu)}{E}(p_w + \sigma_H)r_w^2$

Hence, the stress and displacement are given by

For plane strain problems

$$\sigma_r = \sigma_H - (\sigma_H + p_w)\left(\frac{r_w}{r}\right)^2 - \frac{1-2\nu}{1-\nu}\frac{1}{r^2}\int_{r_w}^{r} r\left\{\alpha\Delta p + \frac{E}{(1-2\nu)}(\eta\Delta T + \Delta S)\right\}dr$$

$$\sigma_\theta = \sigma_H + (\sigma_H + p_w)\left(\frac{r_w}{r}\right)^2 + \frac{1-2\nu}{1-\nu}\frac{1}{r^2}\int_{r_w}^{r} r\left\{\alpha\Delta p + \frac{E}{(1-2\nu)}(\eta\Delta T + \Delta S)\right\}dr$$
$$-\frac{1-2\nu}{1-\nu}\left\{\alpha\Delta p + \frac{E}{(1-2\nu)}(\eta\Delta T + \Delta S)\right\}$$

$\sigma_z = \nu(\sigma_r + \sigma_\theta) - (1-2\nu)\left\{\alpha\Delta p + \dfrac{E}{(1-2\nu)}(\eta\Delta T + \Delta S)\right\}$ for a plane strain around the borehole.

Or

$$\sigma_z = \nu(2\sigma_H) - \frac{1-2\nu}{1-\nu}\left\{\alpha\Delta p + \frac{E}{(1-2\nu)}(\eta\Delta T + \Delta S)\right\}$$

The above solution holds if the problem is in plane condition assuming the in-situ stress components also contribute the deformation. However, if the problem is in plane condition only for the stress disturbance induced by drilling hole, we need to replace $\nu(2\sigma_H)$ by σ_v and the vertical stress is given by

$$\sigma_z = \sigma_v - \frac{1-2\nu}{1-\nu}\left\{\alpha\Delta p + \frac{E}{(1-2\nu)}(\eta\Delta T + \Delta S)\right\}$$

$$u = \frac{1+\nu}{E}(\sigma_H + p_w)\frac{r_w^2}{r} + \frac{(1+\nu)}{(1-\nu)}\frac{(1-2\nu)}{E}\frac{1}{r}\int_{r_w}^{r} r\left\{\alpha\Delta p + \frac{E}{(1-2\nu)}(\eta\Delta T + \Delta S)\right\}dr$$

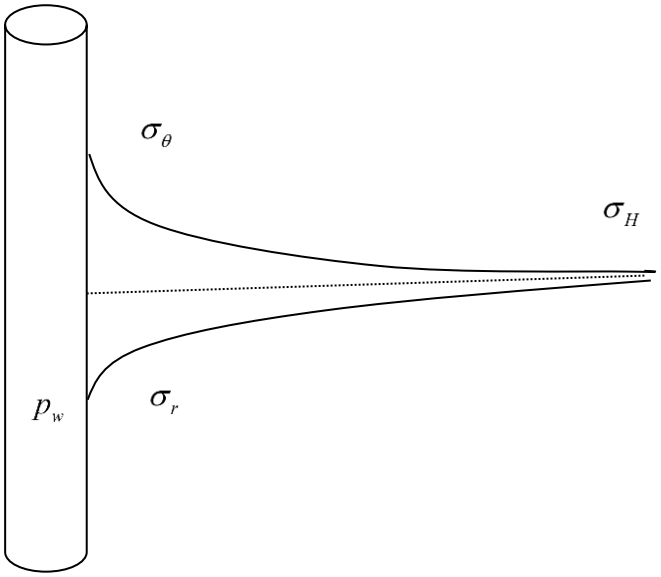

Figure A-1 The stress state around a borehole $P_w > |\sigma_H|$

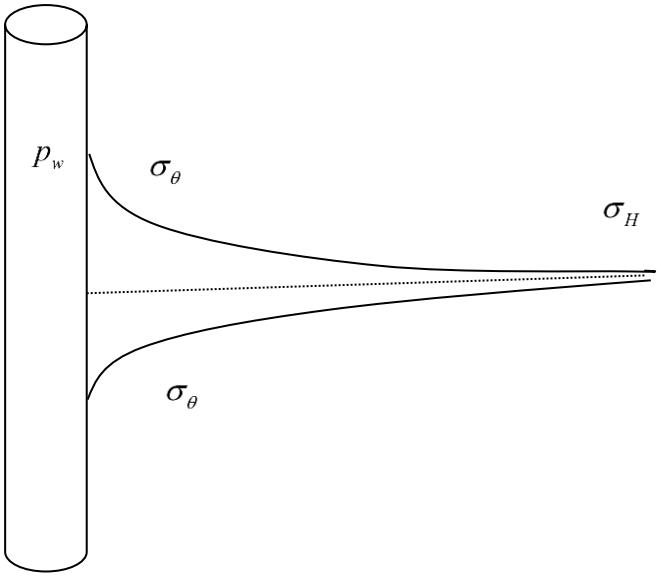

Figure A-2 The stress state around a borehole $P_w < |\sigma_H|$

Displacement after drilling for directional in-situ stresses: Plane strain problems

$$\sigma_r = \frac{1}{2}(\sigma_{H1}+\sigma_{H2}) - (\frac{1}{2}\sigma_{H1}+\frac{1}{2}\sigma_{H2}+p_w)\left(\frac{r_w}{r}\right)^2 - \frac{1-2\nu}{1-\nu}\frac{1}{r^2}\int_{r_w}^{r} r\left\{\alpha\Delta p + \frac{E}{(1-2\nu)}(\eta\Delta T+\Delta S)\right\}dr$$
$$+\frac{1}{2}\left[1+3\left(\frac{r_w}{r}\right)^4 - 4\left(\frac{r_w}{r}\right)^2\right](\sigma_{H2}-\sigma_{H1})\cos 2\theta$$

$$\sigma_\theta = \frac{1}{2}(\sigma_{H1}+\sigma_{H2}) + (\frac{1}{2}\sigma_{H1}+\frac{1}{2}\sigma_{H2}+p_w)\left(\frac{r_w}{r}\right)^2 + \frac{1-2\nu}{1-\nu}\frac{1}{r^2}\int_{r_w}^{r} r\left\{\alpha\Delta p + \frac{E}{(1-2\nu)}(\eta\Delta T+\Delta S)\right\}dr$$
$$-\frac{1-2\nu}{1-\nu}\left\{\alpha\Delta p + \frac{E}{(1-2\nu)}(\eta\Delta T+\Delta S)\right\} - \frac{1}{2}\left[1+3\left(\frac{r_w}{r}\right)^4\right](\sigma_{H2}-\sigma_{H1})\cos 2\theta$$

$$\tau_{r\theta} = -\frac{1}{2}\left[1-3\left(\frac{r_w}{r}\right)^4 + 2\left(\frac{r_w}{r}\right)^2\right](\sigma_{H2}-\sigma_{H1})\sin 2\theta$$

$$\sigma_z = \sigma_v - \frac{1-2\nu}{1-\nu}\left\{\alpha\Delta p + \frac{E}{(1-2\nu)}(\eta\Delta T+\Delta S)\right\} - 2\nu\left(\frac{r_w}{r}\right)^2(\sigma_{H2}-\sigma_{H1})\cos 2\theta$$

$$u = \frac{1+\nu}{E}(\frac{1}{2}\sigma_{H1}+\frac{1}{2}\sigma_{H2}+p_w)\frac{r_w^2}{r} + \frac{(1+\nu)}{(1-\nu)}\frac{(1-2\nu)}{E}\frac{1}{r}\int_{r_w}^{r} r\left\{\alpha\Delta p + \frac{E}{(1-2\nu)}(\eta\Delta T+\Delta S)\right\}dr$$
$$+\frac{1+\nu}{2E\nu}r_w\left[\frac{r}{r_w} - \left(\frac{r_w}{r}\right)^3 + \frac{4\nu}{1+\nu}\left(\frac{r_w}{r}\right)\right](\sigma_{H2}-\sigma_{H1})\cos 2\theta$$

$$v = +\frac{1+\nu}{4E\nu}r_w\left[-(1+\nu)\frac{r}{r_w} + (1-3\nu)\left(\frac{r_w}{r}\right)^3 - \frac{4\nu(1-\nu)}{1+\nu}\left(\frac{r_w}{r}\right)\right](\sigma_{H2}-\sigma_{H1})\sin 2\theta$$

$(u,\ v)$ is the displacement assuming the in-situ stress is built up and the borehole is drilled. The displacement $\left(u^{'}, v^{'}\right)$, after borehole is drilled, requires subtracting the displacement induced by the in-situ stress. Since the displacement induced by the drilling should vanish for $r \to \infty$, the finite and infinite terms for $r \to \infty$ are dropped from u and v.

$$u' = \frac{1+\nu}{E}(\frac{1}{2}\sigma_{H1}+\frac{1}{2}\sigma_{H2}+p_w)\frac{r_w^2}{r} + \frac{(1+\nu)}{(1-\nu)}\frac{(1-2\nu)}{E}\frac{1}{r}\int_{r_w}^{r} r\left\{\alpha\Delta p + \frac{E}{(1-2\nu)}(\eta\Delta T+\Delta S)\right\}dr$$
$$+\frac{1+\nu}{2E\nu}r_w\left[-\left(\frac{r_w}{r}\right)^3 + \frac{4\nu}{1+\nu}\left(\frac{r_w}{r}\right)\right](\sigma_{H2}-\sigma_{H1})\cos 2\theta$$

$$v' = +\frac{1+\nu}{4E\nu} r_w \left[+(1-3\nu)\left(\frac{r_w}{r}\right)^3 - \frac{4\nu(1-\nu)}{1+\nu}\left(\frac{r_w}{r}\right)\right](\sigma_{H2} - \sigma_{H1})\sin 2\theta$$

<u>At $r = r_w$</u>

$$\sigma_r = -p_w$$

$$\sigma_\theta = \sigma_{H1} + \sigma_{H2} + p_w - 2(\sigma_{H2} - \sigma_{H1})\cos 2\theta - \frac{1-2\nu}{1-\nu}\left\{\alpha\Delta p_w + \frac{E}{(1-2\nu)}(\eta\Delta T_w + \Delta S_w)\right\}$$

$$\tau_{r\theta} = 0$$

$$\sigma_z = \sigma_v - \frac{1-2\nu}{1-\nu}\left\{\alpha\Delta p_w + \frac{E}{(1-2\nu)}(\eta\Delta T_w + \Delta S_w)\right\} - 2\nu(\sigma_{H2} - \sigma_{H1})\cos 2\theta$$

$$u = \frac{1+\nu}{E}\left(\frac{1}{2}\sigma_{H1} + \frac{1}{2}\sigma_{H2} + p_w\right)r_w + \frac{1+\nu}{2E\nu} r_w \left[\frac{4\nu}{1+\nu}\right](\sigma_{H2} - \sigma_{H1})\cos 2\theta$$

$$v = -\frac{2}{E} r_w (\sigma_{H2} - \sigma_{H1})\sin 2\theta$$

We may calculate the internal stresses assuming a simple pressure, temperature and swelling distributions.

$$\Delta p = \Delta p_w\left(1 - \ell n\frac{r}{r_w} / \ell n\frac{r_p}{r_w}\right) \text{ for } r_w < r < r_p \text{ and } \Delta p = 0 \text{ for } r_p < r$$

$$\Delta T = \Delta T_w\left(1 - \ell n\frac{r}{r_w} / \ell n\frac{r_T}{r_w}\right) \text{ for } r_w < r < r_T \text{ and } \Delta T = 0 \text{ for } r_T < r$$

$$\Delta S = \Delta S_w\left(1 - \ell n\frac{r}{r_w} / \ell n\frac{r_S}{r_w}\right) \text{ for } r_w < r < r_S \text{ and } \Delta S = 0 \text{ for } r_S < r$$

Displacement after drilling for directional in-situ stresses: Plane strain problems

<u>At $r = r_w$</u>

$$\sigma_r = -p_w$$

$$\sigma_\theta = \sigma_{H1} + \sigma_{H2} - 2(\sigma_{H2} - \sigma_{H1})\cos 2\theta + p_w - \frac{1-2\nu}{1-\nu}\left\{\alpha\Delta p + \frac{E}{(1-2\nu)}(\eta\Delta T + \Delta S)\right\}$$

$$\tau_{r\theta} = 0$$

$$\sigma_z = \sigma_v - \frac{1-2\nu}{1-\nu}\left\{\alpha\Delta p + \frac{E}{(1-2\nu)}(\eta\Delta T + \Delta S)\right\} - 2\nu(\sigma_{H2} - \sigma_{H1})\cos 2\theta$$

$$u' = \frac{1+\nu}{E}(\frac{1}{2}\sigma_{H1} + \frac{1}{2}\sigma_{H2} + p_w)\,\mathrm{r}_w - \frac{1-3\nu}{2E\nu} r_w(\sigma_{H2} - \sigma_{H1})\cos 2\theta$$

$$v' = + \frac{1-6\nu+\nu^2}{4E\nu} r_w(\sigma_{H2} - \sigma_{H1})\sin 2\theta$$

For $r_w < r < r_p$, $r_w < r < r_T$ or $r_w < r < r_S$

$$I = \frac{1}{r^2}\int_{r_w}^{r} r\left\{\alpha\Delta p + \frac{E}{(1-2\nu)}(\eta\Delta T + \Delta S)\right\}dr$$

$$= \frac{1}{r^2}\alpha\Delta p_w \int_{r_w}^{r} r[1 - \frac{1}{\ell n(r_p / r_w)}(\ell nr - \ell nr_w)]dr$$

$$+ \frac{1}{r^2}\frac{E\eta}{(1-2\nu)}\Delta T_w \int_{r_w}^{r} r[1 - \frac{1}{\ell n(r_T / r_w)}(\ell nr - \ell nr_w)]dr$$

$$+ \frac{1}{r^2}\frac{E}{(1-2\nu)}\Delta S_w \int_{r_w}^{r} r[1 - \frac{1}{\ell n(r_S / r_w)}(\ell nr - \ell nr_w)]dr$$

$$= \frac{1}{r^2}\alpha\Delta p_w \left[\frac{1}{2}r^2 - \frac{\frac{1}{2}}{\ell n(r_p / r_w)}\{r^2\ell n(r / r_w) - \frac{1}{2}r^2\}\right]_{r_w}^{r}$$

$$+ \frac{1}{r^2}\frac{E\eta}{(1-2\nu)}\Delta T_w \left[\frac{1}{2}r^2 - \frac{\frac{1}{2}}{\ell n(r_T / r_w)}\{r^2\ell n(r / r_w) - \frac{1}{2}r^2\}\right]_{r_w}^{r}$$

$$+ \frac{1}{r^2}\frac{E}{(1-2\nu)}\Delta S_w \left[\frac{1}{2}r^2 - \frac{\frac{1}{2}}{\ell n(r_S / r_w)}\{r^2\ell n(r / r_w) - \frac{1}{2}r^2\}\right]_{r_w}^{r}$$

$$= \frac{1}{2}\alpha\Delta p_w (\frac{r_w}{r})^2 \left[(\frac{r}{r_w})^2 - 1 - \frac{1}{\ell n(r_p / r_w)}\{(\frac{r}{r_w})^2\ell n(r / r_w) - \frac{1}{2}((\frac{r}{r_w})^2 - 1)\}\right]$$

$$+ \frac{1}{2}\frac{1}{r^2}\frac{E\eta}{(1-2\nu)}\Delta T_w \left[(r^2 - r_w^2) - \frac{1}{\ell n(r_T / r_w)}\{r^2\ell n(r / r_w) - \frac{1}{2}(r^2 - r_w^2)\}\right]$$

$$+ \frac{1}{2}\frac{1}{r^2}\frac{E}{(1-2\nu)}\Delta S_w \left[(r^2 - r_w^2) - \frac{1}{\ell n(r_S / r_w)}\{r^2\ell n(r / r_w) - \frac{1}{2}(r^2 - r_w^2)\}\right]$$

For $r_p < r$, $r_T < r$ or $r_S < r$, we have

$$I = \frac{1}{r^2}\int_{r_w}^{r} r\left\{\alpha\Delta p + \frac{E}{(1-2\nu)}(\eta\Delta T + \Delta S)\right\}dr$$

$$= \frac{1}{2}\frac{1}{r^2}\alpha\Delta p_w\left[(r_p{}^2 - r_w^2) - \frac{1}{\ell n(r_p / r_w)}\{r_p{}^2\ell n(r_p / r_w) - \frac{1}{2}(r_p{}^2 - r_w^2)\}\right]$$

$$+ \frac{1}{2}\frac{1}{r^2}\frac{E\eta}{(1-2\nu)}\Delta T_w\left[(r_T{}^2 - r_w^2) - \frac{1}{\ell n(r_T / r_w)}\{r_T{}^2\ell n(r_T / r_w) - \frac{1}{2}(r_T{}^2 - r_w^2)\}\right]$$

$$+ \frac{1}{2}\frac{1}{r^2}\frac{E}{(1-2\nu)}\Delta S_w\left[(r_S{}^2 - r_w^2) - \frac{1}{\ell n(r_S / r_w)}\{r_S{}^2\ell n(r_S / r_w) - \frac{1}{2}(r_S{}^2 - r_w^2)\}\right]$$

Stress around an inclined well

The stress around a long-inclined well is also solved as a general plane strain problem. The general plane strain problems assume all the variables including the displacement along the well axis are functions of (x, y), hence, the differentiations with respect to z vanish.

Suppose the in-situ stresses are given by $(\sigma_H, \sigma_h, \sigma_V)$ in (x', y', z') coordinate. The azimuth and inclination of an inclined well is given by (θ, γ) where the coordinate of the inclined well is (x, y, z).

The stress in the well coordinate is given by $\sigma_x, \sigma_y, \sigma_z, \tau_{yz}, \tau_{zx}, \tau_{xy}$,where

$$\sigma_x = \ell_1^2\sigma_H + m_1^2\sigma_h + n_1^2\sigma_V$$
$$\sigma_y = \ell_2^2\sigma_H + m_2^2\sigma_h + n_2^2\sigma_V$$
$$\sigma_z = \ell_3^2\sigma_H + m_3^2\sigma_h + n_3^2\sigma_V$$
$$\tau_{yz} = \ell_2\ell_3\sigma_H + m_2m_3\sigma_h + n_2n_3\sigma_V$$
$$\tau_{zx} = \ell_3\ell_1\sigma_H + m_3m_1\sigma_h + n_3n_1\sigma_V$$
$$\tau_{xy} = \ell_1\ell_2\sigma_H + m_1m_2\sigma_h + n_1n_2\sigma_V$$

Directional cosines:

	x'	y'	z'
x	ℓ_1	m_1	n_1
y	ℓ_2	m_2	n_2
z	ℓ_3	m_3	n_3

$\ell_1 = \cos\theta\cos\gamma, \ell_2 = -\sin\theta, \ell_3 = \cos\theta\sin\gamma$

$m_1 = \sin\theta\cos\gamma, m_2 = \cos\theta, m_3 = \sin\theta\sin\gamma$

$n_1 = -\sin\gamma, n_2 = 0, n_3 = \cos\gamma$

$x'y'z'$-original coordinate, xyz-rotated coordinate (perforation in x coordinate direction)

The elastic solution should give the stress state approaches $\sigma_x, \sigma_y, \sigma_z, \tau_{xy}, \tau_{yz}, \tau_{zx}$ in the far field and p_w around the well. To obtain the solution, the stress $\sigma_x, \sigma_y, \sigma_z, \tau_{xy}$ within the plane in perpendicular to the well axis and the stress oriented out of the plane are separated. These two solutions are superposed.

The solution within the plane is identical to the two-dimensional solution with directional stresses.

The stress solution is found for in-situ stress σx.

$$\sigma_r\left(r = r_w\right) = 0$$

$$\tau_{r\theta}\left(x = r_w\right) = 0$$

$$\sigma_x(x \to \infty) = 0.5\sigma_x + 0.5\sigma_x\cos(2\theta)$$

$$\tau_{r\theta}(r \to \infty) = -0.5\sigma_x\sin(2\theta)$$

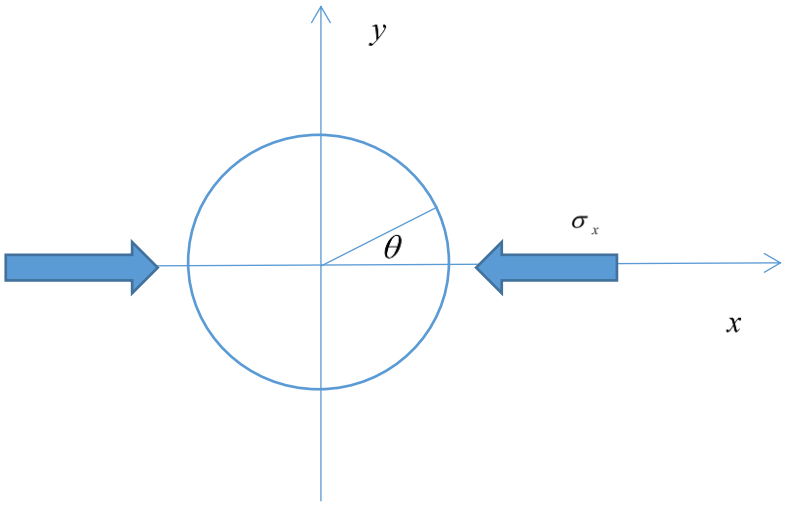

Figure A-3 In-situ stress σx

Decomposing the above stresses into two parts

Part 1: the directional components

$\sigma_r\left(r=r_w\right)=0$

$\tau_{r\theta}\left(r=r_w\right)=0$

$\sigma_x(x\to\infty)=+0.5\sigma_x\cos(2\theta)$

$\tau_{r\theta}(r\to\infty)=-0.5\sigma_x\sin(2\theta)$

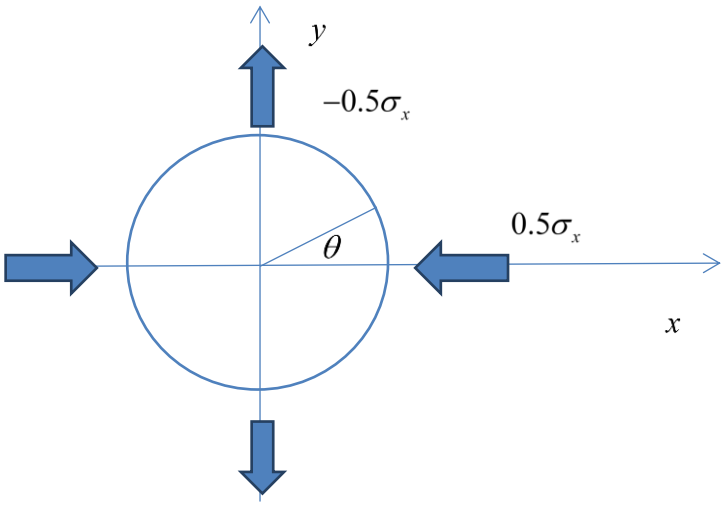

Figure A-4 In-situ stress σx : directional components

Part 2: non-directional components

$\sigma_r\left(r=r_w\right)=0$

$\tau_{r\theta}\left(x=r_w\right)=0$

$\sigma_r(r\to\infty)=0.5\sigma_x$

$\tau_{r\theta}(r\to\infty)=0$

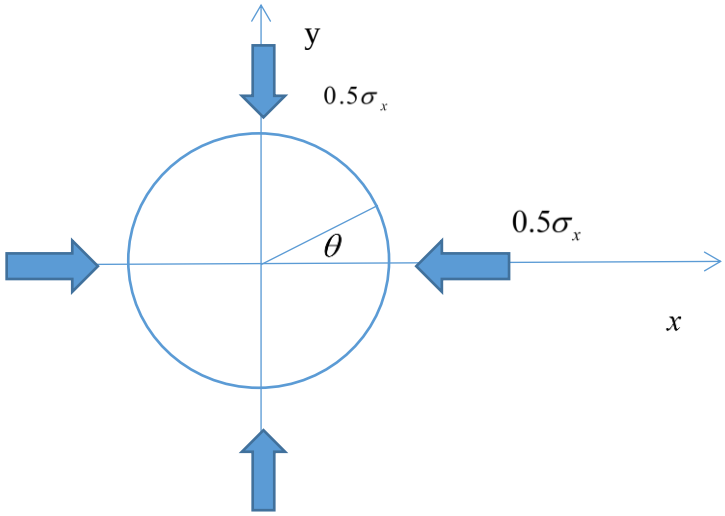

Figure A-5 In-situ stress σx : non-directional components

Part 1 solution

$$\sigma_r = r^{-1}\partial\psi/\partial r + r^{-2}\partial^2\psi/\partial\theta^2 = -\left(2A + 6Cr^{-4} + 4Dr^{-2}\right)\cos(2\theta)$$

$$\sigma_\theta = \partial^2\psi/\partial r^2 = \left(2A + 12Br^2 + 6Cr^{-4}\right)\cos(2\theta)$$

$$\tau_{r\theta} = -(\partial/\partial r)\left(r^{-1}\partial\psi/\partial\theta\right) = \left(2A + 6Br^2 - 6Cr^{-4} - 2Dr^{-2}\right)\sin(2\theta)$$

$$u = [(1+v)/(Ev)]\left[-2Ar + 2Cr^{-3} + 4Dv/(1+v)r^{-1}\right]\cos(2\theta)$$

$$v = [(1+v)/(Ev)]x$$
$$\left[A(1+v)r + 6Bv/(1+v) - C(1-3v)r^{-3} - 2Dv(1-v)/(1+v)r^{-1}\right]\cos(2\theta)$$

The coefficients are determined to satisfied with the boundary conditions.

$$A = -0.25\sigma_x$$
$$B = 0$$
$$C = -0.25\sigma_x r_w^4$$
$$D = 0.5\sigma_x r_{w^2}$$

$$\sigma_r = \sigma_x\left(0.5 + 1.5rd^{-4} - 2rd^{-2}\right)\cos(2\theta)$$

$$\sigma_\theta = \sigma_x \left(-0.5 - 1.5rd^{-4}\right)\cos(2\theta)$$

$$\tau_{r\theta} = \sigma_x \left(-0.5 + 1.5rd^{-4} - rd^{-2}\right)\sin(2\theta)$$

$$u = \sigma_x r_w [(1+v)/(Ev)]\left[0.5rd - 0.5rd^{-3} + 2v/(1+v)rd^{-1}\right]\cos(2\theta)$$

$$v = \sigma_x r_w \left\lfloor (1+v)/\left(E_v\right)\right\rfloor_x$$
$$\left[-0.25(1+v)rd + 0.25(1-3v)rd^{-3} - v(1-v)/(1+v)rd^{-1}\right]\cos(2\theta)$$

Part 2 solution.

$$\sigma_r \left(r = r_w\right) = 0$$

$$\tau_{r\theta}\left(r = r_w\right) = 0$$

$$\sigma_x(r \to \infty) = +0.5\sigma_x$$

$$\tau_{r\theta}(r \to \infty) = 0$$

The following solution is obtained.

$$\sigma_r = 0.5\sigma_x \left(1 - r_d^{-2}\right)$$

$$\sigma_\theta = 0.5\sigma_x \left(1 + r_d^{-2}\right)$$

$$\tau_{r\theta} = 0$$

$$u = 0.5\sigma_x r_w [(1+v)/(E)]\left[(1-2v)r_d + rd^{-1}\right]$$

$$v = 0$$

Superposing part 1 and 2 solution gives:

$$\sigma_r = 0.5\sigma_x \left(1 - rd^{-2}\right) + \sigma_x \left(0.5 + 1.5rd^{-4} - 2rd^{-2}\right)\cos(2\theta)$$

$$\sigma_\theta = 0.5\sigma_x\left(1+rd^{-2}\right)-\sigma_x\left(0.5+1.5rd^{-4}\right)\cos(2\theta)$$

$$\tau_{r\theta} = \sigma_x\left(-0.5+1.5rd^{-4}-rd^{-2}\right)\sin(2\theta)$$

$$u = 0.5\sigma_{xr_w}[(1+v)/(E)]\left\lfloor(1-2v)rd+rd^{-1}\right\rfloor$$
$$+\sigma_x r_w[(1+v)/(Ev)]\left[0.5rd-0.5rd^{-3}+2v/(1+v)rd^{-1}\right]\cos(2\theta)$$

$$v = \sigma_x r_w\left\lfloor(1+v)/\left(E_v\right)\right\rfloor_x$$
$$\left[-0.25(1+v)rd+0.25(1-3v)rd^{-3}-v(1-v)/(1+v)rd^{-1}\right]\cos(2\theta)$$

Similarly, the solution is found for the following boundary conditions.

$$\sigma_r\left(r=r_w\right)=0$$

$$\tau_{r\theta}\left(r=r_w\right)=0$$

$$\sigma_r(r\to\infty)=0.5\sigma_y-0.5\sigma_y\cos(2\theta)$$

$$\tau_{r\theta}(r\to\infty)=0.5\sigma_y\sin(2\theta)$$

The solution is given by

$$\sigma_r = 0.5\sigma_y\left(1-r_d^{-2}\right)-\sigma_y\left(0.5+1.5rd^{-4}-2rd^{-2}\right)\cos(2\theta)$$

$$\sigma_\theta = 0.5\sigma_y\left(1+rd^{-2}\right)+\sigma_y\left(0.5+1.5rd^{-4}\right)\cos(2\theta)$$

$$\tau_{r\theta} = -\sigma_y\left(-0.5+1.5r_d^{-4}-r_d^{-2}\right)\sin(2\theta)$$

$$u = 0.5\sigma_y r_w[(1+v)/(E)]\left\lfloor(1-2v)rd+rd^{-1}\right\rfloor$$
$$-\sigma_y r_w[(1+v)/(Ev)]\left[0.5rd-0.5rd^{-3}+2v/(1+v)rd^{-1}\right]\cos(2\theta)$$

$$v = -\sigma_y r_w[(1+v)/(Ev)]_x$$
$$\left[-0.25(1+v)rd+0.25(1-3v)rd^{-3}-v(1-v)/(1+v)rd^{-1}\right]\cos(2\theta)$$

Now, the solution corresponding to τ_{xy} is determined.

$$\sigma_r\left(r=r_w\right)=0$$

$$\tau_{r\theta}\left(r=r_w\right)=0$$

$$\sigma_r(r\to\infty)=\tau_{xy}\sin(2\theta)$$

$$\tau_{r\theta}(r\to\infty)=\tau_{xy}\cos(2\theta)$$

A general solution with the following form is found.

$$\sigma_r=r^{-1}\partial\psi/\partial r+r^{-2}\partial^2\psi/\partial\theta^2=\left(2A+6Cr^{-4}+4Dr^{-2}\right)\sin(2\theta)$$

$$\sigma_\theta=\partial^2\psi/\partial r^2=-\left(2A+12Br^2+6Cr^{-4}\right)\sin(2\theta)$$

$$\tau_{r\theta}=-(\partial/\partial r)\left(r^{-1}\partial\psi/\partial\theta\right)=\left(2A+6Br^2-6Cr^{-4}-2Dr^{-2}\right)\cos(2\theta)$$

$$u=-[(1+v)/(Ev)]\left[-2Ar+2Cr^{-3}+4Dv/(1+v)r^{-1}\right]\sin(2\theta)$$

$$v=[(1+v)/(Ev)]x$$
$$\left[A(1+v)r+6Bv/(1+v)-C(1-3v)r^{-3}-2Dv(1-v)/(1+v)r^{-1}\right]\cos(2\theta)$$

The coefficients are determined to satisfy the boundary condition.

$$A=0.5T_{xy},B=0,C=0.5\tau_{xy}r_w^4,D=-\tau_{xy}r_w^2$$

The solution is given by

$$\sigma_r=\tau_{xy}\left(1+3rd^{-4}-4r_d^{-2}\right)\sin(2\theta)$$

$$\sigma_\theta=-\tau_{xy}\left(1+3rd^{-4}\right)\sin(2\theta)$$

$$\tau_{r\theta}=\tau_{xy}\left(1-3rd^{-4}+2rd^{-2}\right)\cos(2\theta)$$

$$u=-\tau_{xy}v_w[(1+v)/(Ev)]\left[-r_d+rd^{-3}-4v/(1+v)rd^{-1}\right]\sin(2\theta)$$

$$v = \tau_{xyI'}[(1+v)/(Ev)]x$$
$$\left[0.5(1+v)rd - 0.5(1-3v)rd^{-3} - 2v(1-v)/(1+v)rd^{-1}\right]\cos(2\theta)$$

The solution corresponding to xz is determined.

$$\tau_{rz}\left(r = r_w\right) = 0$$

$$\tau_{rz}(r \to \infty) = \tau_{xz}\cos(\theta)$$

$$\tau_{\theta z}(r \to \infty) = -\tau_{xz}\sin(\theta)$$

The following form of solution is searched.

$$u = Cz\cos(\theta)$$
$$v = -Cz\sin(\theta)$$
$$w = (Ar + B/r)\cos(\theta)$$

If the displacement is substituted in the strain displacement and stress strain relations, the following stresses are calculated.

$$\tau_{rz} = [E/2(1+v)]\left(A + C - B/r^2\right)\cos(\theta)$$

$$\tau_{\theta z} = -[E/2(1+v)]\left(A + C + B/r^2\right)\sin(\theta)$$

The coefficients are determined to satisfy the boundary condition.

$$A = [(1+v)/E]\tau_{xz}, B = [2(1+v)/E]rw^2\tau_{xz}, C = [(1+v)/E]\tau_{rz}$$

Therefore

$$\sigma_r = 0, \sigma_\theta = 0, \tau_{r\theta} = 0$$

$$\tau_{rz} = \tau_{xz}\left(1 - 1/rd^2\right)\cos(\theta)$$

$$\tau_{z\theta} = -\tau_{xz}\left(1 + 1/r_d 2\right)\sin(\theta)$$

$$u = [(1+v)/E]\tau_{xz} z\cos(\theta)$$

$$v = -[(1+v)/E]\tau_{xz} z \sin(\theta)$$

$$w = [(1+v)/E]\tau_{xzT}(rd + 2/rd)\cos(\theta)$$

Similar solution is obtained for τ_{yz} .

$$\sigma_{\mathrm{r}} = 0$$

$$\sigma_{\theta} = 0$$

$$\tau_{r\theta} = 0$$

$$\tau_{rz} = \tau_{yz}\left(1 - 1/r_d 2\right)\sin(\theta)$$

$$\tau_{z\theta} = \tau_{yz}\left(1 + 1/r_d 2\right)\cos(\theta)$$

$$u = [(1+v)/E]\tau_{yz} z \sin(\theta)$$

$$v = [(1+v)/E]\tau_{yz} z \cos(\theta)$$

$$w = [(1+v)/E]\tau_{yz} r_w\left(r_d + 2/r_d\right)\sin(\theta)$$

All the solutions corresponding to the boundary stresses $\sigma_{\mathbf{x}}, \sigma_{\mathrm{y}}, \tau_{\mathrm{xy}}, \tau_{\mathrm{yz}}, \tau_{\mathrm{xz}}$ Pw and Po are added and using the normalized well radius $r_d = r / r_w$, the final solution becomes

$$\begin{aligned}\sigma_r = {} & 0.5*\left(\sigma_x + \sigma_y\right)\left(1 - r_d - 2\right) + 0.5*\left(\sigma_x - \sigma_y\right)\left(1 + 3r_d - 4r_d - 2\right)\cos(2\theta) \\ & + \tau_{xy}\left(1 + 3rd^{-4} - 4rd^{-2}\right)\sin(2\theta) - Pwrd^{-2} \\ & -[E/(1+v)]_{p\cdot 2}\int_{r_w}^{r} r\Delta p dr - [E/(1-v)]_r - 2\int_{r_w}^{r} r(S + \alpha\Delta T)dr\end{aligned}$$

$\beta = [(1+v)/(1-v)](1/3B - 1/3Bi)$ for plane strain.
$\beta = (1+v)(1/3B - 1/3Bi)$ for plane stress.

$$\sigma_\theta = 0.5*\left(\sigma_x+\sigma_y\right)\left(1+r_d^{-2}\right)-0.5*\left(\sigma_x-\sigma_y\right)\left(1+3r_d-4\right)\cos(2\theta)$$
$$-\tau_{xy}\left(1+3r_d^{-4}\right)\sin(2\theta)+P_{Wrd}-2$$
$$+[E/(1+v)]_{fr^{-2}}\int_{r_c}^{r} r\Delta p dr-[E/(1-v)](1/3B\cdot 1/3Bi)\Lambda p\Big]+[E/(1-v)]r^{-2}\int_{r_r}^{r} r(S+\alpha\Delta T)dr$$
$$-[E/(1-v)](S+\alpha\Lambda T)$$
$$\sigma_z=\sigma_{zz}\cdot v\Big\lfloor 2\left(\sigma_x\cdot\sigma_y\right)r_d\cdot 2\cos 2\theta+4\tau_{xy}r_d\cdot z\sin 2\theta\Big\rfloor-[E/(1-v)(1/3B-1/3Bi)\Lambda p$$
$$-[E/(1-v)(S+\alpha\Lambda T)$$

$$\tau_{r\theta}=0.5*\left(\sigma_x\cdot\sigma_y\right)\left(-1+3rd^{-4}-2rd^{-2}\right)\sin 2\theta+\tau_{xy}\left(1-3rd^{-4}+2rd^{-2}\right)\cos 2\theta$$

$$\tau_{\theta z}=\left(-\tau_{xz}\sin\theta+\tau_{yz}\cos\theta\right)\left(1+r_d-z\right)$$

$$\tau_{rz}=\left(\tau_{xz}\cos\theta+\tau_{yz}\sin\theta\right)\left(1-rd^{-2}\right)$$

$$u=0.5\sigma_{xTv}[(1+v)/(E)]\Big\lfloor(1-2v)_{rd}+rd^{-1}\Big\rfloor+\left[r_wP_w(1+v)/E\right]rd^{-1}$$
$$+\left(\sigma_x-\sigma_y\right)r_w[(1+v)/(Ev)]\Big[0.5rd-0.5rd^{-3}+2v/(1+v)rd^{-1}\Big]\cos(2\theta)$$
$$+0.5\sigma_{yr}[(1+v)/(E)]\Big[(1-2v)rd+rd^{-1}\Big]$$
$$-\tau_{xyl_w}[(1+v)/(Ev)]\Big[-rd+rd^{-3}-4v/(1+v)rd^{-1}\Big]\sin(2\theta)$$
$$+[(1+v)/E]\tau_{xz}z\cos(\theta)+[(1+v)/E]\tau_{yz}z\sin(\theta)$$
$$+\beta r^{-1}\int_{r_w}^{r} r\Delta p dr+\frac{1+v}{1-v}r^{-1}\int_{r_w}^{r} r(S+\alpha\Delta T)dr$$

$$v=\left(\sigma_x-\sigma_y\right)_{rw}[(1+v)/(Ev)]\Big[-0.25(1+v)rd+0.25(1-3v)rd^{-3}-v(1-v)/(1+v)rd^{-1}\Big]\cos(2\theta)$$
$$+\tau_{xyrw}[(1+v)/(Ev)]\Big[0.5(1+v)r_w-0.5(1-3v)rd^{-3}-2v(1-v)/(1+v)rd^{-1}\Big]\cos(2\theta)$$
$$-[(1+v)/E]\tau_{xz}z\sin(\theta)+[(1+v)/E]\tau_{yz}z\cos(\theta)$$
$$w=[(1+v)/E]\tau_{xz}r_w\left(r_d+2/rd\right)\cos(\theta)+[(1+v)/E]\tau_{yz}r_w\left(rd+2/r_d\right)\sin(\theta)$$

The displacement u,v,w include the displacement induced with the in-situ stresses. The displacement induced after drilling the well is given by

$$u' = 0.5\sigma_x r_w[(1+v)/(E)]_{rd^{-1}} + \left[r_w P_w(1+v)/E\right] rd^{-1}$$
$$+\left(\sigma_x - \sigma_y\right) r_w[(1+v)/(Ev)]\left[-0.5rd^{-3} + 2v/(1+v)rd^{-1}\right]\cos(2\theta)$$
$$+0.5\sigma_y r_w[(1+v)/(E)]rd^{-1}$$
$$-\tau_{xyI} r_w[(1+v)/(Ev)]\left[rd^{-3} - 4v/(1+v)rd^{-1}\right]\sin(2\theta)$$
$$+\beta r^{-1}\int_{r_w}^{r} r\Delta p dr + \frac{1+v}{1-v} r^{-1}\int_{r_w}^{r} r(S+\alpha\Delta T)dr$$

$$v' = \left(\sigma_{x^-}\sigma_y\right) r_w[(1+v)/(Ev)]\left[0.25(1-3v)rd^{-3} - v(1-v)/(1+v)rd^{-1}\right]\cos(2\theta)$$
$$+\tau_{xy} r_w[(1+v)/(Ev)]\left[-0.5(1-3v)rd^{-3} - 2v(1-v)/(1+v)rd^{-1}\right]\cos(2\theta)$$

$$w' = [(1+v)/E]\tau_{xz} r_w\left(2/r_d\right)\cos(\theta) + [(1+v)/E]\tau_{yz2} r_w\left(2/r_d\right)\sin(\theta)$$

Stress at the borehole

At the borehole, we have

$r_d = 1$

Hence,

$$\sigma_r = -P_W r$$

$$\sigma_\theta = \left(\sigma_x + \sigma_y\right) - 2\left(\sigma_x \cdot \sigma_y\right)\cos(2\theta) - 2\tau_{xy}\sin(2\theta) + P_W - [E/(1-v)](1/3B - 1/3B)\Lambda_P \rfloor$$
$$-[E/(1-v)](S+\alpha\Lambda T)$$

$$\sigma_z = \sigma_{zz}\cdot v\left[2\left(\sigma_x - \sigma_y\right)\right] rd^{-2}\cos 2\theta + 4\tau_{xy}\sin 2\theta\Big] - [E/(1-v)(1/3B - 1/3Bi)\Lambda p - [E/(1-v)(S+\alpha\Lambda T)$$

$$\tau_{r\theta} = 0$$

$$\tau_{\theta z} = 2\left(-\tau_{xz}\sin\theta + \tau_{yz}\cos\theta\right)$$

$$\tau_{rz} = 0$$

Since the net in-situ stresses are used in the above equation, the in situ stresses must be converted from the total in-situ stresses with the following equation.

$$\sigma_{ij}^{net} = \sigma_{ij} + p_o\delta_{ij}$$

Where p_o is the original pore pressure before drilling.
After calculation of the stress around a borehole, the total stresses must be calculated using the following equation.

$$\sigma_{ij} = \sigma_{ij}^{net} - p_o \delta_{ij}$$

Normally, the effective stresses are needed to calculate the borehole stability, the following equation is used if the pore pressure around the borehole is changed by Δp from the original pore pressure.

$$\sigma_r^e = \sigma_r + \Delta p = -P_w + \Delta p$$

$$\sigma_\theta^e = \sigma_x + \sigma_y - 2(\sigma_x - \sigma_y)\cos(2\theta) - 2\tau_{xy}\sin(2\theta) + P_w + \Delta p$$
$$- \frac{E}{1-\nu}\left(\frac{1-2\nu}{E} - \frac{1-2\nu_m}{E_m}\right)\Delta p - \frac{E}{1-\nu}(S + \alpha\Delta T)$$

$$\sigma_z^e = \sigma_{zz} - 2\nu\left\lfloor(\sigma_x - \sigma_y)\cos(2\theta) + 2\tau_{xy}\sin(2\theta)\right\rfloor$$
$$+ \Delta p - \frac{E}{1-\nu}\left(\frac{1-2\nu}{E} - \frac{1-2\nu_m}{E_m}\right)\Delta p - \frac{E}{1-\nu}(S + \alpha\Delta T)$$

$$\tau_{r\theta} = 0$$

$$\tau_{\theta z} = 2\left(-\tau_{xz}\sin\theta + \tau_{yz}\cos\theta\right)$$

$$\tau_{rz} = 0$$

APPENDIX B

TRANSFORMATION FOR INCLINED FORMATION AND INCLINED WELL

Mesh transformation

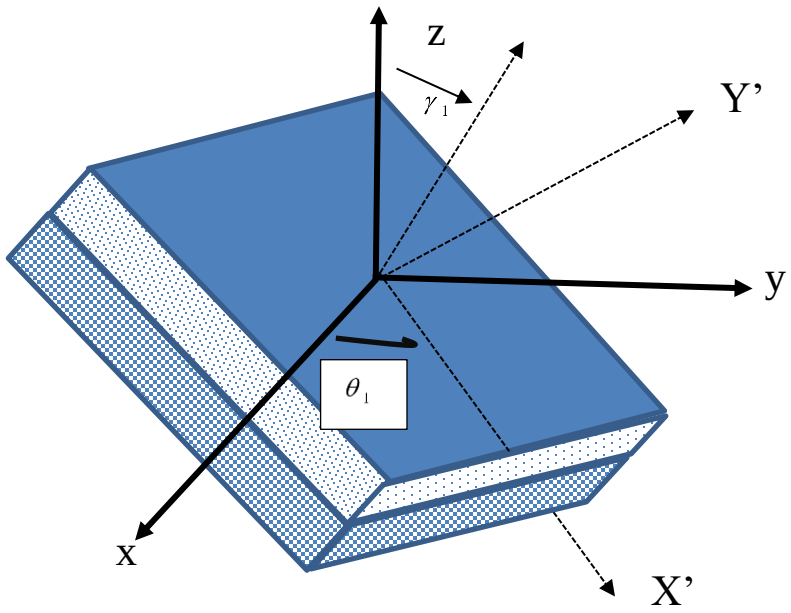

Figure B-1 Mesh transformation

Table B-1 Relation of coordinate transformation

	x	y	z
X'	$\cos\theta_1$	$-\sin\theta_1$	0
Y'	$\sin\theta_1$	$\cos\theta_1$	0
Z'	0	0	1

After rotation $x' = \cos\theta_1 - \sin\theta_1$, $y' = \sin\theta_1 + \cos\theta_1$,

Shift $\Delta z = -x' \tan\gamma_1$